공학박사 학위논문

Development of Seismic Reliability Analysis Methods for Large-scale Infrastructure Networks

대규모 사회기반시설 네트워크의
내진 신뢰성 평가 방법론 개발

2023년 8월

서울대학교 대학원

건설환경공학부

이 동 규

Development of Seismic Reliability Analysis Methods for Large-scale Infrastructure Networks

대규모 사회기반시설 네트워크의
내진 신뢰성 평가 방법론 개발

지도교수 송 준 호

이 논문을 공학박사 학위논문으로 제출함
2023년 8월

서울대학교 대학원
건설환경공학부
이 동 규

이동규의 공학박사 학위논문을 인준함
2023년 8월

위 원 장 김 동 규 (인)

부 위 원 장 송 준 호 (인)

위 원 이 영 주 (인)

위 원 양 수 현 (인)

위 원 변 지 은 (인)

Abstract

With the advancement of technology and the densification of modern society, infrastructure facilities are closely interconnected, thereby forming a vast infrastructure network. Seismic damage to individual structures can result in socio-economic costs to the entire infrastructure network. To quantify the risk of networks and ensure efficient operation and maintenance, there is a need for network seismic reliability analysis. To this end, the seismic failure probability of structures should first be assessed, and then the network reliability is evaluated under different combinations of structural conditions. It is challenging to apply such network seismic reliability analysis for large-scale networks due to common source effects of earthquakes throughout the network, interdependent seismic demands, and It is challenging to apply such network seismic reliability analysis for large-scale networks. Monte Carlo Simulation (MCS) has been used to overcome these limitations, but still has several limitations, including inefficiency for low probability events and difficulty in probabilistic inference.

This dissertation proposes three main methodologies for seismic network reliability analysis. The first approach introduces Bayesian networks (BNs) and junction trees (JTs) to evaluate network reliability and quantify the complexity. Based on the JT constructed from the dual representation of a given network, the reliability of directed acyclic networks can be evaluated by one-way message passing. Even for a cyclic network, the reliability can be accurately assessed using a set of equivalent directed acyclic subnetworks through cycle decomposition. Meanwhile, although it is common to quantify the complexity of network reliability analysis only by the number of components, the network topology also affects the actual

computational complexity. Numerical examples demonstrate that the proposed method can not only evaluate network reliability and component importance measures in real time, but also quantify the complexity using the maximum clique size in JT.

Second, a centrality-based selective recursive decomposition algorithm (CS-RDA) is proposed to identify critical components that play a key role in terms of connectivity based on the network centrality, thereby (1) simplifying the network for multi-scale approaches and (2) significantly increasing the convergence of recursive decomposition algorithm (RDA). Compared to other RDAs, CS-RDA can achieve the target bound width using significantly fewer subgraphs. The efficiency and accuracy of CS-RDA are demonstrated by numerical examples including large-scale highway bridge networks. The application examples also investigate the trade-off between efficiency and accuracy with respect to the degree of network simplification.

Finally, a variance-reduction sampling method is proposed to enhance the scalability and efficiency of direct MCS. The binary limit-state function for network connectivity is reformulated into more informative continuous limit-state functions that quantify how close each sample is to the network failure event. The proposed functions facilitate the construction of intermediate relaxed failure events, thereby enabling network reliability analysis using subset simulation. Furthermore, a single implementation of subset simulation can generate the network reliability curve by configuring each intermediate failure domain as a network failure event under a given earthquake intensity. Numerical examples demonstrate that the proposed method can accurately and efficiently evaluate network reliability curves in terms of k-terminal reliability and maximum flow, as well as two-terminal reliability.

Keyword: Network reliability analysis; Seismic reliability; Infrastructure network; Large-scale networks; Graph theory; Bayesian network; Junction tree algorithm; Complexity quantification; Probabilistic inference; Multi-scale approach; Clustering; Recursive decomposition algorithm; Subset simulation; Hamiltonian Monte Carlo; Network reliability curve.

***Student Number*:** 2017-27849

List of Contents

List of Figures

List of Tables

보존용 학위논문 정오표

페이지	정정 전	정정 후
p. 115 : 2	Section 2.4.1	Section 3.4.1
p. 118 : 3	Section 2.4.2	Section 3.4.2
p. 122 : 4	mink	maxk
p. 122 : 5	mink	maxk
p. 122 : 6	smallest	largest
p. 122 : 7	Section 2.4.2	Section 3.4.2

Chapter 1. Introduction

1.1 Motivations

As cities become denser and more complex than ever before, modern societies are highly dependent on the reliability of complex urban infrastructure networks such as transportation, electricity, and gas networks. These networks are critical to ensuring the safety of communities by providing necessary services for survival such as access to food, water, shelter, or medical care. The importance of their post-earthquake performance is even more pronounced. Damaged infrastructure networks cause disproportionate socio-economic losses, although they should be used to facilitate evacuation and relief activities. Therefore, to make appropriate decisions about infrastructure networks and to allocate available resources, it is essential to quickly evaluate the post-disaster network performance, such as network disconnection.

To perform an accurate network reliability analysis (NRA) for an earthquake causing widespread damage, the interdependency between uncertainty demands reaching each site should be considered, along with the failure probabilities of components. This makes seismic reliability analysis of large-scale networks inherently time consuming. For example, the computational complexity of analyzing their interdependencies is given as $O(N^2)$, where N denotes the number of components. Besides, NRA faces various obstacles including complex network topologies and the curse of dimensionality due to exponentially growing combinations of component states. The most prominent limitation is that the network state is not explicitly known by the combination of component states. In addition,

complex networks have extremely low failure probabilities due to their redundancy, which requires an enormous number of iterations to achieve a statistically significant level of convergence especially for sampling-based methods.

1.2 Objectives

Traditional methods for NRA can be classified into three categories: (1) analytical approaches; (2) decomposition approaches; and (3) sampling-based approaches. However, there are scalability problems in applying each method to large-scale infrastructure networks. To facilitate the seismic reliability analysis of large-scale networks, this dissertation proposes three main NRA methods, one for each category.

Exact computation based on traditional analytical approaches has been limited to small networks or simple network topologies, such as series and parallel systems. In the first proposed method, Bayesian networks (BNs) and their junction trees (JTs) are used to assess the exact reliability of general networks. This JT-based NRA method is inspired by the fact that BNs are graphical models representing random variables and dependencies and can be used to perform probabilistic inference. The message-passing process, scheduled to update the network failure probability, specializes in complexity quantification using maximum clique size and probabilistic inference, as well as accurate NRA.

The second method decomposes the target network into cut sets and link sets, thereby narrowing down the upper and lower bounds of network reliability. To effectively decompose large-scale networks into subnetworks, components that play a key role in network connectivity should be identified. For this purpose, a centrality-based selective recursive decomposition algorithm (CS-RDA) is proposed by

combining betweenness centrality (BC) and selective recursive decomposition algorithm (S-RDA). In addition to node centrality for network decomposition, edge centrality is also used for cluster detection. The complexity of NRA can be greatly reduced by network simplification based on detected clusters, which greatly expands the size of networks that can be handled.

Finally, the third method combines a variance-reduction sampling with NRA. Although various sampling approaches, including the crude MCS, have been adopted with high flexibility and scalability, they are highly inefficient for low-failure events. To this end, the binary limit-state function for network connectivity analysis is reformulated into more informative continuous limit-state functions, quantifying how close each sample is to a network failure. These proposed functions allow subset simulation to be performed for NRA. Therefore, a single implementation of Hamiltonian Monte Carlo-based subset simulation (HMC-SS) can generate the network reliability curve by configuring each intermediate failure domain as a network failure event under an earthquake intensity. Table 1.1 provides an overview of the proposed methods.

Table 1.1. Overview of proposed methods

Method	Approach	Features
Junction-tree-based analysis	Analytical method	- Exact NRA - Complexity quantification - Probabilistic inference
Centrality-based selective recursive decomposition algorithm	Decomposition-based method	- Bounds of network reliability - Multi-scale NRA - Component importance measure
Subset simulation-based analysis	Sampling method	- *k*-terminal reliability & *k*-out-of-*N* reliability analysis - Network reliability curves

1.3 Organization

The organization of the dissertation is as follows. In Chapter 2, BNs and JT algorithms based on the dual representation of networks are combined for NRA. The constructed JT is used for probabilistic inference and complexity quantification as well as for NRA. Chapter 3 proposes a non-simulation-based network reliability algorithm, and uses centrality for clustering the network and identifying critical nodes belonging to min-cuts. BC of each component, combined with the failure probability, is proposed as a measure of component importance to replace the computationally expensive conditional probability-based importance measures (CPIMs). In Chapter 4, new continuous network limit-state functions are proposed to apply variance-reduction sampling methods to NRA. Owing to the flexibility of the sampling methods, the proposed algorithm can evaluate the reliability curve of networks through a single implementation of subset simulation. Finally, Chapter 5 summarizes the developed methods and recommends topics for future research.

Throughout this dissertation, networks or systems are modeled as graphs with nodes (also called vertices) and edges (also called links or arcs) for NRA. It should be noted that nodes and edges in the graph do not always correspond to node-type and line-type components, respectively, in the given network. Chapter 2 only considers the failure of line-type components, which are represented as nodes in the corresponding BN. In contrast, the nodes of the graphs in Chapter 3 represent both node-type components (e.g., stations and bridges) and line-type components (e.g., pipelines and roads). Their respective failure probabilities are modeled as neighboring edges in the graph. In Chapter 4, the graph can be modeled as the original network to use the proposed sampling-based algorithm.

Chapter 2. Network reliability analysis (NRA) and complexity quantification using Bayesian network and dual representation

2.1 Introduction

For the exact failure probability of a network consisting of N arcs, one should perform the probabilistic analysis over N-dimensional probability spaces. Since the size of such a distribution grows exponentially with the number of components (N), a complete quantification of these distributions becomes infeasible even for a moderate number of components (typically $N \geq 30$). To overcome such limitations, several sampling-based methods have been proposed. However, such an approach is computationally inefficient when the failure probability is low. Another limitation of the sampling-based approach is that a new analysis should be performed to update the failure probabilities based on available information or evidence.

To overcome these limitations, an efficient NRA method is proposed where the failure event is defined as the disconnection of an OD pair of interest. The main idea is to separate the modeling of structural failures and functional failures of network components (i.e., edges and/or nodes) by employing a BN. Thereby, the analysis complexity depends not only on the network size (i.e., the number of component events), but also on the network topology. Once a BN model is established, one can utilize existing BN inference algorithms to carry out reliability analysis.

The advantages of the proposed method are three-fold. First, the method can compute the exact failure probability of large-scale networks that were previously

considered to be too large for an exact analysis. Second, existing BN algorithms that are readily available in general-purpose software programs facilitate implementation. Finally, the method enables us to quantify the complexity of network topology from the perspective of reliability analysis, which remains as an unresolved task.

In this chapter, only arc failures are considered. However, this is not necessarily a limitation since it is straightforward to modify the proposed method to consider node failures (Ball *et al.* 1995). In addition, the proposed method deals only with a given network that does not have a directed cycle, which is a fundamental requirement for BNs. This drawback also can be mitigated by preprocessing to decompose cycles. The cycle decomposition preprocessing still works for networks with multiple cycles.

Chapter 2 is organized as follows. Section 2.2 summarizes the background theories of BN and JT and introduces the concept of dual representation of networks. Section 2.3 proposes a new NRA method based on BN and dual graphs, as well as cycle decomposition and network simplification preprocessing. In Section 2.4, the proposed method is applied to the NRA, and the network complexity is quantified in terms of the number of arcs in various network topologies. Then, a large-scale transportation network is analyzed as a numerical example to demonstrate the efficiency and usefulness of the proposed method in Section 2.5. Finally, the conclusions and future work are presented in Section 2.6.

2.2 Background

2.2.1 Bayesian network (BN)

A BN is one of the probabilistic graphical models (PGMs) that visualize directional dependence between random variables (r.v.'s). A BN is represented by a directed acyclic graph (DAG), $G(\boldsymbol{N}, \boldsymbol{E})$, where $\boldsymbol{N}$ and $\boldsymbol{E}$ denote a set of nodes that stand for r.v.'s and a set of directed edges that represent statistical or causal dependencies between a node pair, respectively. When an edge points from node N_i to node N_j, they are called parent and child nodes, respectively.

Once a BN graph is set up, each node $N_i \in \boldsymbol{N}$ needs to be quantified by a probability distribution being conditioned on its parent nodes $Pa(N_i)$, i.e., $P\big(N_i \big| Pa(N_i)\big)$. Then, the joint probability distribution $P(\boldsymbol{N})$, represented by a BN graph, becomes a product of the conditional probabilities of all nodes, i.e.,

$$P(\boldsymbol{N}) = \prod_{N_i \in \boldsymbol{N}} P\big(N_i \big| Pa(N_i)\big). \tag{2.1}$$

Eq. (2.1) shows how a BN factorizes a full joint distribution $P(\boldsymbol{N})$ into lower-dimensional distributions $P\big(N_i \big| Pa(N_i)\big)$, which can significantly reduce the memory required to store distributions. In other words, a BN enables efficient modeling of a high-dimensional probability distribution by visualizing conditional independence between r.v.'s.

BNs have a few limitations. As the number of parent nodes increases, the memory required to store the conditional probability $P(N_i|Pa(N_i))$ grows exponentially. In other words, given too many parent nodes, it becomes infeasible to quantify a BN. Another limitation is that a BN graph must not have any directed cycle, which limits the class of problems that can be handled by the BN methodology.

2.2.2 Junction tree (JT) algorithm

A junction tree (JT) is a graphical method that enables a structured way for inferring a BN model. A BN graph can be transformed into a JT graph, for which multiple general-purpose algorithms are available for computing marginal probabilities (Barber 2012). Once a JT graph is constructed, one can perform probabilistic inference by passing messages (which are in the form of probability distributions) between the cliques in the tree. This message-passing process is equivalent to distributing and combining local probability information across a JT graph. After updating the message of all cliques, one can compute the marginal probability distribution of any r.v. by visiting a clique that the r.v. of interest belongs to.

JT models are advantageous for inferring BN models especially because of accessible computer programs that can manage the whole analysis process of a JT model. To implement the proposed method, the BRML toolkit (Barber 2012) is used.

2.2.3 Dual representation of networks

A dual representation of a network converts arcs and nodes from a primal network. In other words, in a dual network, arcs in a primal network become nodes, and node pairs are connected if their corresponding arcs are directly connected in a primal network. Such alternative representation often reveals hidden properties of a network that do not appear apparent in a primal network (Porta *et al*. 2006).

2.3 Proposed JT-based NRA method

For a new NRA method, BN, JT, and dual graphs are utilized. Advantages of the proposed method are three-fold: (1) the method can evaluate the reliability of

networks whose exact solution was previously considered unattainable, (2) the computational complexity of an arbitrary network can be quantified from the perspective of NRA, and (3) it can be extended to compute probabilistic indices, e.g., CPIM.

Figure 2.1 illustrates a summary of the proposed procedure. First, one simplifies a target network by eliminating components that are not connected to an OD pair of interest. Then, a BN graph is built by using a dual representation of the simplified network. Next, the BN graph is transformed into a JT graph, for which a message-passing is scheduled; this can be done by employing one of the existing JT algorithms. The final JT model can be used for three purposes: (1) quantifying the computational complexity of NRA; (2) performing NRA; and (3) probabilistic inference.

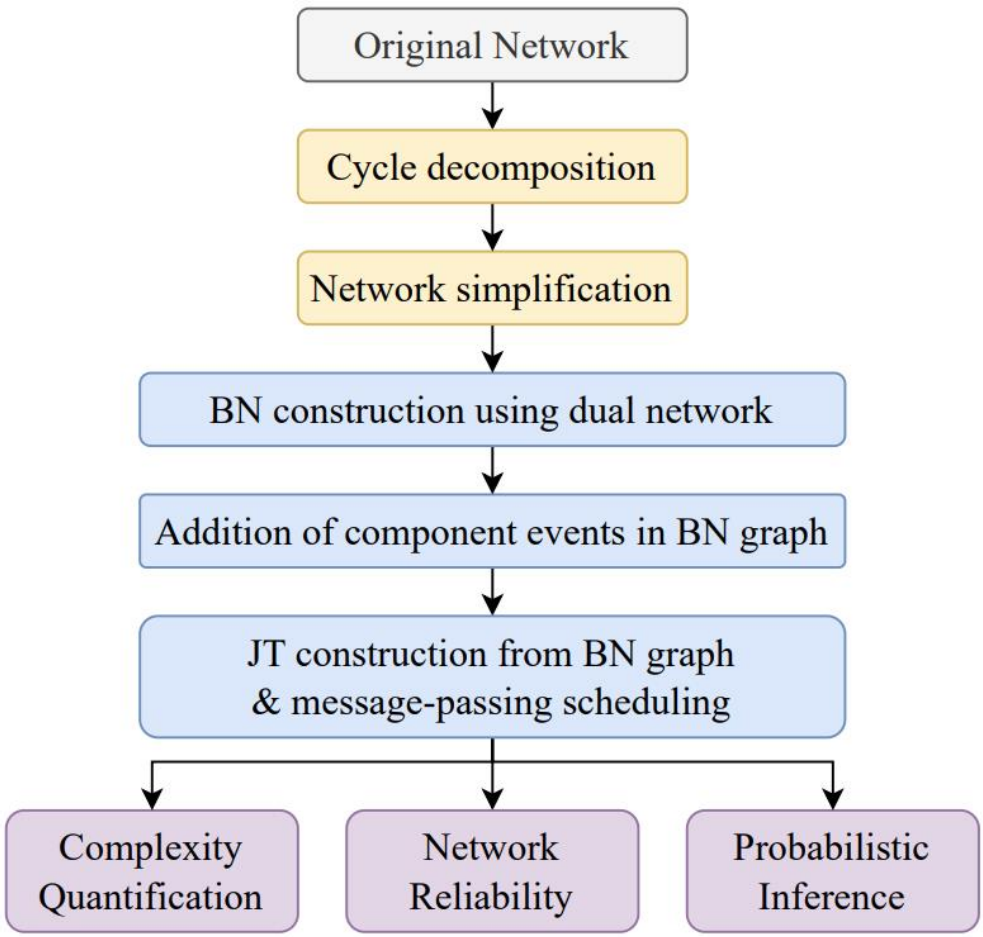

Figure 2.1. Flowchart of proposed JT-based NRA method

2.3.1 Preprocessing

The proposed method utilizes BN, and thus inherently cannot handle directed cyclic networks. To mitigate this limitation, this section proposes a scheme for decomposing the original cyclic network into multiple acyclic subnetworks. A cycle is defined as multiple arcs forming a closed polygon, so that the cycle is broken when one or more arcs fail. If all arcs in the cycle survive, the cycle can be considered as a single component. This means that a graph with a single cycle consisting of n arcs can be decomposed into $n+1$ directed acyclic subgraphs. More specifically, the first subgraph represents the graph where one arc of the cycle fails, and the second represents the one where the first arc works but another arc fails. In the same way, one can create up to the n^{th} subgraph, where $(n-1)$ arcs work but the other is broken. Finally, the $(n+1)^{th}$ subgraph with all functional arcs is equivalent to a graph where the inflow and outflow arcs to the cycle are concentrated at a single vertex within the cycle. The reliability analysis for the network with n_{cyc} cycles requires the following number of decomposed subgraphs:

$$n_{sub} = \prod_{i=1}^{n_{cyc}} (n_i + 1), \tag{2.2}$$

where n_i is the number of arcs in i^{th} cycle. Then, network failure probability $P(S)$ is computed using the decomposed subgraphs, i.e.,

$$P(S) = \sum_{j=1}^{n_{sub}} \left[P_j \cdot P\left(S^j\right)\right], \tag{2.3}$$

where P_j denotes the likelihood of subgraph j; and $P\left(S^j\right)$ is the failure probability of the j^{th} subgraph. This scheme has the limitation that the

computational cost increases rapidly as the number of cycles increases as shown in Eq. (2.2). In such cases, prioritizing and analyzing the most likely subgraphs first can provide an approximation to the solution without having to analyze all the subgraphs. Figure 2.2 shows a graph G with a single cycle consisting of three arcs, and the four subgraphs generated after cycle decomposition are shown in Figure 2.3.

When dealing with large networks, a sizeable portion of the vertices may be unreachable from either the origin or destination. Such vertices unnecessarily complicate the NRA. Therefore, the proposed method first removes those vertices and their connected arcs that can be identified by any basic connectivity analysis algorithm. Numerical experiments show that this strategy significantly improves the efficiency of the proposed algorithm.

Unlike cycle decomposition preprocessing, the network simplification is not mandatory. Even if this is omitted, unnecessary nodes can be eliminated through marginalization during the message-passing in a JT graph. However, with the proposed preprocessing, computation becomes much more efficient than with marginalization. Especially in random networks that often have many isolated components from an OD pair, this strategy enables solving problems that seem intractable in their original forms.

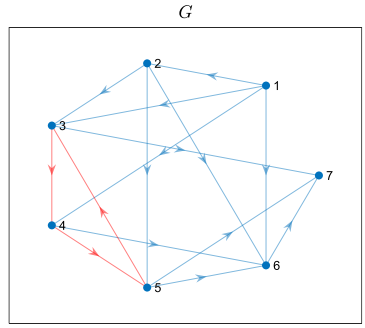

Figure 2.2. Example graph with a cycle

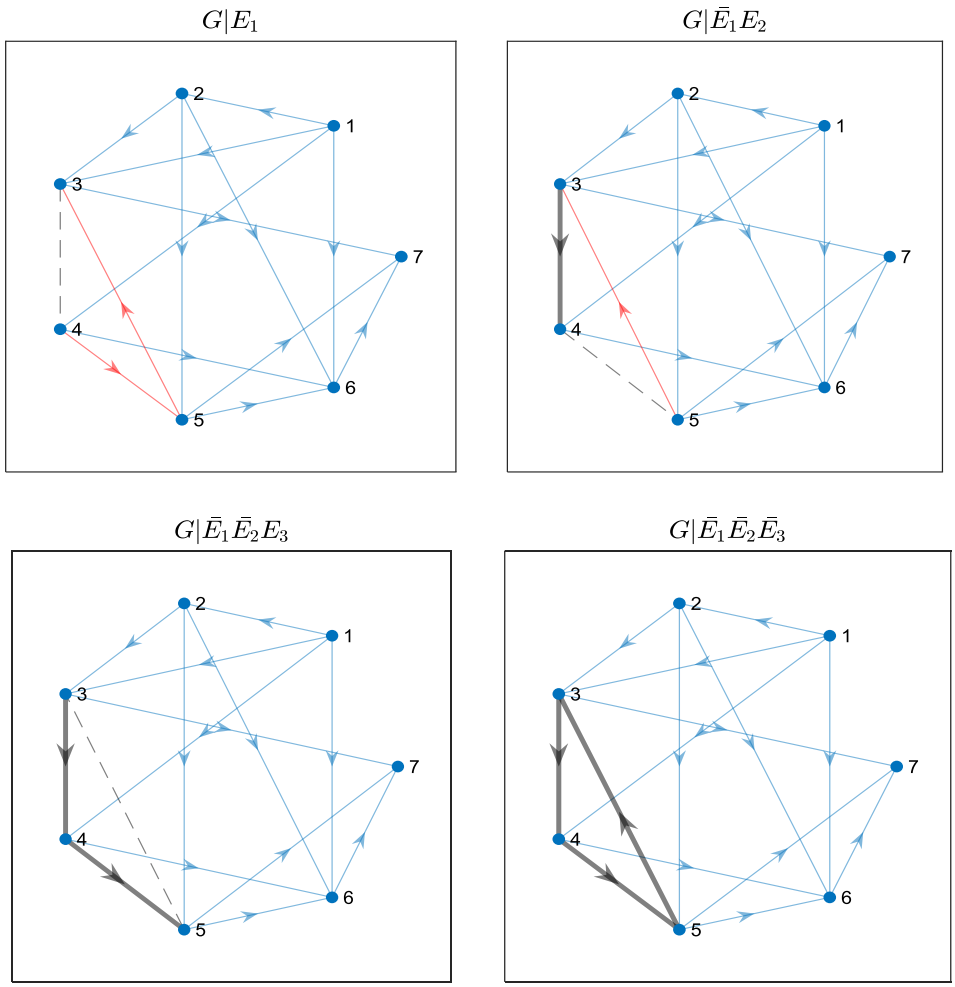

Figure 2.3. Equivalent subgraphs after cycle decomposition (dashed: failed edges, bold black: survival edges, red: unknown)

2.3.2 Bayesian network (BN)

2.3.2.1 BN construction using dual graph

The method builds a BN, in which nodes represent components that can fail. Then, a directed edge is created for each pair of nodes whose corresponding arcs are connected in the target network. Since this study considers arc failures only, the resulting BN has a topology equivalent to the dual representation of a target network.

For example, consider an example network in Figure 2.4, which consists of four vertices (blue circles) and five directed arcs (green arrows). The origin and destination vertices are denoted by O and D, respectively. Then, using the dual representation, the corresponding BN can be constructed as in Figure 2.5. In the BN, $T_1, \dots, T_N$ (in this case, $N = 5$) are binary r.v.'s that take 1 if the head of arc i is reachable from the origin vertex, and 0 otherwise. S is a binary r.v. whose state becomes 1 if the destination vertex can be reached from the origin vertex, and 0, otherwise. While conditional probability tables (CPTs) of T_i will be discussed in Section 2.3.2.3, the CPT of S is constructed as Table 2.1 (Byun and Song 2021a).

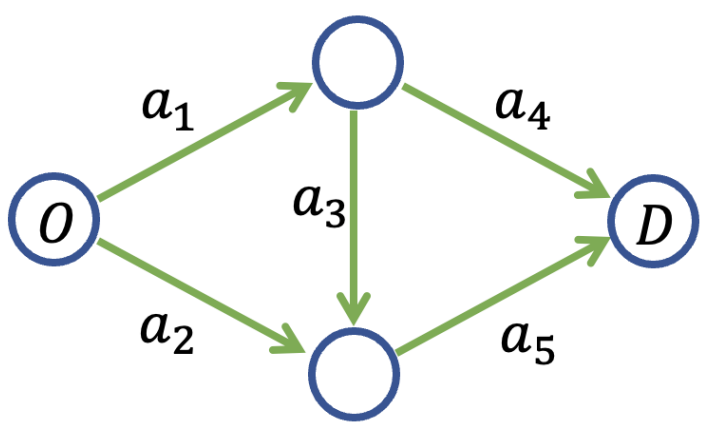

Figure 2.4. Example network with five arcs

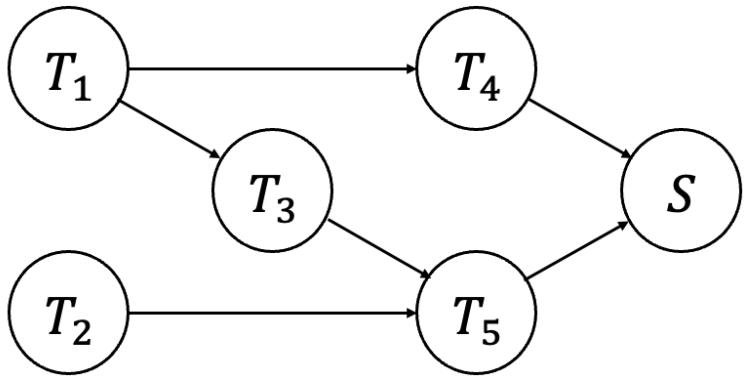

Figure 2.5. BN graph constructed via dual representation of example network

Table 2.1. CPT of S given $T_1, \dots, T_N$

$P(S\|T_1, \dots, T_N)$	$S = 1$	$S = 0$
$\sum_{T_i \in Pa(S)} T_i \geq 1$	1	0
$\sum_{T_i \in Pa(S)} T_i = 0$	0	1

The proposed method is applicable only to maximum flow analysis (for which connectivity analysis is a special case). This is because the method achieves efficiency by exploiting conditional independence between arcs that are not directly connected; that is, the connectivity status of an arc (from an origin vertex) is independent to the status of other vertices when the status of directly connected arcs is known. For instance, in the BN graph in Figure 2.5, the connectivity of arc 5 to the origin vertex is independent to arcs 1 and 4, being conditioned on the connectivity of arcs 2 and 3.

Such conditional independence may not hold for other types of analysis. For example, in a traffic simulation analysis, traffic is sequentially assigned by referring to traffic flows on both preceding and succeeding arcs.

2.3.2.2 Addition of component events

The node T_i represents a topology-based perspective of NRA. In addition, one needs to include r.v.'s to represent the states of component events, denoted as X_i, i.e., X_i represents whether arc i is functional $(X_i = 1)$ or not $(X_i = 0)$. By construction, X_i becomes a parent node of T_i for each $i = 1, \dots, N$. Then, the CPT of T_i can be constructed as shown in Table 2.2 if arc i is directly connected to the origin node. If arc i is reachable from the origin node but not directly connected to it, one can use the CPT in Table 2.3.

In quantifying the CPTs of X_i, there are largely two cases: (1) component events are statistically independent and (2) dependent. In the first case, one can simply add a node X_i and an edge heading from T_i to X_i for each i. For instance, for the example network, a BN is constructed as shown in Figure 2.6. Then, each node X_i, $i = 1, \dots, N$, is assigned a CPT that represents $P(X_i)$.

Table 2.2. CPT of T_i given X_i

$P(T_i \mid X_i)$	$T_i = 1$	$T_i = 0$
$X_i = 1$	1	0
$X_i = 0$	0	1

Table 2.3. CPT of T_i given X_i and $T_1, \dots, T_N$

$P(T_i \mid X_i, T_1, \dots, T_N)$	$T_i = 1$	$T_i = 0$
$\left(\sum_{T_k \in Pa(T_i)} T_k\right) \cdot X_i \geq 1$	1	0
$\sum_{T_k \in Pa(T_i)} T_k = 0$	0	1
$X_i = 0$	0	1

On the other hand, in the second case, where nodes are connected to each other, the computation becomes complicated. For example, Figure 2.7 illustrates a modified BN graph of the example network. In this case, it is required to quantify a single joint CPT $P(X_1, \dots, X_N)$ over all nodes $X_1, \dots, X_N$, whose size increases exponentially with N.

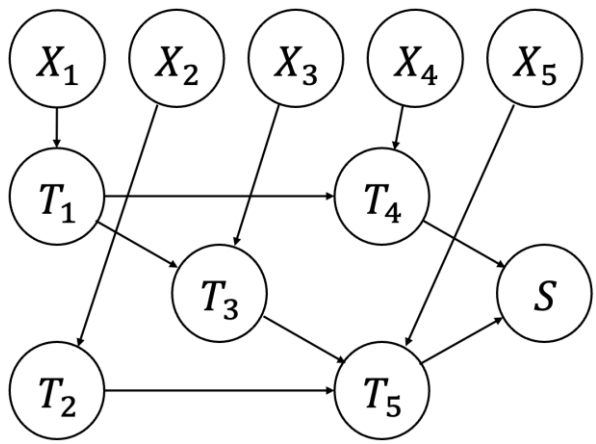

Figure 2.6. BN graph of example network with independent component events

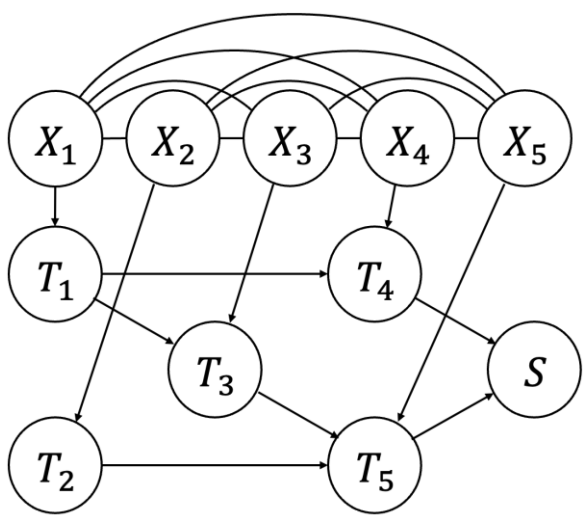

Figure 2.7. BN graph of example network with dependent component events

2.3.2.3 JT construction and message-passing scheduling

For probabilistic inference, the BN graphs constructed in Section 2.3.2.2 can be used to build JT graphs. This can be done automatically using existing algorithms such as the maximum weight spanning tree algorithm (Barber 2012). Once a JT graph is constructed, message-passing can be scheduled, for which several algorithms can be used (Barber 2012).

For example, the JT graph for the BN graph in Figure 2.6 can be constructed as Figure 2.8. To update the system probability $P(S)$ at the end, the message-passing is scheduled from low to high numbered cliques as $1 \rightarrow 6,\ 2 \rightarrow 6,\ \ldots,\ 8 \rightarrow 9$. Note that the yellow cliques come from the addition of component events, which only propagates the component failure probabilities and is irrelevant to the maximum clique size. This means that one can infer the complexity of the target NRA just by comparing the size of the largest clique in the JT composed of white cliques. In contrast, the JT graph corresponding to the BN in Figure 2.7 becomes a large single clique including all nodes $X_1, \ldots, X_N, T_1, \ldots, T_N$, and S as shown in Figure 2.9.

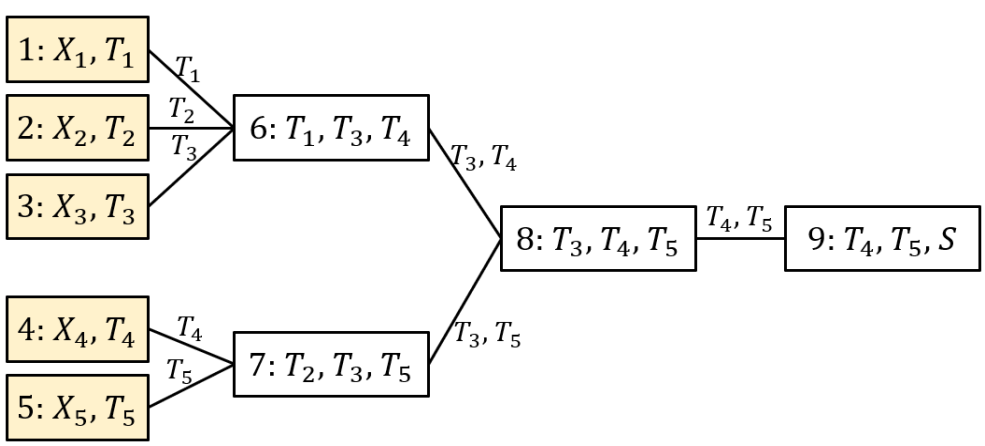

Figure 2.8. JT graph corresponding to Figure 2.6

$$1: T_1, T_2, T_3, T_4, T_5, S, X_1, X_2, X_3, X_4, X_5$$

Figure 2.9. JT graph corresponding to Figure 2.7

2.4 Utilization of constructed JT graph

2.4.1 Complexity quantification of NRA

A constructed JT graph can be used to quantify the computational complexity of NRA by evaluating the sum of the memory required to store the CPTs of the cliques. Specifically, the memory demanded by a clique C_j is the product of the number of states of the r.v.'s in C_j. Therefore, the required memory is proportional to 2^{N_j} where N_j is the number of r.v.'s in clique C_j. For instance, the number of probabilities to be stored in Figure 2.8 is $2^2 \times 5 + 2^3 \times 4 = 52$ as five cliques consist of two components and four cliques consist of three components. It is noted that the largest clique governs a required memory in general.

Such utility is beneficial in that the quantification of network topology complexity remains inconclusive. While there are several metrics developed to this end (e.g., Valiant 1979; Ball 1986), the proposed approach provides a direct metric for NRA. Before performing NRA, one can use the proposed approach to measure the complexity of a given network topology and select an appropriate NRA method. For instance, if the given topology is too complicated to apply analytical methods, one can use a sampling method or advanced BN inference algorithms.

2.4.2 JT-based NRA

Once a junction graph and a message-passing schedule are set up, NRA can be carried out by evaluating the marginal distribution of the system event, $P(S)$. This procedure is straightforward when component events are statistically independent (e.g., JT in Figure 2.8).

On the other hand, when they are dependent (e.g., Figure 2.9), advanced inference strategies such as Rao-Blackwellized particles or conditioning (Koller and Friedman 2009; Byun and Song 2021b) can be employed to make the analysis affordable. The Rao-Blackwellized approach circumvents memory issues by applying sampling to a subset of r.v.'s while performing exact inference over other r.v.'s. Meanwhile, if there are common-cause variables (e.g., intensity of an earthquake), applying the conditioning technique to those variables can significantly reduce a required memory (Byun and Song 2021b). Even when there is no common-source variable, one can artificially model such variables, e.g., Bensi *et al.* (2011) and Song and Kang (2009).

The most notable thing about this method is that it can handle multiple states, not just the binary state of a component. By defining multiple states of a component, it can be easily extended to analyze the connectivity of the network as well as the maximum flow.

2.4.3 Probabilistic inference

Accurate and fast JT-based NRA using one-way message-passing can easily be extended to probabilistic inference, including CPIM (Song and Kang 2009). Scheduling message-passing in the other direction from the JT could be an option,

but simply iterating the message-passing proposed with the modified failure probabilities is sufficient owing to the fast computation time. More specifically, CPIM can be updated by the conditional network failure probability given one component fails, the component failure probability, and the original network failure probability as

$$CPIM_i = P(E_i|E_{net}) = \frac{P(E_i E_{net})}{P(E_{net})} = \frac{P(E_{net}|E_i)P(E_i)}{P(E_{net})}. \quad (2.4)$$

2.5 Numerical examples

2.5.1 Application I: typical network topologies

This section investigates the computational complexity of four typical network topologies: line, grid, tree, and complete networks in Figure 2.10. Since the largest clique governs computational complexity, the largest clique size of the corresponding JT graphs is examined, along with the computable range (red area) on a personal computer with 16GB of RAM in Figure 2.11, where the number of arcs varies from 4 to 184. In the line and tree networks, the complexity is not affected by an increasing number of arcs. On the other hand, the maximum clique size in complete networks increases linearly, indicating that the memory demand increases exponentially. The maximum clique size of the grid structure also increases with the number of arcs, but at a much slower rate than the complete network.

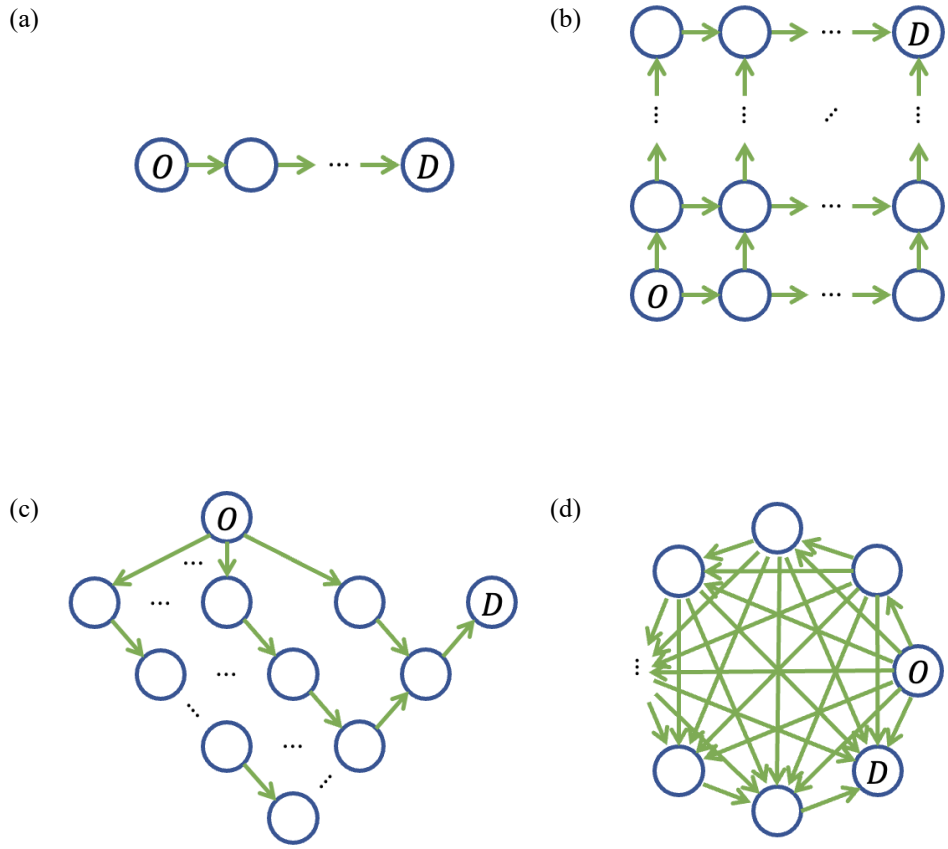

Figure 2.10. Typical network topologies: (a) line, (b) grid, (c) tree, and (d) complete

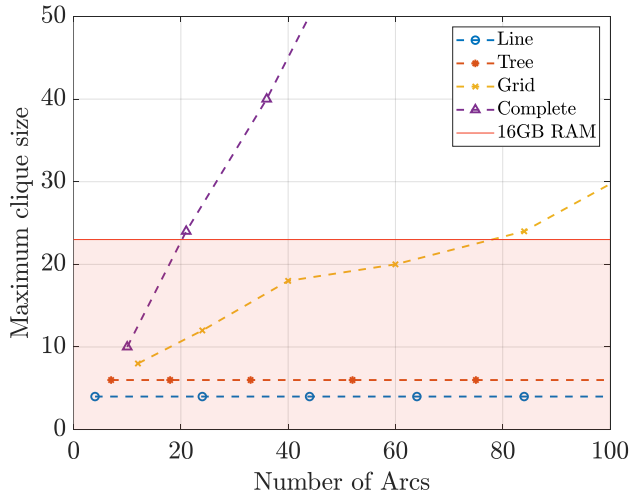

Figure 2.11. Maximum clique size of each topology with network size represented by number of arcs

2.5.2 Application II: random network with a cycle

Consider the random network with a cycle mentioned in Figure 2.2, where the probability of any two vertices being connected is uniformly assumed to be 50%. The edges connecting vertices 3 and 4, 4 and 5, and 5 and 3 are defined by edge 1, edge 2, and edge 3, respectively. E_1, E_2, and E_3 denote the failure events of corresponding edge with probabilities of 0.115, 0.107, and 0.105, respectively. Based on this information, one can compute the likelihood of each subgraph in Figure 2.3, since the failure of every component is independent to each other.

Although quantifying the complexity of NRA for the original network is impossible because one cannot build a BN, the generated acyclic subgraphs make it possible. Table 2.4 shows the computation time, quantified complexity in terms of maximum clique size, likelihoods, and failure probabilities for each subgraph. There is minor difference in the computation time, and in terms of the complexity of NRA, the more surviving edges there are, the larger the maximum clique size since inflows and outflows are concentrated on the vertices connected to surviving edges. In the end, Table 2.5 shows that the network reliability evaluated by their weighted sum is almost identical to the MCS result, but the computation time is about 1/1,000 of that by MCS.

Table 2.4. NRA results for subgraphs

Subgraph	Computation time	Max. clique size	Likelihood	P_f
$\{G\|E_1\}$	0.0714 s	5	0.115	2.97×10^{-3}
$\{G\|\bar{E}_1 E_2\}$	0.0710 s	5	0.095	6.10×10^{-3}
$\{G\|\bar{E}_1 \bar{E}_2 E_3\}$	0.0812 s	6	0.083	2.46×10^{-3}
$\{G\|\bar{E}_1 \bar{E}_2 \bar{E}_3\}$	0.0713 s	7	0.707	2.11×10^{-3}

Table 2.5. Comparison of NRA results

Methods	Computation time	P_f
JT-based NRA	0.295 s	2.61×10^{-3}
MCS	337.8 s	2.67×10^{-3}

2.5.3 Application III: Shelby County water distribution network

A real-world water distribution network is a prime example of directed networks, where most edges points in a single direction. Figure 2.12 shows the water distribution network in Shelby County, TN (Lim and Song 2012). It consists of 49 vertices including storage tanks and pumping stations, and 71 directional arcs. The direction of some edges are modified from the original network, and the location of several storage tanks and pumping stations are set based on the network topology. Under emergency events, such as an earthquake, it is important to have a guaranteed water supply based on the connection from any storage tanks to pumping stations. Accordingly, the disconnection probability from one or more tanks to each pumping station is evaluated using the proposed JT-based NRA method.

Prior to the probability evaluation, the maximum clique size in the constructed

JT for complexity quantification is given by 8, which is independent of the target pumping stations. The failure probability of each component is assumed to be 5%, and the water shut-off probability for each station, $P(S_1)$, $P(S_2)$, and $P(S_3)$, evaluated by the proposed method is shown in Table 2.6 with the computation time. Moreover, the results are compared with those by MCS. The evaluated network failure probabilities vary from 0.234% to 7.16%, and the proposed JT-based NRA evaluates them accurately within about 0.4 seconds regardless of the probability. In contrast, the efficiency of MCS is highly dependent on the target probability; the lower the probability, the longer MCS takes. On the problem with the highest computational cost, MCS takes about 369 seconds for a target coefficient of variance of 1%. This is about 1,000 times longer than that of the proposed method, and if the more robustly the components are designed, the worse the efficiency of the MCS.

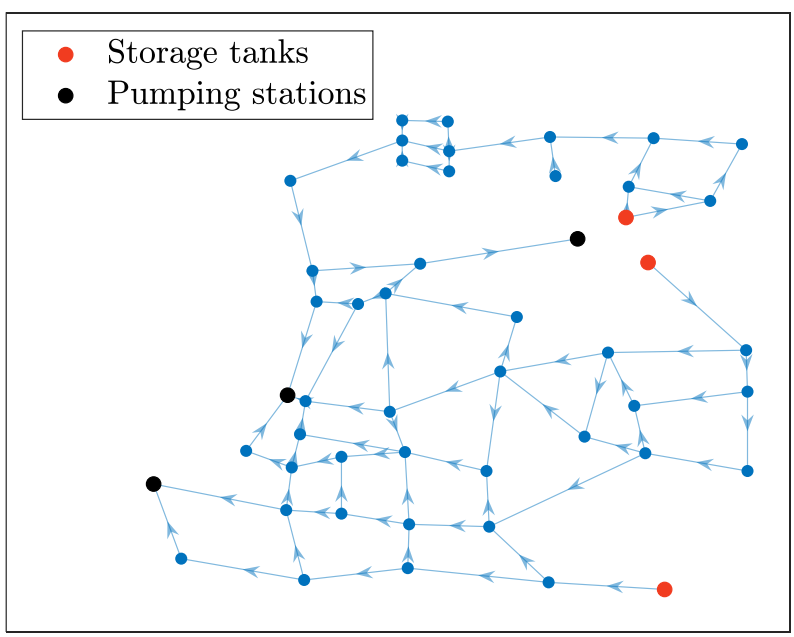

Figure 2.12. Water distribution network in Shelby County, TN, with three storage tanks and three pumping stations.

Table 2.6. NRA results on water distribution network in Shelby County, TN.

Methods	$P(S_1)$	Time	$P(S_2)$	Time	$P(S_3)$	Time
JT-based NRA	0.234%	0.382 s	7.16%	0.348 s	4.72%	0.292 s
MCS	0.251%	369 s	7.29%	11.1 s	4.63%	19.4 s

2.5.4 Application IV: EMA benchmark network

The Eastern Massachusetts (EMA) highway network, modified from Zhang *et al*. (2018), consists of 129 directional arcs and 74 vertices, as shown in Figure 2.13(a). The failure probability of each arc, $P(X_i = 0)$, is set as 0.1 for $i = 1, \dots, 129$. Using the network simplification strategy described in Section 2.3.1, the network is simplified to that in Figure 2.13(b), where the numbers of arcs and vertices are reduced to 85 and 47, respectively.

Considering the independent component events X_i, the maximum clique sizes of the JT graph with and without preprocessing are identical as 16. The result implies that, in this example, the preprocessing does not incur any difference in computational complexity while slightly shortening the time by reducing message-passing between cliques. Table 2.7 compares the computation time, and the network failure probability estimates by the proposed method with and without preprocess, compared to the results of Monte Carlo simulation (MCS). The results confirm that the proposed method provides consistent estimates of the network failure probability, while taking only about 2.6~3.8% of the computation time taken by MCS. It is noted that the result computed by the proposed method is an exact solution.

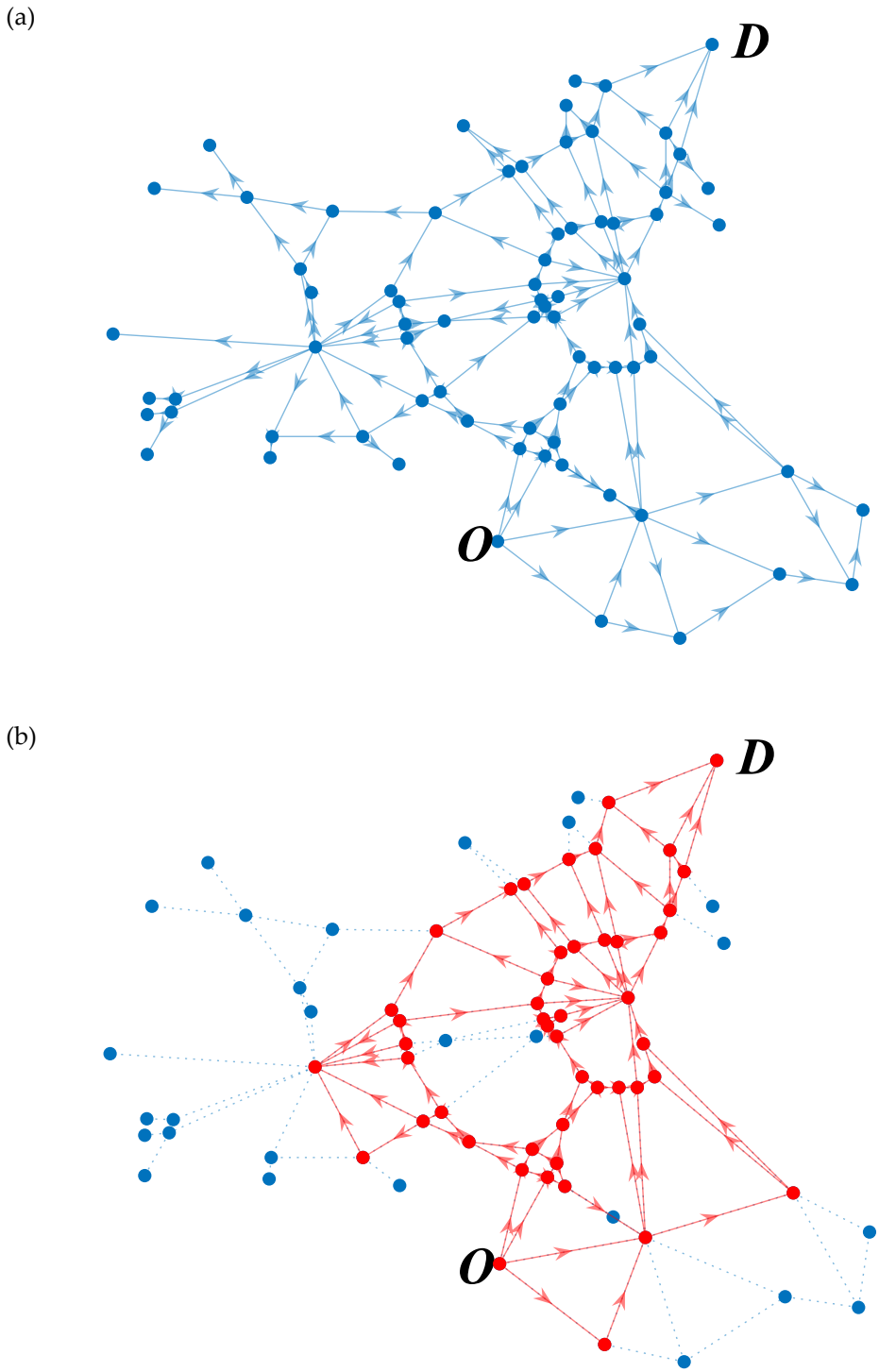

Figure 2.13. EMA highway network: (a) original network, and (b) simplified network by preprocess

Table 2.7. Analysis results of EMA highway network

Methods	Computation time	P_f
MCS	19.99 s	2.952 %
JT-based NRA (w/ preprocess)	0.525 s	2.957 %
JT-based NRA (w/o preprocess)	0.757 s	2.957 %

Figure 2.14 shows the results of probabilistic inference in terms of CPIM using Eq. (2.4); components with high CPIM are highlighted with red solid lines. Since the edges removed by network simplification (blue dashed lines) have no effect on the OD connectivity, CPIMs for these edges are identical to the initial failure probability of network. On the other hand, the remaining edges (red or black solid lines) are engaged in network reliability, and each CPIM varies depending on their locations, even though the individual failure probabilities are unified to 0.1. Table 2.8 shows the five edges with the highest CPIMs, i.e., those with the greatest impact on the network reliability, and their CPIMs. Figure 2.15 shows the maximum clique sizes for the networks in Sections 2.5.2 through 2.5.4.

Table 2.8. Edges with highest CPIM

Edge ID	CPIM
73	0.613
85	0.424
82	0.386
63	0.195
61	0.171

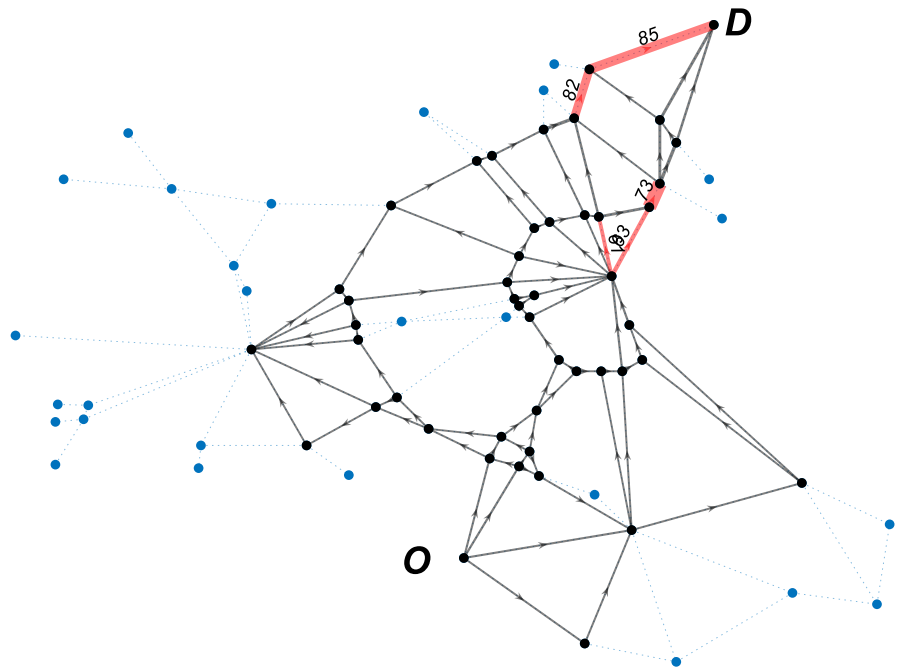

Figure 2.14. Results of probabilistic inference: edges with highest CPIM

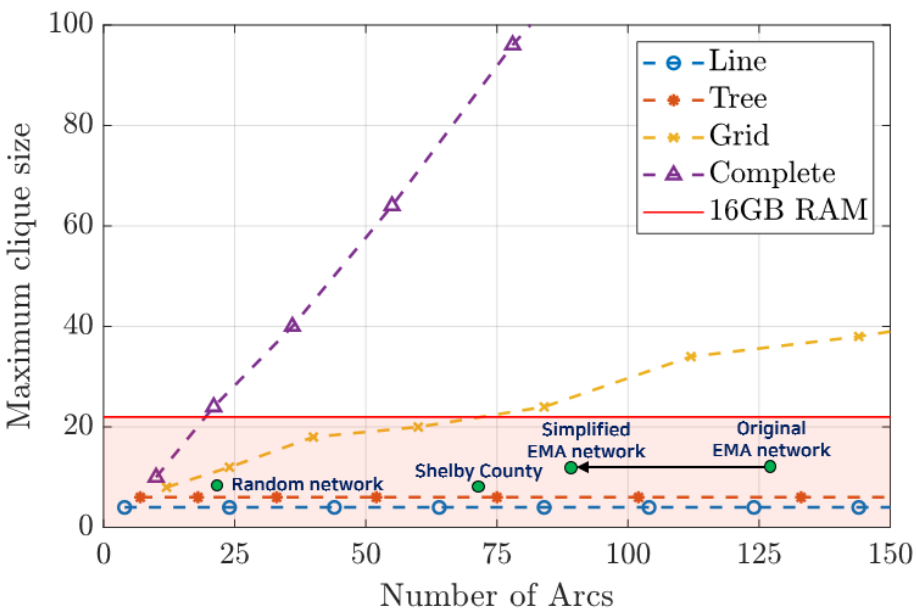

Figure 2.15. Comparison of application examples and typical topologies in terms of maximum network clique size.

Chapter 3. Multi-scale NRA using Centrality-based Selective Recursive Decomposition Algorithm

3.1 Introduction

Various non-simulation-based approaches such as first-order system reliability method approximations (Hohenbichler and Rackwitz 1982) have been developed. However, most of these methods are too complicated and inaccurate to analyze non-series or non-parallel systems. To compute the failure probability of general systems, Song and Kang (2009) proposed the matrix-based system reliability method, which divides the sample space of the component events into mutually exclusive and collectively exhaustive events. Li and He (2002) proposed the recursive decomposition algorithm (RDA), which decomposes a network into subgraphs recursively to compute the network disconnection probability. RDA systematically identifies disjoint (mutually exclusive) link sets (i.e., sets of components whose joint survivals ensure the connectivity between predefined two terminal nodes) and cut sets (i.e., sets of network components whose joint failures cause the disconnection of the node pair), which allows us to compute the network reliability simply by summing up the probabilities of the identified sets. However, applying these non-simulation-based methods to the reliability analysis of complex infrastructure networks may require unrealistic computational costs and an excessive amounts of computer memory.

To obtain narrow bounds on the network reliability in a relatively short time,

Lim and Song (2012) proposed the selective recursive decomposition algorithm (S-RDA) that preemptively identifies critical disjoint link sets and cut sets with the highest probability of network connection or disconnection in the RDA process, along with an efficient risk assessment framework considering the spatial correlation of ground motions. By prioritizing the identification of link sets and cut sets that make dominant contributions to the network reliability and failure probability, S-RDA significantly enhances the convergence speed of the bounds, thus saving the computational cost in terms of time and memory. This improved efficiency has allowed for the analysis of larger infrastructure networks that traditional non-simulation-based algorithms could not handle due to the excessive computational cost. However, despite the improved performance of S-RDA, there are still fundamental limitations in applying RDA to large infrastructure networks because the numbers of critical disjoint link sets and cut sets grow exponentially as the network size increases. In addition, as the number of components constituting each disjoint link set and cut set also increases, evaluating the joint probability in higher dimensions can become time-consuming and inaccurate.

To alleviate this computational challenge, methods to identify a simplified network representation have been developed. Gómez *et al.* (2013) proposed a hierarchical network representation method for large-scale networks. Clusters are identified by the Markov clustering method based on the network topology to construct a simplified network consisting of the identified clusters and inter-cluster connections. To facilitate the network reliability analysis (NRA), the nodes connecting the clusters and inter-cluster connections were assumed to be indestructible. Lim *et al.* (2015) proposed a multi-scale approach using spectral

clustering algorithms to efficiently evaluate the network reliability by considering not only the failure probability of each node, but also the spatial correlations between component failures for accurate seismic risk assessment (Lim and Song 2012). However, the spectral clustering methods used in this approach have a critical disadvantage for large-scale networks: expensive computational cost. The computational cost problem is quite critical for dimensionality reduction computations in large and dense networks.

This chapter aims to address the computational complexity problems in large-scale network analysis by using the network centrality index. To this end, a network reliability method called centrality-based selective recursive decomposition algorithm (CS-RDA) is proposed (Lee and Song 2021). The critical nodes, i.e., those which are most likely to be included in the minimum cut set, are detected based on network centrality, and preferentially decomposed in each identified link set to find cut sets with higher probabilities, thereby promoting fast convergence of the algorithm. This chapter also introduces a network clustering algorithm based on the centrality concept to simplify large-scale networks that make non-simulation-based approaches intractable. After obtaining a simplified network representation, the reliability of each cluster and that of the simplified network are evaluated by the proposed CS-RDA.

The remainder of this chapter is organized as follows. Section 3.2 describes how the uncertainty of seismic capacity and demand for each component and statistical dependencies are handled throughout the dissertation as well as in this chapter, along with the two existing non-simulation-based approaches that provide a foundation for CS-RDA: the original RDA and S-RDA. Section 3.3 provides an overview of

network centrality measures, and proposes two new algorithms based on the network centrality: (1) the edge-betweenness algorithm and (2) CS-RDA. The simplified network representation using super-components proposed by Lim *et al.* (2015), and how to handle the uncertainty in the seismic capacity and demand of each super-component and the statistical dependencies between them are also discussed together. Finally, the applicability of the proposed algorithm is demonstrated and tested by the reliability analysis of numerical examples in Section 3.4 in which its performance is compared with that of existing algorithms.

3.2 Background and related works

3.2.1 Seismic risk assessment in infrastructure networks

In assessing the failure probabilities of components, two major uncertainties need to be considered: (1) seismic demands throughout the network, and (2) seismic capacity of each component. These uncertainties of components form the basis for computing the network seismic reliability and component importance measures.

3.2.1.1 Ground motion intensities and spatial correlation

To predict ground motion intensities based on a seismic attenuation model, a ground motion prediction equation (GMPE) (Abrahamson and Youngs 1992; Joyner and Boore 1993; Goda and Hong 2008) is often used in the form

$$\ln D_i(T_n) = f(M, R_i, \boldsymbol{\lambda}_i, T_n) + X_i(T_n), \tag{3.1}$$

where $D_i(T_n)$ is a ground-motion intensity measure at the i^{th} site, such as peak ground acceleration (PGA), peak ground velocity (PGV), and spectral acceleration

(SA); $f(M, R_i, \boldsymbol{\lambda}_i, T_n)$ is the attenuation relation given in terms of the earthquake magnitude M, the distance between the earthquake source and the i^{th} site, R_i, and a set of other explanatory variables $\boldsymbol{\lambda}_i$; and $X_i(T_n)$ is the random residual at the i^{th} site with zero mean and standard deviation σ_X. The residual $X_i(T_n)$ is described as the sum of $\eta(T_n)$ and $\varepsilon_i(T_n)$, which are the inter- and intra-event residuals with zero means and standard deviations $\sigma_\eta(T_n)$ and $\sigma_\varepsilon(T_n)$, respectively. It is assumed that $\eta(T_n)$ and $\varepsilon(T_n)$ are statistically independent of each other and both follow Gaussian distributions. As a result, the standard deviation of the residual $X_i(T_n)$ is derived as $\sigma_X(T_n) = \left(\sigma_\eta^2(T_n) + \sigma_\varepsilon^2(T_n)\right)^{\frac{1}{2}}$. Because only PGA or PGV is considered as the ground motion intensity measure D_i in this dissertation, the natural period T_n is omitted to simplify Eq. (3.1) as

$$\ln D_i = \ln \overline{D}_i + \eta + \varepsilon_i, \tag{3.2}$$

where D_i and $\overline{D}_i$ are the actual PGA or PGV demand at the i^{th} site and its prediction by the GMPE, respectively (Lim and Song 2012).

To consider uncertainties in the spatial distribution of the seismic demands, researchers including Goda and Hong (2008) suggested models for correlation coefficient between residuals at the i^{th} and j^{th} site. The correlation coefficient between ε_i and ε_j is often expressed as a function of the distance Δ_{ij} between the two sites. From Eq. (3.2), the correlation between $\ln D_i$ and $\ln D_j$, i.e., $\rho_{\ln D_i \ln D_j}(\Delta_{ij})$, is derived in terms of characteristics of inter-event residual (σ_η), intra-event residual (σ_ε), and distance Δ_{ij}, that is,

$$\rho_{\ln D_i \ln D_j}(\Delta_{ij}) = \frac{\sigma_\eta^2 + \rho_{\varepsilon_i \varepsilon_j}(\Delta_{ij})\sigma_\varepsilon^2}{\sigma_\eta^2 + \sigma_\varepsilon^2}. \tag{3.3}$$

The attenuation relation model in Boore and Akinseen (2008) is adopted to predict the natural logarithm of the PGA demand at the i^{th} component as

$$\begin{aligned} \ln \overline{PGA}_i = &-0.5265 - 0.0115\sqrt{R_i^2 + 1.35^2} \\ &+ \ln\left(R_i^2 + 1.35^2\right)[-0.3303 + 0.0599(M_w - 4.5)], \end{aligned} \tag{3.4}$$

where M_w is the moment magnitude; and R_i is the distance between the epicenter and the i^{th} site given in km. For calculating intra-event spatial correlation, the model proposed by Goda and Hong (2008) is used, which is given as follows:

$$\rho_{\varepsilon_i \varepsilon_j}(\Delta_{ij}) = \exp\left(-0.27\Delta_{ij}^{0.40}\right). \tag{3.5}$$

3.2.1.2 Probability and statistical dependence of failures

Following HAZUS-MH (FEMA 2013), the uncertain limit-state capacity of the i^{th} structure, C_i, is assumed to follow a lognormal distribution with parameters $\bar{C}_i$ and ζ_i, which are the median and the lognormal standard deviation of C_i, respectively. The failure probability of the i^{th} structure in a network is then computed as

$$P(E_i) = P(C_i \leq D_i), \tag{3.6}$$

where E_i denotes the event that the i^{th} structure is closed due to serious seismic damage. The seismic damage and the limit-state capacity are assumed to be statistically independent of each other. By substituting Eq. (3.2) into Eq. (3.6), and applying the natural logarithm, the failure probability is computed as

$$P(E_i) = P(\ln C_i \le \ln D_i) = \Phi\left(\frac{\ln \bar{D}_i - \ln \bar{C}_i}{\sqrt{\zeta_i^2 + \sigma_\eta^2 + \sigma_\varepsilon^2}}\right), \tag{3.7}$$

where $\Phi(\cdot)$ denotes the cumulative distribution function (CDF) of the standard Gaussian distribution.

Next, the joint failure probability of the i^{th} and j^{th} structures is derived as

$$\begin{aligned} P(E_iE_j) &= P\left[(\ln C_i \le \ln D_i) \cap (\ln C_j \le \ln D_j)\right] \\ &= \Phi_2(-\beta_i, -\beta_j, \rho_{ij}), \end{aligned} \tag{3.8}$$

where $\Phi_2(\cdot,\cdot,\rho_{ij})$ denotes the bivariate normal CDF with zero means, unit standard deviations and the correlation coefficient ρ_{ij}; and $\beta_i = -\Phi^{-1}[P(E_i)]$ and $\beta_j = -\Phi^{-1}[P(E_j)]$ are the generalized reliability indices, which can be computed from Eq. (3.7). The correlation coefficient between safety factors, ρ_{ij} is also derived as

$$\begin{aligned} \rho_{ij} &= \frac{\zeta_i\zeta_j\delta_{ij} + (\sigma_\eta^2 + \sigma_\varepsilon^2)\rho_{\ln D_i \ln D_j}(\Delta_{ij})}{\sqrt{\zeta_i^2 + \sigma_\eta^2 + \sigma_\varepsilon^2}\sqrt{\zeta_j^2 + \sigma_\eta^2 + \sigma_\varepsilon^2}} \\ &= \frac{\zeta_i\zeta_j\delta_{ij} + \sigma_\eta^2 + \rho_{\varepsilon_i\varepsilon_j}(\Delta_{ij})\sigma_\varepsilon^2}{\sqrt{\zeta_i^2 + \sigma_\eta^2 + \sigma_\varepsilon^2}\sqrt{\zeta_j^2 + \sigma_\eta^2 + \sigma_\varepsilon^2}}, \end{aligned} \tag{3.9}$$

where δ_{ij} is the Kronecker delta, which is 1 if $i = j$, and 0 otherwise. This derivation of the correlation coefficients not only dramatically shortens the computation time compared to the numerical methodology, but also ensures the accuracy. When the limit-state capacity follows a distribution other than lognormal distribution, the correlation coefficient ρ_{ij} should be calculated using a numerical method, which may decrease efficiency. Since the failure probability of each structure can be represented by the CDF of the standard Gaussian distribution, the

probability of the disjoint link set or cut set can be computed by a multivariate normal CDF algorithm such as a dimension reduction scheme (Kang and Song 2010) or quasi-Monte Carlo simulation (Genz 1992).

3.2.2 Recursive decomposition algorithm (RDA)

A network can be considered as a graph $G = (\boldsymbol{N}, \boldsymbol{E})$ where $\boldsymbol{N}$ and $\boldsymbol{E}$ denote the sets of the nodes and edges, respectively. In the graph, the set $\boldsymbol{N}$ is composed of the nodes representing both node-type and line-type components, while the set $\boldsymbol{E}$ consists of edges connecting the node-type and line-type elements in the given network. In the numerical examples in Section 3.4, only the failures of node-type elements, e.g., bridges, are considered while the line-type elements are assumed to be undamaged.

Consider a network consisting of nodes including two terminal nodes, which is represented by a graph G. After a natural or human-made disaster occurs, the node pair may remain connected or disconnected from each other. Suppose each component also has a binary state: operative or failed. To express the origin-destination (OD) connectivity in terms of the states of components, a 'structure function' $\Psi(G)$ and 'node functions' $a_i,\ i = 1, \dots, n,$ i.e., Bernoulli random variables representing the connectivity of the graph G and the state of the i^{th} component respectively, are introduced as follows:

$$\Psi(G) = \begin{cases} 1, & \text{if OD pair is connected,} \\ 0, & \text{if OD pair is disconnected,} \end{cases} \tag{3.10}$$

$$a_i = \begin{cases} 1, & \text{if } i^{\text{th}} \text{ component operates,} \\ 0, & \text{if } i^{\text{th}} \text{ component fails.} \end{cases} \tag{3.11}$$

To represent the structure function $\Psi(G)$ of a given network as a linear function of node functions a_i, the recursive decomposition algorithm (RDA) (Li and He 2002) identifies disjoint link sets and cut sets by the following procedure, which is illustrated in Figure 3.1. Since the structure function $\Psi(G)$ will be decomposed according to the Boolean operation laws in RDA, it is difficult to deal with networks with components having more than two states without generalization of the formulation.

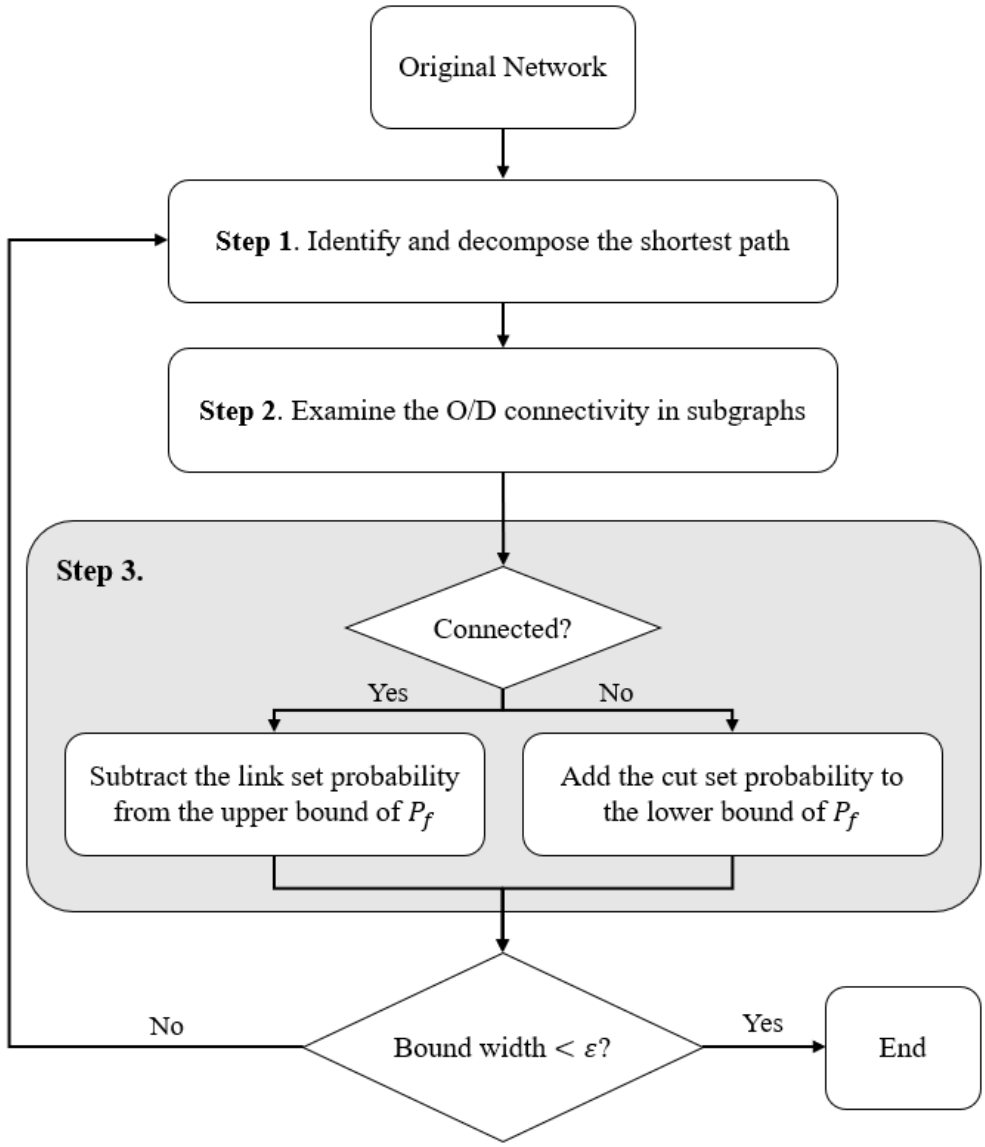

Figure 3.1. Flowchart of recursive decomposition algorithm

3.2.2.1 Step 1: Identification of shortest paths for network decomposition

Consider the Bernoulli random variable for the shortest path between OD nodes $L_1 = a_1 a_2 \dots a_n$, which is equal to the product of node functions a_i, $i = 1, \dots, n$, constituting the shortest path. Then, the structure function $\Psi(G)$ is expressed as

$$\Psi(G) = a_1 a_2 \dots a_n \Psi(G) + \overline{(a_1 a_2 \dots a_n)} \Psi(G), \tag{3.12}$$

where $\bar{a}_i$ is equal to $1 - a_i$. According to the Boolean operation laws, Eq. (3.12) is expanded as a linear function of node functions and structure functions of subgraphs in ascending order of component numbering as

$$\begin{aligned} \Psi(G) &= a_1 a_2 \dots a_n \Psi(G) + \overline{(a_1 a_2 \dots a_n)} \Psi(G) \\ &= a_1 a_2 \dots a_n + \bar{a}_1 \Psi(G_1) + a_1 \bar{a}_2 \Psi(G_2) + \cdots \\ &\quad + a_1 a_2 \cdots a_{n-1} \bar{a}_n \Psi(G_n), \end{aligned} \tag{3.13}$$

where G_i represents the subgraph of G, obtained by removing the i^{th} node in the link set L_1 from the original graph G.

3.2.2.2 Step 2: Examination of OD connectivity in subgraphs

Even if the reliability of each component is known, the structure function $\Psi(G)$ cannot be accurately assessed due to structure functions of some subgraphs on the right-hand side in Eq. (3.13). To define all these terms as the product of node functions or a constant, it is necessary to investigate whether the OD pair is connected in each subgraph. The selection of subgraphs to explore the OD connectivity follows a breadth-first search (BFS) (Ahuza *et al*. 1993; Cormen *et al*. 2009) ordering, which gives a priority to the existing subgraphs. If the OD pair is disconnected in the subgraph G_i, $\Psi(G_i)$ will be zero and its coefficient

$a_1 a_2 \cdots a_{i-1} \bar{a}_i$ will be classified as the Bernoulli random variable for a disjoint cut set C_{n_c+1}, where n_c represents the number of disjoint cut sets found so far. On the contrary, if the OD pair is still connected in the subgraph G_i, the subgraph G_i will be saved separately, and in Step 1 of the subsequent iteration, the shortest path will be searched among the stored subgraphs.

3.2.2.3 Step 3: Calculating bounds on network reliability

In a simple network, one can identify all disjoint link sets and cut sets, and evaluate the exact network reliability R or network failure probability P_f using all disjoint link sets or cut sets, respectively. If all disjoint link sets between the OD node L_i, $i = 1, \dots, N_L$, are identified, the network reliability R, i.e., the probability that the structure function $\Psi(G)$ is equal to 1, is calculated as

$$R = P[\Psi(G) = 1] = P\left(\bigcup_{i=1}^{N_L} L_i\right) = \sum_{i=1}^{N_L} P(L_i). \tag{3.14}$$

On the other hand, the network failure probability P_f can be obtained by summing up the probabilities of all disjoint cut sets C_i, $i = 1, \dots, N_C$, i.e.

$$P_f = P[\Psi(G) = 0] = P\left(\bigcup_{i=1}^{N_C} C_i\right) = \sum_{i=1}^{N_C} P(C_i). \tag{3.15}$$

In a large-scale complex network, however, many disjoint link sets and cut sets could make it intractable to assess the exact network reliability or failure probability due to the exorbitant memory or computation time required. In this case, one can alternatively compute the bounds on the network reliability or failure probability using a set of the identified disjoint link sets and cut sets, i.e.,

$$\sum_{i=1}^{n_L} P(L_i) \le R \le 1 - \sum_{i=1}^{n_C} P(C_i), \tag{3.16a}$$

$$\sum_{i=1}^{n_C} P(C_i) \le P_f \le 1 - \sum_{i=1}^{n_L} P(L_i), \tag{3.16b}$$

where n_L and n_c are the numbers of identified disjoint link sets and cut sets, respectively. From either Eq. (3.16a) or (3.16b), the bound width ΔB can be computed as

$$\Delta B = 1 - \sum_{i=1}^{n_L} P(L_i) - \sum_{i=1}^{n_C} P(C_i). \tag{3.17}$$

Steps 1 to 3 are repeated until the bound width ΔB becomes smaller than the target width. During iterations, the Bernoulli random variable for shortest path between the OD pair within the subgraph G_k is represented as $L' = a'_1 a'_2 \dots a'_m$, and its structure function $\Psi(G_k)$ is expanded recursively in Step 1, i.e.,

$$\begin{aligned} \Psi(G_k) = a'_1 a'_2 \dots a'_m + \bar{a}'_1 \Psi\left(G_{1,k}\right) + a'_1 \bar{a}'_2 \Psi\left(G_{2,k}\right) + \cdots \\ + a'_1 a'_2 \cdots a'_{m-1} \bar{a}'_m \Psi\left(G_{m,k}\right), \end{aligned} \tag{3.18}$$

where $G_{i,k}$ represents the second-order subgraph of G, obtained by removing the i^{th} node from the subgraph G_k. The constant term $(a_1 a_2 \cdots a_{k-1} \bar{a}_k) \times (a'_1 a'_2 \dots a'_m)$ newly created by substituting Eq. (3.18) into Eq. (3.13) is the Bernoulli random variable for a disjoint link set L_{n_L+1}, where n_L represents the number of disjoint link sets discovered until the current iteration.

3.2.3 Selective RDA (S-RDA)

To achieve faster convergence of the bounds in Eq. (3.16a) or (3.16b), selective RDA (S-RDA) was proposed to make improvements in two aspects: (1) selective

identification of *critical* disjoint link sets and cut sets, and (2) decomposition of subgraphs indicating the highest likelihood (Lim and Song 2012). These improvements are applied to Step 1 of the original RDA as described below. The methods of examining the OD connectivity and calculating the bounds on the network reliability are the same as those described in Steps 2 and 3.

On the other hand, there is a difference in Step 1: S-RDA identifies the most reliable paths instead of the shortest paths. Because each reliable path has a higher probability than the shortest path, S-RDA can reduce the bound width more rapidly than the original RDA. To find the link sets with the highest probability of survival, a modified Dijkstra's algorithm (Ahuza *et al.* 1993; Cormen *et al.* 2009) is utilized instead of BFS. For quick calculations in Step 1, statistical dependence between component failures is ignored. That is, the reliability of each link set is estimated as the product of the reliability estimates of the components in the link set while identifying the paths. The statistical dependence is fully considered when calculating the bounds in Step 3.

There is another difference in the selection of a subgraph to decompose. In the original RDA, subgraphs are selected following the component ordering choice. In contrast, S-RDA decomposes subgraphs with the highest likelihood of survival or failure first. This facilitates the convergence of the bounds computed by S-RDA.

3.3 Centrality-based network simplification and NRA

Despite the merits and technical advances discussed above, the applicability of RDA and S-RDA are still limited due to the large computation time and memory required for complex infrastructure networks. To further expedite the convergence of the

bounds, this chapter proposes a centrality-based selective RDA (CS-RDA), which singles out the *critical nodes* whose failures can cause the disconnection between the OD pair from network topology viewpoint. This section first reviews network centrality measures and introduces CS-RDA for efficient network reliability analysis based on BC. In addition, for an efficient clustering-based multi-scale approach, a network simplification method is proposed based on edge-centrality.

3.3.1 Network centrality measures

Evaluating the impact of each component on network performance is essential in analysis and management of a network. Various network centrality indices have been developed to quantify node importance in a network and modified to investigate influential people in social networks, key nodes on the Internet, and super-spreaders of diseases (Özgür *et al.* 2008). In this section, three major network centrality indices are reviewed: (1) degree centrality, (2) closeness centrality, and (3) betweenness centrality.

First, degree centrality of a node is defined as the number of its neighboring nodes (Nieminen 1974). The definition is based on the presumption that the more nodes are connected to a given node, the greater impact the node tends to make on the whole network. Using the adjacency matrix A, whose element A_{ij} takes 1 if there is an edge from node i to node j, and 0 otherwise, the degree centrality of the i^{th} node, $C_D(i)$, is calculated as

$$C_D(i) = \sum_{j \neq i} A_{ij}. \tag{3.19}$$

Second, closeness centrality of a node is defined as the average distance of the

shortest paths to the other nodes in the network (Beauchamp 1965). On this account, the distances of all edges in the network should be defined to find the shortest path. It is noted that the directivity of edges can lead to completely different results. For example, a famous person in a social network tends to have high closeness centrality from incoming edges, but low closeness centrality from outgoing edges. The closeness centrality of the i^{th} node, $C_C(i)$, is defined as

$$C_C(i) = \frac{N_n}{\sum_{j \neq i} d_{ij}}, \tag{3.20}$$

where N_n is the number of nodes in the given network; and d_{ij} represents the shortest distance between node i and node j, which will be replaced by the probability of the most reliable path between the two nodes later in this chapter.

Finally, betweenness centrality quantifies the importance of a given node in terms of the proportion of shortest paths passing through the node (Freeman 1977). While the closeness centrality concentrates on the lengths of the shortest paths starting from or ending at a given node, betweenness centrality focuses on how often the shortest paths between all OD pairs in the network go through the node. In detail, the betweenness centrality of the i^{th} node, $C_B(i)$, is given as

$$C_B(i) = \sum_{s \neq i} \sum_{t \neq s,i} \frac{v_i(s,t)}{v(s,t)}, \tag{3.21}$$

where $v(s,t)$ is the number of shortest paths between node s and node t; and $v_i(s,t)$ is the number of those passing through node i. Later in this chapter, $v(s,t)$ and $v_i(s,t)$ will be substituted with the number of the most reliable paths between node s and node t, and the number of those via node i, respectively.

3.3.2 Network simplification using edge-centrality

As the number of disjoint sets within the network increases exponentially, the accuracy of calculating the probability of each disjoint set may get worse because the computational errors caused by the high-dimensional calculation may accumulate.

To overcome the computational limitation, the idea of network simplification via clustering has been explored (Gómez *et al.* 2013; Lim *et al.* 2015). The network simplification methods aim to minimize the computational complexity of network analysis while preserving information on each component and network topology. However, for large-size networks, simplification by a spectral clustering algorithm (Lim *et al.* 2015) still entails a prominent level of computational complexity, which makes the approach infeasible. To overcome the computational limitation of the existing method at a slight expense of accuracy, the following section proposes a clustering algorithm using edge-betweenness. A network modelling framework is also introduced to describe the simplified network (Lim *et al.* 2015) in terms of the clusters identified by the proposed algorithm.

3.3.2.1 Edge-betweenness algorithm

Modularity is one of the network descriptors often used for measuring the goodness of a given clustering choice (Newman and Girvan 2004). To be more specific, modularity Q is defined as the normalized difference between the actual and the expected numbers of the edges connecting a pair of nodes both of which are currently located in the same cluster, i.e.,

$$Q = \frac{1}{2m}\sum_i \sum_j \left\{ [A_{ij} - 2mp_i p_j]\delta_{c_i c_j} \right\}, \tag{3.22}$$

where $m = \frac{1}{2}\sum_i \sum_j A_{ij}$ is the total number of the edges in the network; p_i represents the likelihood that an edge is connected to the i^{th} node after the network edges are re-distributed randomly while keeping the degree centralities of individual nodes and total number of edges unchanged; and $\delta_{c_i c_j}$ is the Kronecker delta, which gives 1 if both the i^{th} and j^{th} nodes belong to the same cluster, and 0 otherwise. Since p_i is derived as $C_D(i)/2m$, the modularity can be described in terms of degree centralities as

$$Q = \frac{1}{2m}\sum_i \sum_j \left\{ \left[A_{ij} - \frac{C_D(i)C_D(j)}{2m} \right] \delta_{c_i c_j} \right\}. \tag{3.23}$$

Although it is NP-hard to find the network clustering choice maximizing the modularity (Brandes *et al.* 2007), it is known that a heuristic edge-betweenness algorithm, called the Girvan-Newman algorithm, can provide remarkable and swift solutions (Newman and Girvan 2004). The edge-betweenness algorithm detects clusters in a network by progressively removing the edges with the highest edge-betweenness, whose definition is almost identical to the BC used in Section 3.3.1. The edge-betweenness aims to measure how often an edge, instead of a node, lies on the shortest path between each pair of nodes in the network. The detected edges with the highest edge-betweenness are removed until the modularity Q has the maximum value. At this time, the edges that have been eliminated but cannot detach clusters are restored. This algorithm can be further extended to the multi-scale approach by deeming each detected cluster as a super-node in the upper level of clustering.

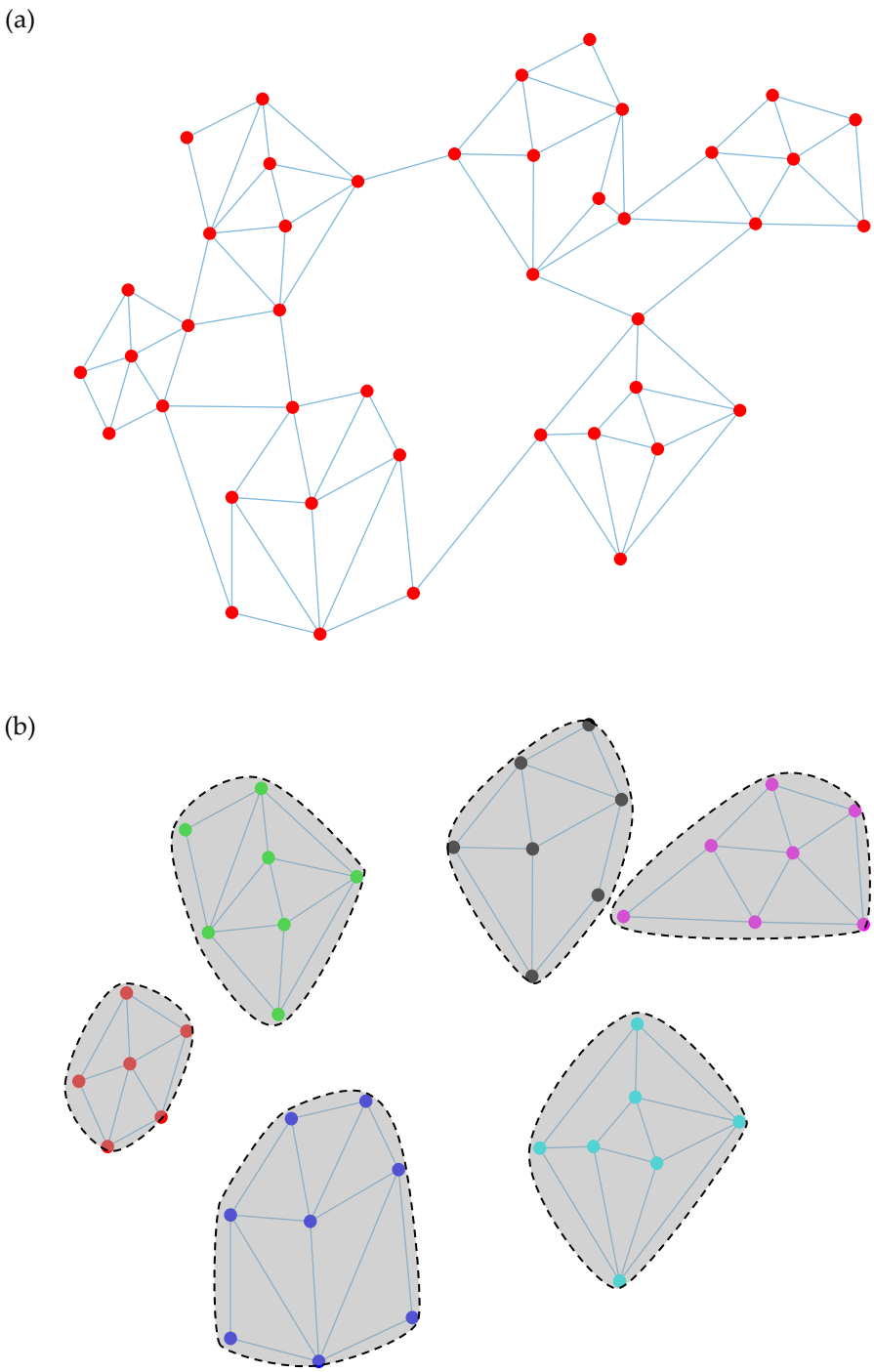

Figure 3.2. Hypothetical network example: (a) original topology, and (b) clusters identified using edge-betweenness algorithm

Table 3.1 Modularity and number of clusters by edge-betweenness algorithm

No. of eliminated edges	0	5	10	**15**	20	25
Modularity	0	0.476	0.642	**0.675**	0.631	0.578
No. of clusters	1	2	4	**6**	8	10

For example, let us consider a hypothetical network in Figure 3.2(a), which has 42 nodes (red dots) and 85 bi-directional edges. The modularity of the network shows the maximum value when the network is divided into 6 clusters (gray facets in black dashed lines in Figure 3.2(b)) by the edge-betweenness algorithm. Table 3.1 shows that the more edges are removed, the more clusters are formed, whereas the modularity tends to decrease as more than 15 edges are removed.

3.3.2.2 Representation of simplified network

Using the identified clusters, one can obtain a simplified representation of the network in terms of super-components such as inter-cluster edges, inter-cluster nodes, and super-edges (Lim *et al.* 2015). Inter-cluster edges refer to those connecting different clusters (thick red lines in Figure 3.3) while inter-cluster nodes are the those connected with each other by inter-cluster edges (blue dots in Figure 3.3). Super-edges (thick gray lines in Figure 3.3) are virtual edges that stand for connectivity between inter-cluster nodes within the same cluster. The reliability of a super-edge is defined as the probability that the corresponding inter-cluster nodes lose their connectivity, while the reliability of an inter-cluster node is the same as that of the corresponding actual node. To represent the simplified network following a 'node-weighted' network modelling approach that constructs a graph with only node weights, the virtual 'edge node' is introduced at the midpoint of each super-edge (Lim and Song 2012). There are three methods of evaluating the reliability of super-

edges depending on the number of OD nodes included in the cluster, which were detailed by Lim *et al.* (2015).

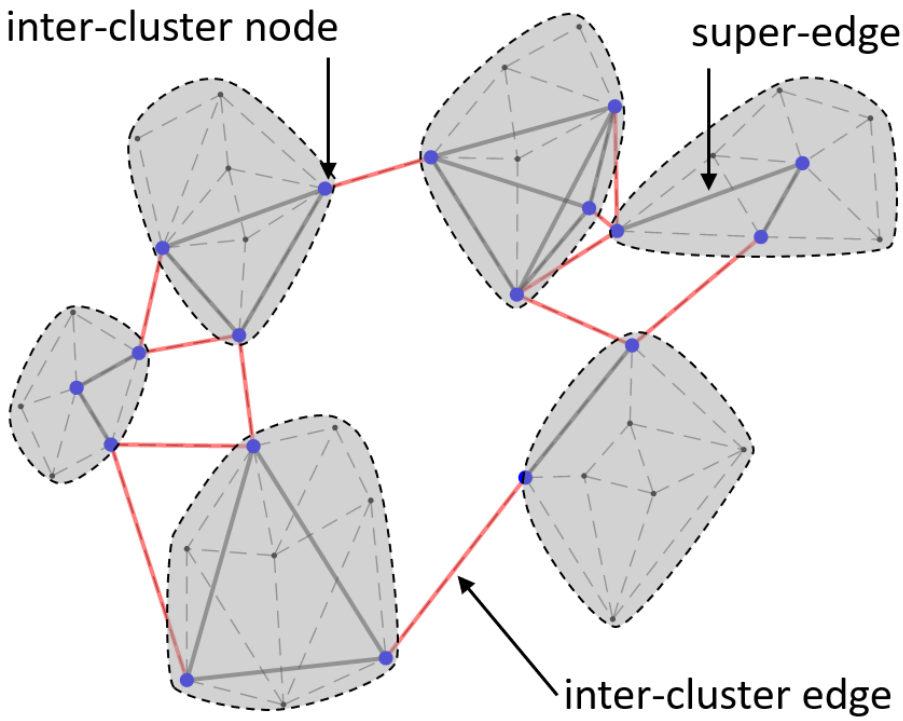

Figure 3.3. Representation of simplified hypothetical network using super-components

3.3.3 Centrality-based selective RDA (CS-RDA)

This section proposes a new selective recursive decomposition algorithm based on the network centrality concept. Whereas S-RDA prioritizes paths and subgraphs in terms of their potential contributions to the reduction of the probability bound width ΔB in Eq. (3.17), the proposed algorithm termed 'centrality-based selective RDA' (CS-RDA) additionally focuses on critical nodes whose removals would make maximum effects on the OD connectivity from the network topology viewpoint. In detail, the critical nodes are defined as those whose removals would minimize the

number of branches in the following network decomposition process, e.g., the OD nodes themselves. The algorithm identifies nodes with higher centrality as critical ones based on the observations that the removal of nodes with high centrality accelerates network disconnection compared to the removals of randomly selected nodes (Petreska *et al.* 2010). To incorporate the proposed idea of using network centrality into the algorithm, the following process is added to Step 1 of S-RDA: the components in the identified critical disjoint link set are sorted in descending order of network centrality before decomposing them as shown in Eq. (3.21). This process enables the algorithm to decompose the graph into the smaller number of link sets and cut sets having high probabilities. The performance of CS-RDA naturally relies on the choice of the network centrality.

One can compare the performance of CS-RDA with different types of centrality in network examples. In addition to the three centralities introduced in Section 3.3.1, the commonly used 'eigenvector centrality' and 'PageRank centrality' are also tested. Assuming that all components in the hypothetical network in Figures 3.2 and 3.3 have a failure probability of 3%, and that the correlation coefficients between them are 5%, the bounds of network failure probability and bound widths for each centrality are shown in Figure 3.4(a) and (b). Table 3.2 shows the number of disjoint sets for each centrality required to achieve the bound width of 0.1%. CS-RDA with BC converges most efficiently across all the network centralities, and this behavior is commonly observed in other networks (Cetinay *et al.* 2018).

However, CS-RDA might have a critical disadvantage for networks in which the centralities of the OD nodes are extremely low. For example, Figure 3.5 shows the Eastern Massachusetts highway network (Zhang *et al.* 2018), and the colors

represent BC of each component. It is noted that BCs of the OD nodes are exactly zero. In this case, the failures of the OD nodes related directly to the disconnection of the OD pair can be found later in the process, which makes the performance of CS-RDA identical to that of S-RDA or even worse. To overcome this, one can assign virtual nodes to each OD node. Connections among the virtual nodes that are introduced to the same OD node increase the centralities of the OD nodes while connections between virtual nodes connected to different OD nodes increase centralities of nodes included in the most reliable path. The process to determine the number of virtual nodes involves a trade-off between the computational cost of network centrality and the improvement in efficiency of network reliability analysis. The optimal number of virtual nodes depends on the network size and the location of the OD pair. In this algorithm, the diameter of the network, i.e., the maximum of the shortest path lengths, is set to the number of virtual nodes based on the experience of the authors. The link sets and cut sets identified by the abovementioned process lead to a smaller number of components having higher probabilities than those by S-RDA, which make the convergence of the bounds faster.

Table 3.2. Modularity and number of clusters by edge-betweenness algorithm

Centrality	S-RDA	Between ness	Closeness	Degree	Eigen-vector	Pagerank
Required disjoint sets	231,174	48,244	51,684	53,407	56,306	81,818

(a)

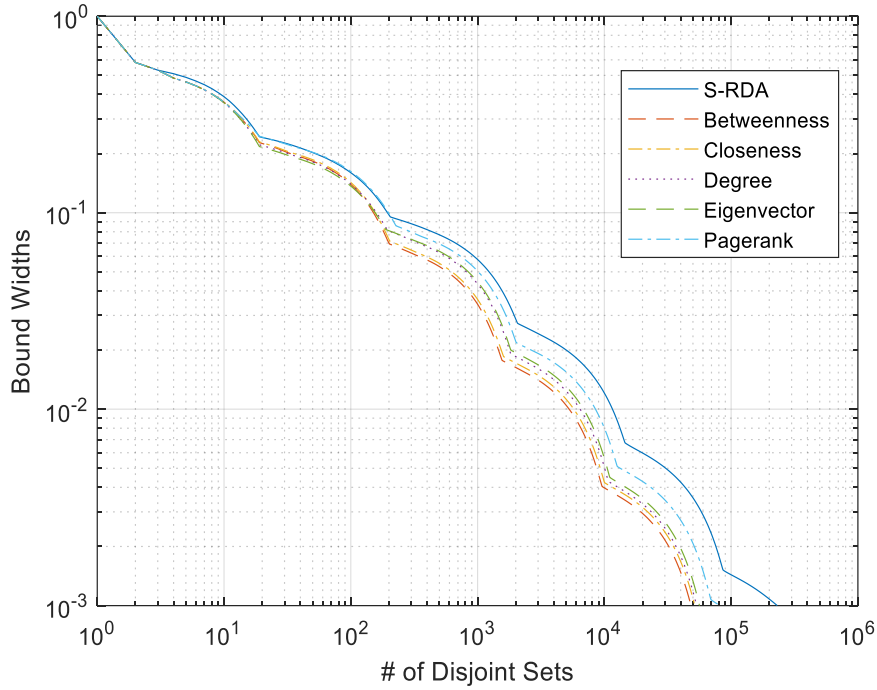

(b)

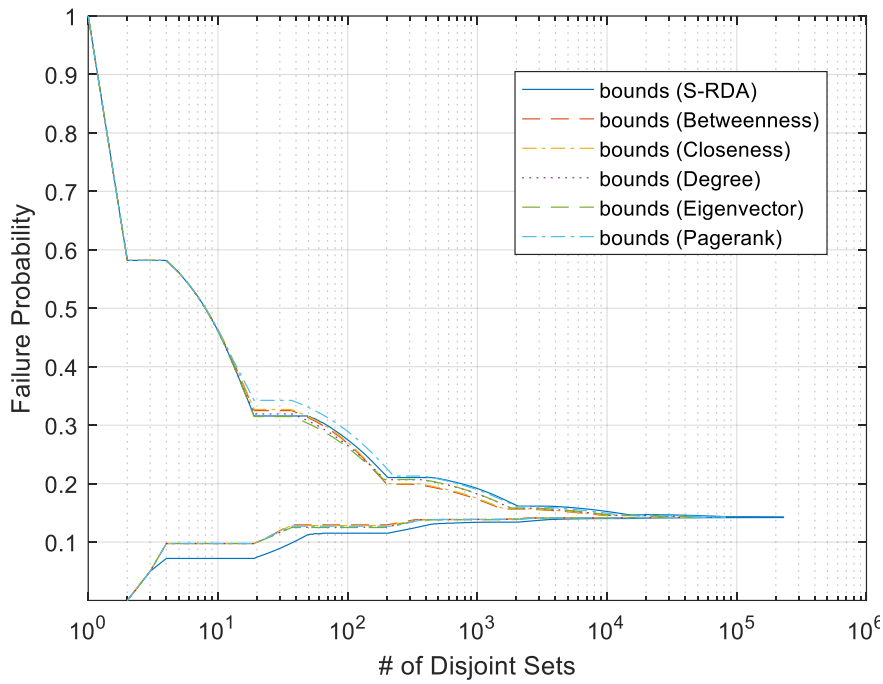

Figure 3.4. Performance of CS-RDA with different centralities: (a) bound widths, and (b) bounds on the network failure.

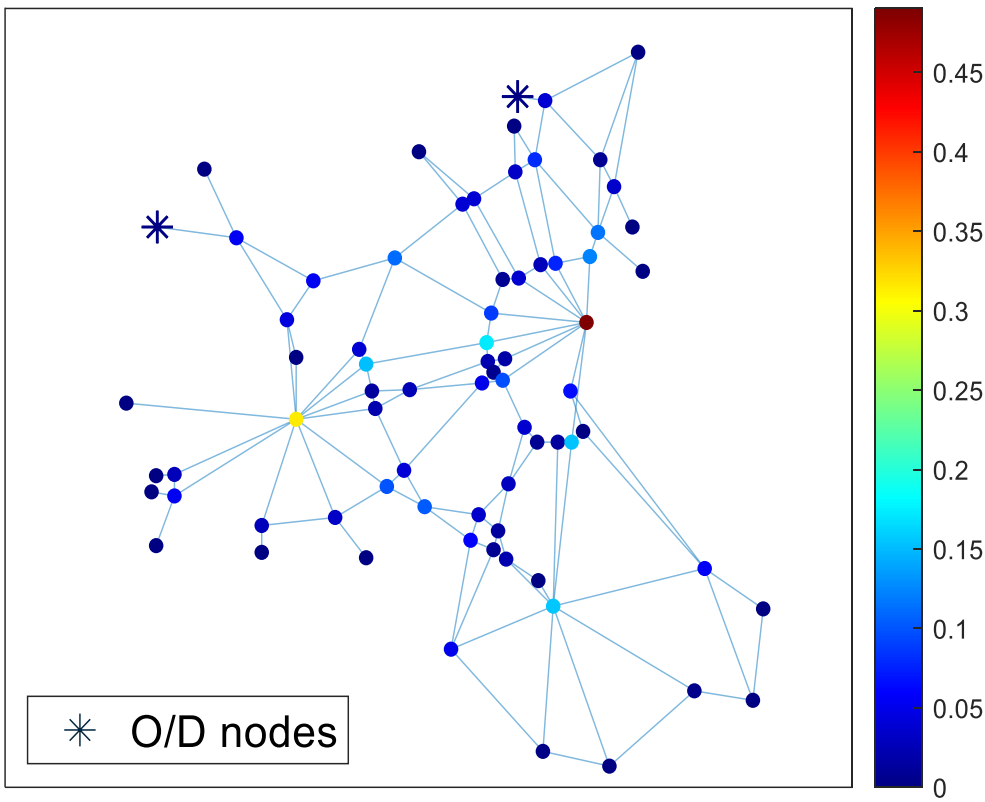

Figure 3.5. Example of OD nodes with low BC: Eastern Massachusetts highway network

For details of CS-RDA, let us consider a simple network reliability assessment example in Figure 3.6, where the surviving nodes and failed nodes in (sub)graphs are represented by thick gray circles and orange dotted circles, respectively. The analysis examines the connectivity between the origin node 1 and destination node 5. It is assumed that the reliability of node 3 is 0.8, the reliability of the other nodes is 0.9, and their failure events are statistically independent of each other. In the original RDA and S-RDA, the Bernoulli random variable for the most reliable path L_1 between the OD pair is represented as the product of the node functions constituting the path, that is, $L_1 = a_1 a_2 a_4 a_5$ (see Figure 3.6(a)). On the other hand, as shown in Figure 3.6(b), CS-RDA rearranges the node functions in L_1 in the descending order of BC so that $L_1 = a_1 a_5 a_4 a_2$ (after 4 virtual nodes are attached to each of the OD nodes following the aforementioned recommendation regarding the number of virtual nodes). The re-ordering affects the network decomposition in Eq. (3.13). Figure 3.6 shows four subgraphs originating from the identified link set L_1 for each approach. In the results by CS-RDA, the first three subgraphs are identified as disjoint cut sets, and only the last one is recognized as a disjoint link set $L_2 = a_1 a_5 a_4 \bar{a}_2 a_3$. The subsequent decomposition of the path L_2 leads to a disjoint cut set $C_4 = a_1 a_5 a_4 \bar{a}_2 \bar{a}_3$. The algorithm is then terminated because no more paths are available. As a result, the network reliability is calculated as 0.714 according to Eq. (3.14), i.e., by summing the probabilities of the identified link sets L_1 and L_2. While existing RDAs enumerate at least 8 disjoint sets (Figure 3.6(a)), CS-RDA can complete the network decomposition by 6 disjoint sets (Figure 3.6(b)). This disparity in the number of disjoint sets increases exponentially as the network size increases.

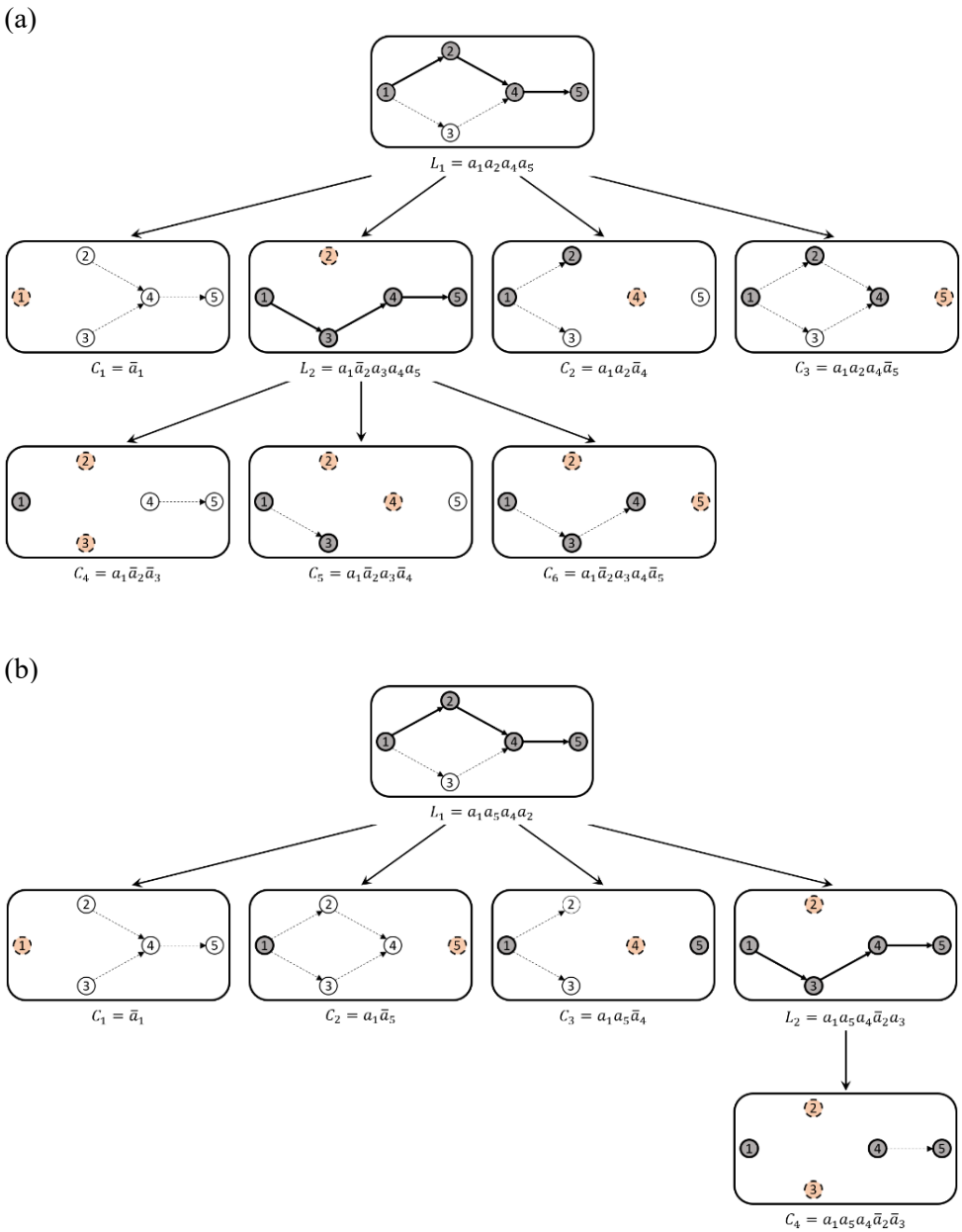

Figure 3.6. Decomposition of an example network by (a) existing RDAs, and (b) CS-RDA

A simplified network identified by a multi-scale analysis approach has a significantly reduced number of components compared to the original network. On the other hand, the approach may introduce a new challenge in calculating the failure probability and the statistical dependence of super-components, especially super-edges within the simplified network. When the i^{th} and j^{th} super-components are inter-cluster nodes, the failure probabilities $P(E_i)$ and $P(E_j)$, and the correlation coefficient ρ_{ij} are equal to those in Eqs. (3.7) and (3.9), respectively. However, if either or both are super-edges, one should find the correlation coefficient ρ_{ij} describing the statistical dependence between two super-components numerically, which may result in extremely complex and time-consuming calculations.

The failure probability of the i^{th} super-edge is assessed using CS-RDA by setting the nodes at both ends of the super-edge to the OD pair and expressed as

$$P(E_i) = \mathrm{P}\left(\bigcup_{k=1}^{n_C^i} C_k^{E_i}\right) = \sum_{k=1}^{n_C^i} P\left(C_k^{E_i}\right), \tag{3.24}$$

where $C_k^{E_i}$ is the k^{th} disjoint cut set in the i^{th} super-edge, $k = 1, \dots, n_C^i$; and n_C^i the total number of the identified disjoint cut sets in the i^{th} super-edge. Suppose E_i and E_j represent the failure events of the i^{th} and j^{th} super-components, respectively. The joint failure probability $P(E_iE_j)$ can be computed as

$$P(E_iE_j) = \mathrm{P}\left[\left(\bigcup_{k=1}^{n_C^i} C_k^{E_i}\right) \bigcap \left(\bigcup_{l=1}^{n_C^j} C_l^{E_j}\right)\right] = \sum_{k=1}^{n_C^i}\sum_{l=1}^{n_C^j} P\left(C_k^{E_i} C_l^{E_j}\right), \tag{3.25}$$

where $C_k^{E_i}$ and $C_l^{E_j}$ are the k^{th} and l^{th} disjoint cut set identified by CS-RDA in the i^{th} and j^{th} super-components (Lim *et al.* 2015), respectively, $k = 1, \dots, n_C^i$

and $l = 1, \dots, n_C^j$.

However, in large-scale networks, the probability $P(E_i E_j)$ obtained by Eq. (3.25) is inaccurate and time-consuming due to the extremely large n_C^i and n_C^j. To enhance the efficiency and accuracy of the calculation above, $P(E_i)$ and $P(E_i E_j)$ in Eqs. (3.24) and (3.25) respectively can be calculated by sampling sufficient component failure events that satisfy Eqs. (3.7) and (3.9). Then, one can find the correlation coefficient ρ_{ij} numerically by substituting $P(E_i)$ and $P(E_i E_j)$ obtained by the sampling into the following equation:

$$P(E_i E_j) = \Phi(-\beta_i)\Phi(-\beta_j) + \int_0^{\rho_{ij}} \varphi_2(-\beta_i, -\beta_j, \rho)\, d\rho, \tag{3.26}$$

where $\varphi_2(\cdot,\cdot,\rho)$ is the joint probability density function of the bi-variate standard Gaussian distribution with a correlation coefficient ρ. While the number of iterations of Eq. (3.26) increases in proportion to the square of the number of super-components, the individual computation time is proportional to the cluster diameter, resulting in a trade-off between the calculation of correlations and the reliability analysis of the simplified network. In general, the rate of increase in the number of super-components exceeds that of cluster diameters, which implies that the higher the analysis scale is, the shorter the total computation time becomes.

3.3.4 Conditional probability-based importance measure

In efforts to establish an efficient and cost-effective maintenance planning for infrastructure networks, it is helpful to identify components making critical contributions to network reliability based on topological importance and component failure probabilities (i.e., structural vulnerability). To quantify and rank the contributions of components to a network, various component importance measures (Henley and Kumamoto 1981; Der Kiureghian *et al.* 2007; Song and Kang 2009) have been proposed, and CPIM is utilized in this section. The network failure probability $P(E_{net})$ and joint probability $P(E_i E_{net})$ in Eq. (2.4) can be computed by $\sum_{j=1}^{n_C} P(C_j)$ and $\sum_{j=1}^{n_C} P(E_i C_j)$ from Eq. (3.15) through CS-RDA, respectively, under the assumption that the bound width of CS-RDA is negligible (Lim and Song 2012).

3.4 Numerical examples

Three numerical examples are presented to demonstrate the proposed CS-RDA and multi-scale analysis approach based on the edge-betweenness algorithm: the hypothetical network shown in Figure 3.5, a highway bridge network in San Jose, CA (modified from Nabian and Meidani (2018)), and a highway bridge network in San Diego, CA. The computation times reported hereinafter are based on the use of MATLAB® on a personal computer with AMD Ryzen 5 3600 3.60 GHz CPU and 16GB RAM.

To compare the performance of existing algorithms with that of the proposed algorithm, the number of disjoint sets and the computation time required to achieve the target bound width are presented. Subsequently, it is discussed how the

computational cost and accuracy of the analysis change as the scale increases with the edge-betweenness algorithm, compared to the results of the uni-scale approach. Note that uni-scale analysis refers to original-scale network analysis, and networks that have been simplified once and twice are defined as bi-scale and tri-scale networks, respectively. Finally, the most critical components using the CPIMs are explored and compared to those with high BC to discuss the implications of network centrality.

Because of the lack of information on bridge types, the standard deviations of the inter- and intra-event residuals are assumed to be 0.265 and 0.502, respectively. The parameters of limit-state capacities C_i for all the nodes in the hypothetical network and all the bridges in the highway bridge network in San Jose, CA are assumed to be 0.85 for the median PGA, $\bar{C}_i$ (g), and 0.69 for the standard deviation of the natural logarithm, ζ_i. For the bridges in the highway bridge network in San Diego, CA, it is assumed to be 0.77 for $\bar{C}_i$, and 0.65 for ζ_i.

3.4.1 Example I: Hypothetical example

The hypothetical network example illustrated in Figures 3.2 and 3.3 has 42 nodes and 85 bi-directional edges (42+85×2=212 network components). Figure 3.7 shows the OD nodes and the epicenter location along with BC of each node (using colors); a red-color node has a higher BC while a blue node has a lower BC. The earthquake scenario considered has a moment magnitude $M_w = 7.0$. This network is relatively small, so the multi-scale analysis is not applied.

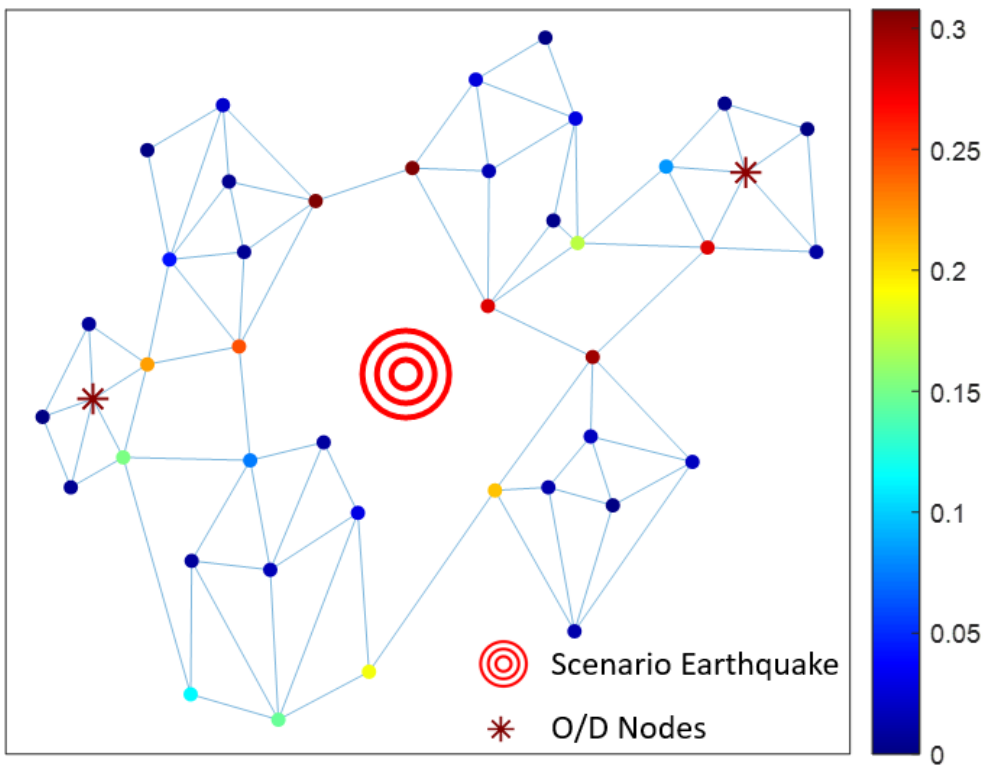

Figure 3.7. Hypothetical network example and BC of nodes

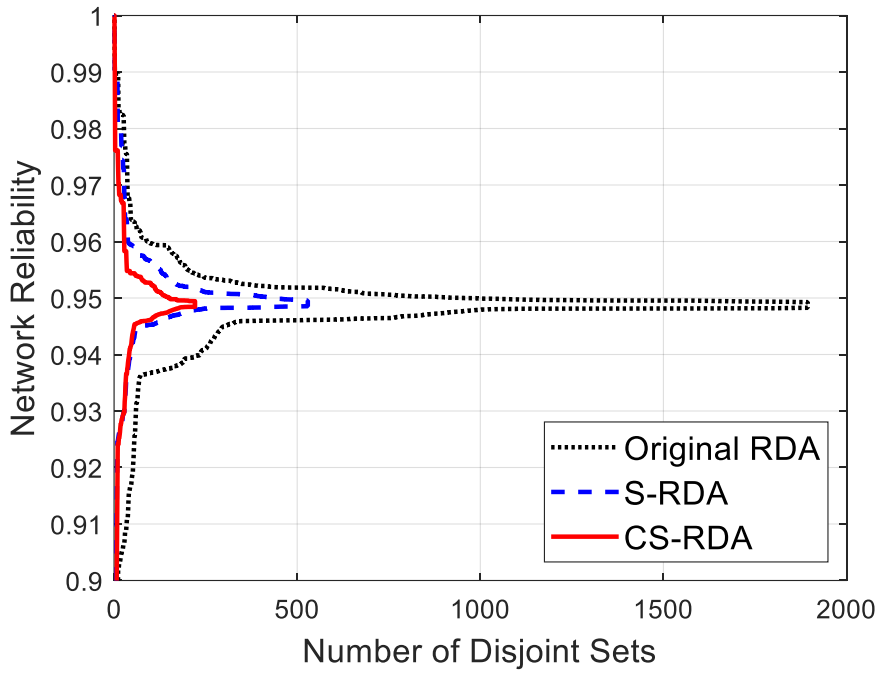

(a)

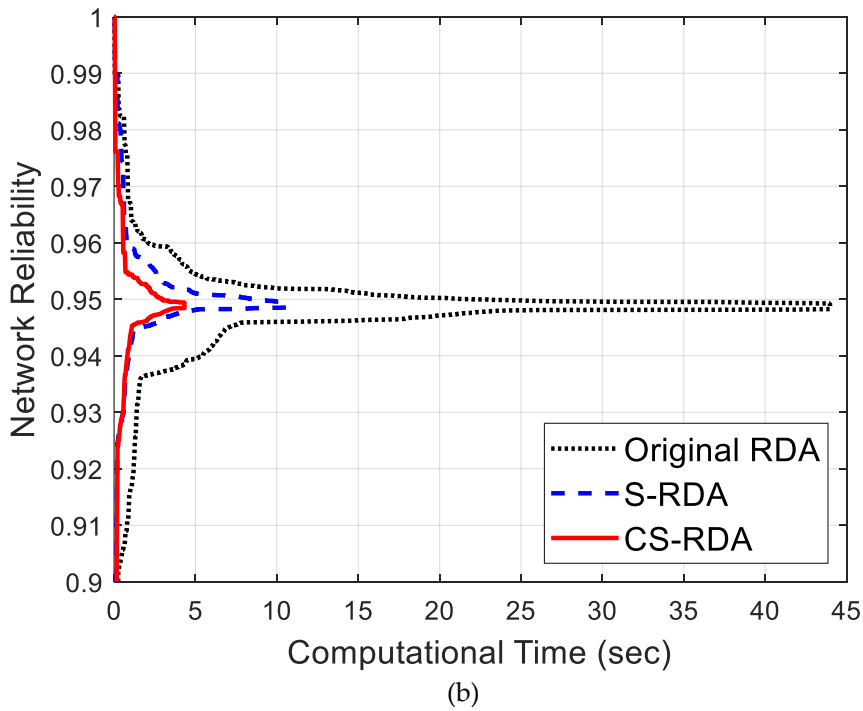

(b)

Figure 3.8. Bounds on the network reliability for the hypothetical network in terms of (a) number of disjoint sets, and (b) computation time

Table 3.3. Analysis results for hypothetical network example ($M_w = 7.0$)

Methods	P_f	# of disjoint sets	Computational time
MCS	0.0510	-	169 s
Original RDA	0.0507~0.0517	1,895	44.0 s
S-RDA	0.0505~0.0515	530	10.6 s
CS-RDA	**0.0506~0.0516**	**220**	**4.32 s**

Figure 3.8 compares the bounds on the network reliability obtained by the original RDA (Li and He 2002), S-RDA (Lim and Song 2012) and CS-RDA (Lee and Song 2021), in terms of the number of identified disjoint link sets and cut sets, and the computation time required to achieve the target bound width of 0.1%. Table 3.3 provides the results in more detail. The number of the identified disjoint sets needed for CS-RDA is only 220, which is only about 11.72% and 41.89% of that for the original RDA and S-RDA, respectively. The computation time ratios of CS-RDA to the original RDA and S-RDA are similar to the disjoint set ratios, respectively, which means that the computation time relies only on the number of disjoint sets. Even with this remarkably reduced computation time and memory for CS-RDA, the upper and lower bounds on the reliability of the given hypothetical network are close to those using existing algorithms, as well as to the value $R = 0.9490$ obtained by MCS.

Table 3.4. CPIMs, BC, and failiure probabilities of nodes with highest CPIMs in hypothetical network example

Comp ID	CPIM	CPIM Rank	BC	BC Rank	P_f	P_f Rank
8	0.274	1	0.308	1	0.047	5
42	0.271	2	0.305	3	0.014	35
22	0.266	3	0.209	10	0.065	4
5	0.258	4	0.307	2	0.044	7
Time	92.5 s		0.085 s		0.0025 s	

Table 3.4 shows the values and ranks of the CPIMs, BC (virtual nodes are still assigned to OD pairs), and failure probabilities (P_f) for the nodes with the highest CPIMs. While the highest CPIMs are not explained by the corresponding failure probabilities, their high BC complements the blind spot. The CPIMs of the three nodes (5, 8, 42) with the highest BC are ranked 1st, 2nd, and 4th. It is noteworthy that node 22 with relatively low BC has a high failure probability. This indicates that CPIM can consider both topological importance and vulnerability of components in quantifying the relative contributions of components to the network failure event. Table 3.4 also reports the computation time required to obtain the measures.

For calculating the CPIM of each node, the probabilities of the intersection of the disjoint cut sets are found by CS-RDA, and the failure event of each node should be calculated as described in Section 3.3.1. The total computational cost was 92.5 seconds. Meanwhile, it took 0.0850 seconds and 0.0025 seconds to measure the BC and failure probabilities of all nodes, respectively. For a relatively quick identification of important components from network topology viewpoint, one can use BC. If one wishes to evaluate the importance of components accurately considering both effects, CPIMs can be computed by CS-RDA.

3.4.2 Example II: San Jose highway bridge network

The San Jose highway bridge network in Figure 3.9 has 125 bridges (blue circles) and 153 bi-directional edges (solid lines), i.e., a total of 125+153×2=431 network components, which is a modified version of the network in Nabian and Meidani (2018). An earthquake event with the moment magnitude $M_w = 7.0$ is chosen, and the latitude and longitude of the epicenter shown at the lower left corner in Figure

3.9 are N35.24° and W122.05° respectively. The OD nodes (red stars) are located in the northwest and southeast. When the number of components in the target network exceeds 100, performing NRA with CS-RDA alone becomes too computationally intensive, resulting in memory and computation time issues. To address this issue, the edge-betweenness algorithm identifies nine clusters for the bi-scale analysis and two clusters for the tri-scale analysis respectively, as shown in Figures 3.10(a) and (b). The simplified network in the bi-scale analysis has 38 nodes and 70 bi-directional edges (38+70×2=178 network components), and that in the tri-scale analysis has only 14 nodes and 19 bi-directional edges (14+19×2=52 network components).

Figure 3.9. Highway bridge network in San Jose, CA

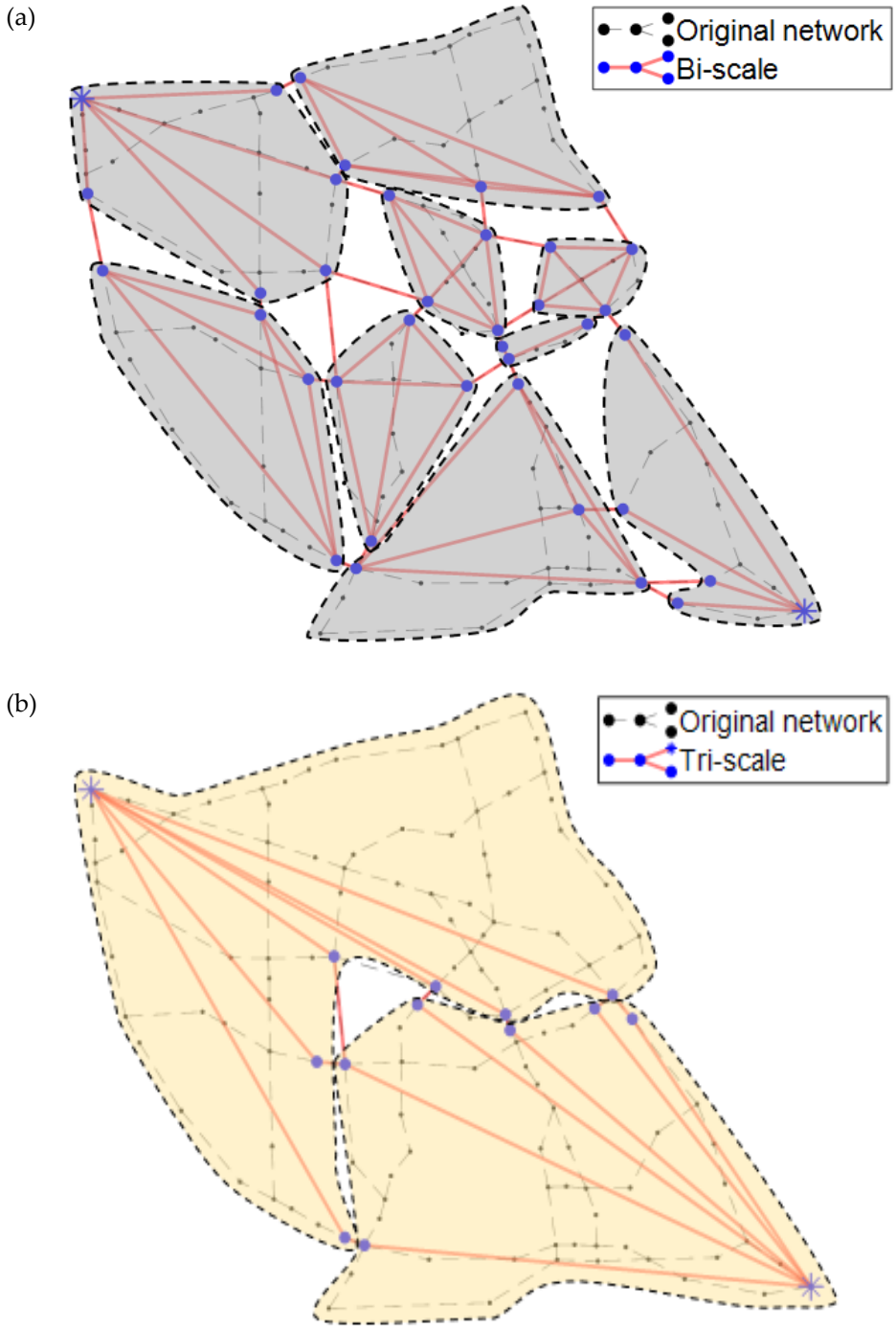

Figure 3.10. Hierarchical representation of San Jose highway bridge network example for (a) bi-scale, and (b) tri-scale analysis

(a)

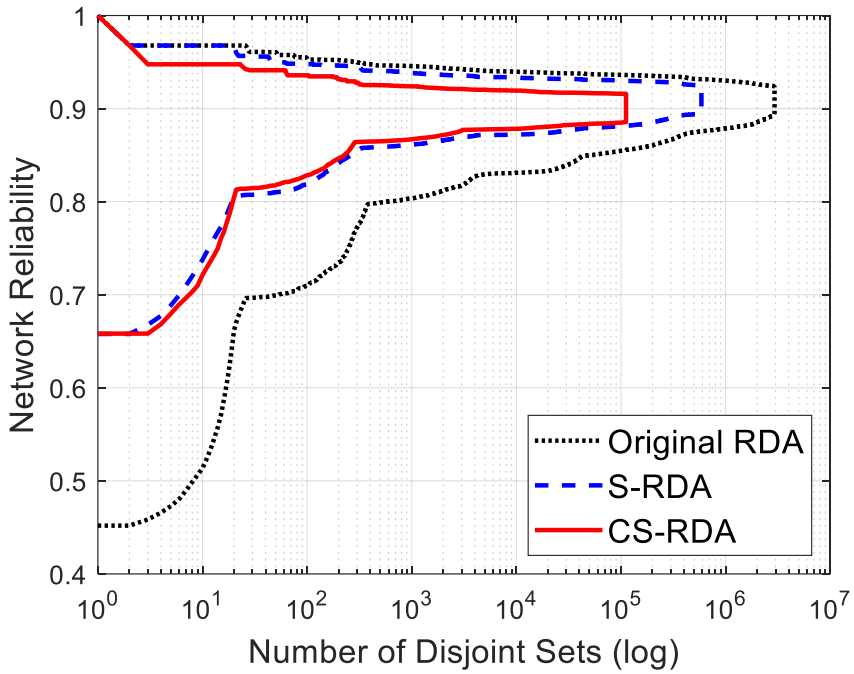

(b)

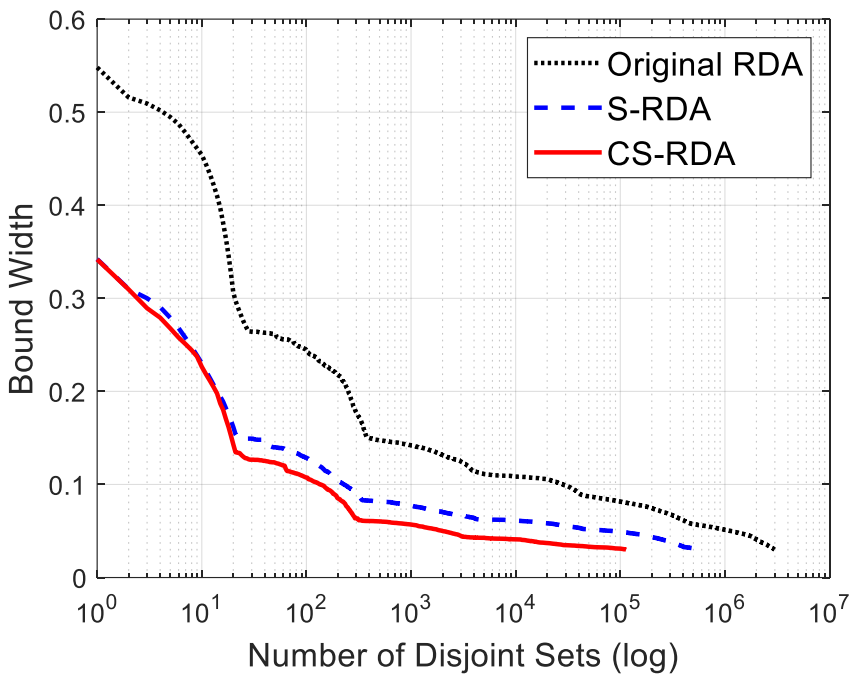

Figure 3.11. (a) Bounds on network reliability for San Jose highway bridge network, and (b) bound widths in terms of number of disjoint sets

The results in Figure 3.11 demonstrate the efficiency of CS-RDA in terms of the number of identified disjoint link sets and cut sets through comparison with the original RDA and S-RDA. The bounds by CS-RDA converge to the target bound width of 3% by 113,694 disjoint sets, which are only 3.82% and 19.26% of those by the original RDA and S-RDA, respectively.

Table 3.5 summarizes the results of uni-, bi-, and tri-scale network reliability analyses using CS-RDA. Unlike the uni-scale approach, the bi- and tri-scale approaches require additional data preprocessing, which consists of the edge-betweenness algorithm and the probabilistic analysis to evaluate the failure probability and statistical dependency of super-components. Despite the relatively long preprocessing time, the total computation time decreases significantly at the higher scale, while there is little loss in terms of accuracy. The analysis time excluding the preprocessing was only 6,085 seconds and 1.37 seconds for the bi- and tri-scale approaches, respectively, which are only 1/34 and 1/150,000 of the computation time of the uni-scale approach. However, the trade-off for increased efficiency is reduced accuracy. As the scale increases, the network reliability is overestimated compared to the MCS results. This is due to the overestimation of the reliability of super-links during network simplification, which requires additional procedures to compensate.

Table 3.6 shows the CPIMs, BC, and failure probabilities of some nodes in the highway bridge network. Since the network is distributed over a large area, the failure probabilities of bridges vary depending on the location. Consequently, nodes with high CPIMs (nodes 10, 74, 81) depend on the failure probabilities of bridges, unlike Example 1. Only node 1 has the same ranks in terms of CPIM and BC.

Table 3.5. Analysis results for San Jose highway bridge network ($M_w = 7.0$)

Scale	P_f	# of disjoint sets	Preprocessing time	Total computation time
MCS	0.0891	-	-	280 s
Uni-scale	0.0905~0.1005	991,603	-	206,374 s
Bi-scale	0.0925~0.1025	115,933	240 s	6,375 s
Tri-scale	0.0935~0.0951	66	46.7 s	48.1 s

Table 3.6. CPIMs, BC, and failiure probabilities of nodes with highest CPIMs in San Jose highway bridge network

Comp ID	CPIM	CPIM Rank	BC	BC Rank	P_f	P_f Rank
1	0.297	1	0.304	1	0.032	88
81	0.279	2	0.022	92	0.119	1
10	0.273	3	0.048	53	0.113	2
74	0.265	4	0.037	66	0.108	3
Time	21,740 s		0.197 s		0.0027 s	

3.4.3 Example III: San Diego highway bridge network

Figure 3.12 shows the San Diego highway bridge network that consists of 317 bridges (blue circles), 339 bi-directional actual edges (solid lines), and four subjunctive edges (red dashed lines). The network thus features a total of 1,003 (=317+343×2) network components. The Southwest of San Diego and five intercity highways connected by subjunctive edges are set as the OD nodes (red stars). An earthquake event with the moment magnitude $M_w = 6.0$ is chosen, and the latitude and longitude of the epicenter are respectively $\mathrm{N}32.65°$ and $\mathrm{W}117.25°$.

Because of the complexity of the network, for the uni-scale analysis, only CS-RDA analysis is performed, and the results are compared with those by the bi- and tri-scales analyses. The edge-betweenness algorithm identifies 16 clusters for the bi-scale analysis and two clusters for the tri-scale analysis. Most of their inter-cluster

nodes are located at the intersections (junctions) or at the center of the edges as shown in Figures 3.13(a) and (b). The simplified network of the bi-scale analysis has 91 nodes and 117 bi-directional edges (91+117×2=325 network components), and that of the tri-scale analysis has only 12 nodes and 15 bi-directional edges (12+15×2=42 network components).

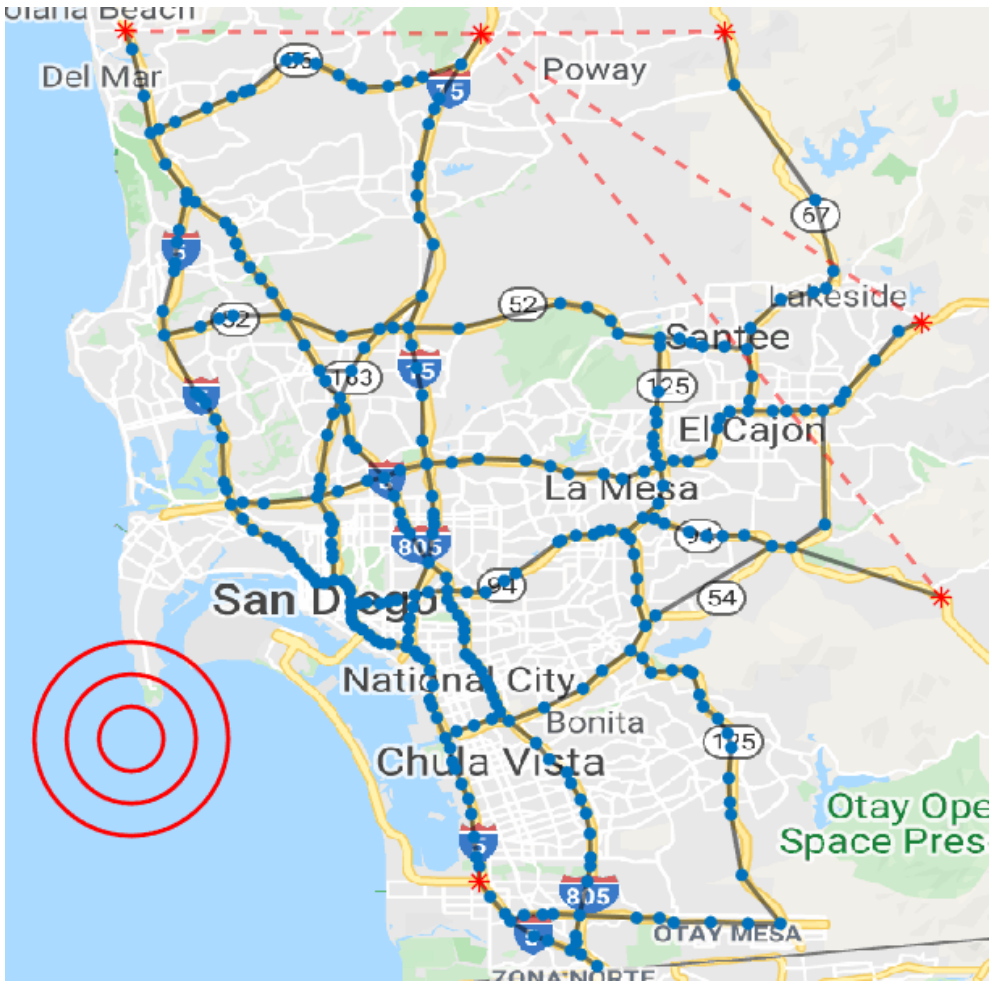

Figure 3.12. Highway bridge network in San Diego, CA

(a)

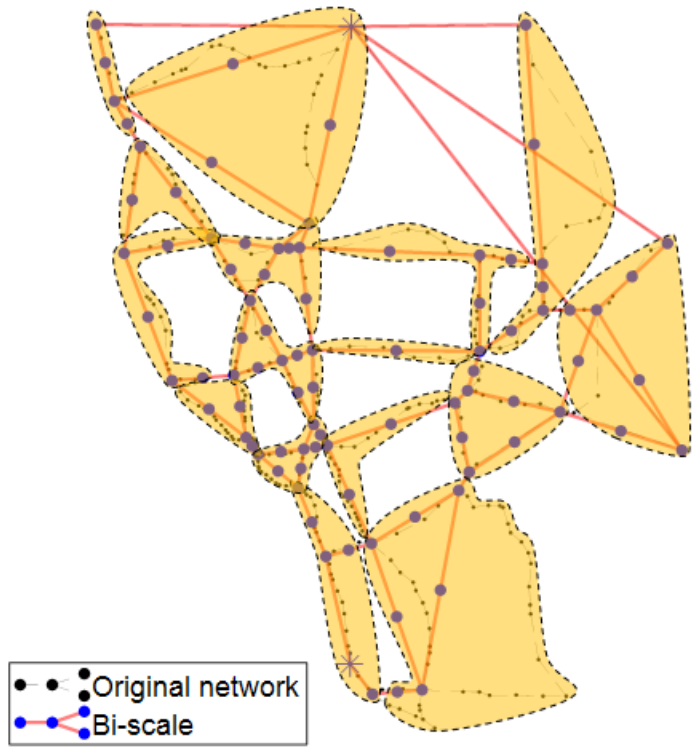

(b)

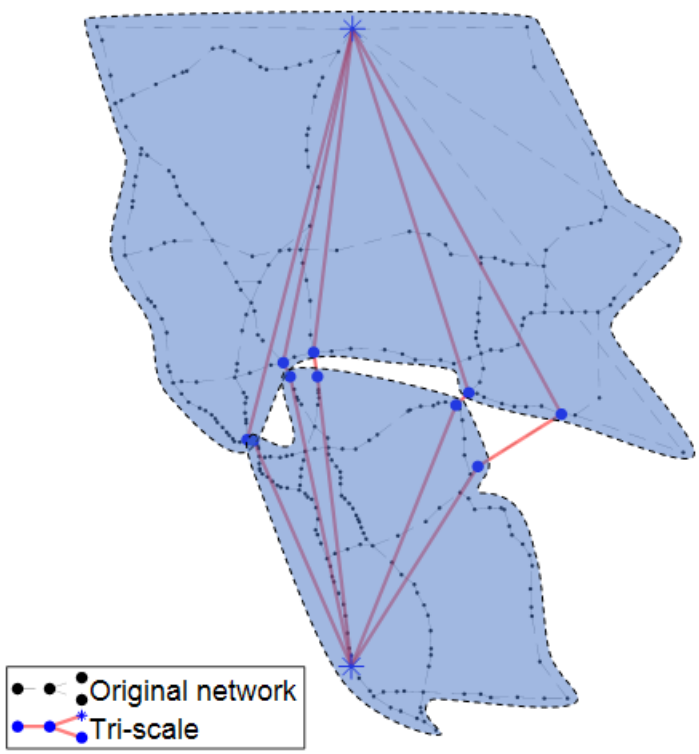

Figure 3.13. Hierarchical representation of San Diego highway bridge network example for (a) bi-scale, and (b) tri-scale analysis

Table 3.7 shows that the bound width by the uni-scale analysis does not decrease below 2.40% even after a week-long calculation. By contrast, the multi-scale analysis provides converged estimate within minutes or seconds. This is because the dimension of each disjoint cut set or link set grows rapidly as the number of nodes constituting each disjoint set increases in this large network. In calculating the high-dimensional multivariate normal CDF, the calculation time increases exponentially regardless of the methodology used, such as the dimensionality reduction system or the quasi-Monte Carlo simulation, while the accuracy of the calculated values is poor. On the other hand, despite the preprocessing time for clustering as required in Example 2, the reliability assessment of a large-scale network is possible in a shorter time. The results at higher scales inevitably contain errors caused by the network simplification; the results of the MCS are outside the bounds on the tri-scale in Table 3.7. This is due to the overestimation of the reliability of clusters containing sources or terminals proposed by Lim *et al*. (2015), which can be corrected by downward standardization.

Table 3.8 shows that three nodes with the highest CPIMs (node 59, 60, and 69) have high BCs because of their topological characteristics. On the other hand, node 44 is identified as an important component because of its high failure probability, caused by its proximity to the epicenter.

Table 3.7. Analysis results for San Diego highway bridge network ($M_w = 6.0$)

Scale	P_f	# of disjoint sets	Preprocessing time	Total computation time
MCS	0.0634	-	-	441 s
Uni-scale	0.0455~0.0695	1,000,000	-	More than a week
Bi-scale	0.0566~0.0660	714	129.8 s	199.3 s
Tri-scale	0.0564~0.0618	49	83.6 s	84.8 s

Table 3.8. CPIMs, BC, and failiure probabilities of nodes with highest CPIMs in San Diego highway bridge network

Comp ID	CPIM	CPIM Rank	BC	BC Rank	P_f	P_f Rank
69	0.271	1	0.362	3	0.017	104
59	0.142	2	0.353	6	0.025	53
60	0.138	3	0.313	14	0.025	56
44	0.135	4	0.027	177	0.034	1
Time	14,845 s		0.0750 s		0.0019 s	

Chapter 4. Efficient Monte Carlo simulation for seismic reliability curves of networks

4.1 Introduction

To quantify the seismic vulnerabilities of infrastructure networks, it is imperative to evaluate network reliability based on information about individual components, network topology, and seismic hazards. However, the seismic reliability analysis of large-scale networks can be computationally demanding or even infeasible; the computational cost typically grows exponentially with the number of components. Various sampling-based approaches have been proposed to analyze network reliability owing to their ease of implementation and high flexibility, but the direct MCS is extremely inefficient for rare events, such as the loss of connectivity in large infrastructure networks.

To overcome the limitations of direct MCS, an efficient variance-reduction sampling approach is proposed for seismic reliability analysis of infrastructure networks. The main idea is to reformulate the binary limit-state function into a more informative continuous function. The reformulated continuous limit-state function encodes the same failure domain as its binary counterpart, but at the same time, it implicitly provides information about the location of the failure domain. The latter property is crucial for formulating efficient variance-reduction sampling strategies.

The proposed limit-state functions quantify how close each sample is to the network failure, thereby facilitating the construction of intermediate relaxed failure events. A single implementation of Hamiltonian Monte Carlo-based subset

simulation (HMC-SS) can generate the network reliability curve by configuring each intermediate failure domain as a network failure event under a given earthquake intensity. This chapter contributes to the proposal of a method that streamlines MCS for assessing the seismic reliability of infrastructure networks, thereby enabling us to address large-scale networks that were untreatable with existing sampling-based approaches. In numerical examples, the efficiency and accuracy of the proposed method are demonstrated by seismic reliability analyses of hypothetical and realistic large-scale transportation networks.

4.2 Background

4.2.1 Failure domain of network reliability

An infrastructure network consists of line-type components such as pipelines and roads, and node-type components such as stations and bridges. The network can be represented as a graph $G(\boldsymbol{N}, \boldsymbol{E})$, where $\boldsymbol{N}$ is defined as the set of nodes (or vertices) that represents both types of components, and $\boldsymbol{E}$ is defined as the set of links (or edges) that conceptually expresses the connectivity between nodes. Therefore, one can assume that all links in set $\boldsymbol{E}$ are perfectly reliable, and this assumption does not cause any error in the accurate assessment of network reliability. For networks with link failures, one can make the abovementioned assumption still valid by converting them to equivalent networks with node failures in polynomial time (Colbourn 1987; Ball *et al.* 1995).

Let $z_i = \ln C_i - \ln D_i$ be the logarithmic safety margin for the i^{th} component. $\boldsymbol{z} = [z_1, \dots, z_N]$ is defined as the network state vector (i.e., a vector of the logarithmic safety margins of components), where $N = |\boldsymbol{N}|$ is the number of

nodes (i.e., the total number of node-type and line-type components) in the target network. Then, the network reliability problem is performed by evaluating the failure probability P_f via multi-dimensional integration as

$$P_f = \int_{\mathcal{F}} f(\boldsymbol{z})d\boldsymbol{z} = \int_{\mathbb{R}^N} \mathbb{I}(G(\boldsymbol{z}) \leq 0) f(\boldsymbol{z})d\boldsymbol{z}, \tag{4.1}$$

where $\mathcal{F} = \{\boldsymbol{z}|G(\boldsymbol{z}) \leq 0\}$ is the failure domain for the network reliability problem, such as connectivity reliability analysis (e.g., two-terminal, k-terminal, all-terminal reliability) and capacity reliability analysis (Nabian and Meidani 2018); $G(\boldsymbol{z}) \in \mathbb{R}$ is the network limit-state function; $f(\boldsymbol{z})$ is the joint probability density function (PDF) of the network state vector $\boldsymbol{z}$ through seismic reliability analysis with correlation coefficients.

For two-terminal reliability analysis between the predefined OD node pair, the network limit-state function in Eq. (4.1) is replaced with the following binary network reliability function, $G_{\mathrm{OD}}^{\mathrm{Bi}}(\boldsymbol{z})$, as

$$G_{\mathrm{OD}}^{\mathrm{Bi}}(\boldsymbol{z}) = \begin{cases} 1, & \text{if OD pair is connected in } \boldsymbol{z}, \\ 0, & \text{otherwise.} \end{cases} \tag{4.2}$$

$G_{\mathrm{OD}}^{\mathrm{Bi}}(\boldsymbol{z})$ is completely dependent on the network topology. For example, in a series system, only the joint survival of all components guarantees connectivity. In contrast, a parallel system fails only when all components do not work. Therefore, the failure domains of N-component series and parallel systems, $\mathcal{F}_{\mathrm{series}}$ and $\mathcal{F}_{\mathrm{parallel}}$, are respectively defined as

$$\mathcal{F}_{\mathrm{series}} = \left\{G_{\mathrm{series}}^{\mathrm{Bi}}(\boldsymbol{z}) = 0\right\} = \bigcup_{i=1}^{N} \{B_i = 1\} = \left\{\min_{i=1,\ldots,N} z_i \leq 0\right\}, \tag{4.3}$$

$$\mathcal{F}_{\text{parallel}} = \left\{G^{\text{Bi}}_{\text{parallel}}(\boldsymbol{z}) = 0\right\} = \bigcap_{i=1}^{N}\{B_i = 1\} = \left\{\max_{i=1,\ldots,N} z_i \leq 0\right\}. \tag{4.4}$$

where $G^{\text{Bi}}_{\text{series}}$ and $G^{\text{Bi}}_{\text{parallel}}$ represent binary network reliability functions with series and parallel systems between an OD pair, respectively; and B_i is the Bernoulli variable representing the failure event of component i as

$$B_i = \mathbb{I}(C_i \leq D_i) = \mathbb{I}(z_i \leq 0), \tag{4.5}$$

where $\mathbb{I}(\cdot)$ denotes a binary indicator function that returns 1 if the given inequality or equation holds, and 0 otherwise.

For example, let us consider a two-component series system and a two-component parallel system. According to Eqs. (4.3) and (4.4), the failure domains for each system, $\mathcal{F}_{\text{series}}$ and $\mathcal{F}_{\text{parallel}}$, are illustrated in red in Figures 4.1(a) and (b), respectively. The exact failure probabilities of each system P_f is evaluated by integrating $f(\boldsymbol{z})$ over each failure domain $\mathcal{F}$.

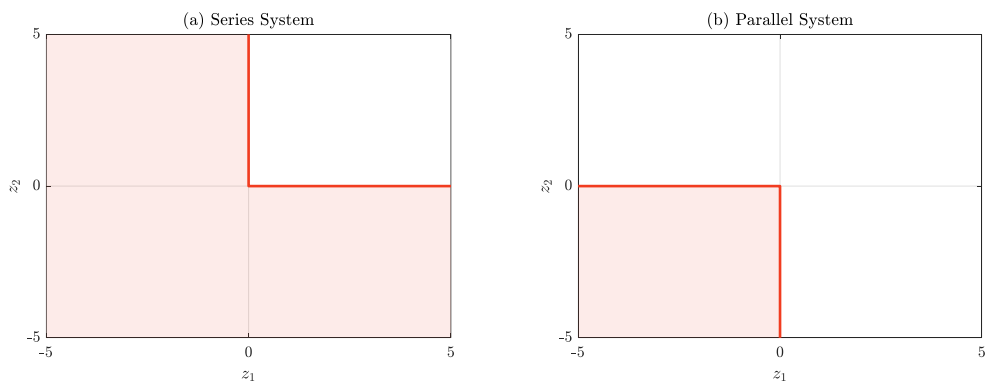

Figure 4.1. Failure domains of (a) two-component series system, and (b) two-component parallel system

Series and parallel systems can be considered as networks with a link set (i.e., a set of nodes forming a path between the OD pair) and a cut set (i.e., a set of nodes whose simultaneous failure results in the disconnection of the OD pair), respectively. In other words, by generalizing Eqs. (4.3) and (4.4) respectively, the failure domain of a general network, $\mathcal{F}$, is given in two ways (Song and Der Kiureghian 2003) as

$$\mathcal{F} = \bigcap_{k} \bigcup_{i \in L_k} \{B_i = 1\} = \left\{ \max_{k} \min_{i \in L_k} z_i \leq 0 \right\}, \tag{4.6}$$

$$\mathcal{F} = \bigcup_{l} \bigcap_{i \in C_l} \{B_i = 1\} = \left\{ \min_{l} \max_{i \in C_l} z_i \leq 0 \right\}, \tag{4.7}$$

where L_k and C_l denote the k-th link set and the l-th cut set, respectively.

Once all the cut sets or link sets in a network with N components are known, the exact network reliability can be evaluated by combining Eq. (4.1) with Eq. (4.6) or (4.7). To this end, various non-simulation-based methods have been developed to identify all link sets (Abraham 1979; Aziz *et al.* 1993) or cut sets (Brown 1971; Rosenthal 1979), and recursive decomposition algorithms (Li and He 2001; Lim and Song 2012; Lim *et al.* 2015; Lee and Song 2021) use both sets to compute the upper and lower bounds of the network reliability. However, network reliability problems are NP-hard (Rosenthal 1977; Colbourn 1987), i.e., there is no polynomial-time algorithm for general networks, thereby making the accurate reliability analysis of large-scale networks infeasible. More specifically, the main challenges of NRA include: (1) failure domain exploration in 2^N combinations of component states, and (2) fast and accurate computation in the high-dimensional space $\mathbb{R}^N$.

4.2.2 Review of subset simulation

Subset simulation (Au and Beck 2001) is one of the most widely-used variance-reduction sampling approaches. The main idea of subset simulation is to represent the failure domain of interest, $\mathcal{F}$, as nested intermediate failure domains, $\mathcal{F}_1 \supset \mathcal{F}_2 \supset \cdots \supset \mathcal{F}_M = \mathcal{F}$. The failure probability P_f is expressed as a product of the conditional probabilities $P(\mathcal{F}_i|\mathcal{F}_{i-1})$, which are the transition probabilities to the next intermediate failure domain at each step.

$$P_f = \prod_{i=1}^{M} P(\mathcal{F}_i|\mathcal{F}_{i-1}), \tag{4.8}$$

where $\mathcal{F}_0 = \mathbb{R}^N$ denotes the initial failure domain. By setting each conditional probability identically to a constant p_0, the intermediate failure domains $\mathcal{F}_i$, $i = 1, \dots, M-1$, are adaptively determined based on the p_0 quantile in $\mathcal{F}_{i-1}$ by sampling. Au and Beck (2001) suggested setting $p_0 = 0.1$, and Zuev *et al*. (2012) demonstrated that $p_0 \in [0.1, 0.3]$ shows similar performance.

While generating independent identically distributed samples from the initial failure domain is easily accomplished by the crude MCS, it becomes a completely different and considerably challenging problem in the intermediate failure domains $\mathcal{F}_{i-1}$ for $i \geq 2$. To this end, various Markov chain Monte Carlo (MCMC) methods such as Metropolis-Hastings algorithm (Metropolis *et al.* 1953; Hastings 1970) have been utilized. Using MCMC methods, each conditional probability $P(\mathcal{F}_i|\mathcal{F}_{i-1})$, and the failure probability of interest $\hat{P}_{f,SS}$, can be estimated as follows, respectively.

$$P(\mathcal{F}_i|\mathcal{F}_{i-1}) = \int_{\mathcal{F}_i} f(\boldsymbol{z}|\mathcal{F}_{i-1})d\boldsymbol{z} \cong \frac{1}{n}\sum_{j=1}^{n} \mathbb{I}\left(\boldsymbol{z}^{(j)} \in \mathcal{F}_i \middle| \mathcal{F}_{i-1}\right), \tag{4.9}$$

$$\hat{P}_{f,SS} = \prod_{i=1}^{M} P(\mathcal{F}_i|\mathcal{F}_{i-1}) \cong \frac{p_0^{M-1}}{n}\sum_{j=1}^{n} \mathbb{I}\left(\boldsymbol{z}^{(j)} \in \mathcal{F} \middle| \mathcal{F}_{M-1}\right), \tag{4.10}$$

where n is the number of samples required for each intermediate failure domain; and $\boldsymbol{z}^{(j)}$ is the j^{th} sample vector. Subset simulation is particularly efficient for extremely sparse events with $P_f \ll 1$; whereas the crude MCS requires $n_{MCS} \propto \frac{1}{P_f}$ simulations, the number of samples required for a single implementation of subset simulation is theoretically given as $n_{SS} \coloneqq M \cdot n \propto \left|\log P_f\right|$ (Au and Beck 2001).

MCMC methods have a critical limitation; the samples from MCMC methods are identically distributed under the stationary state of the Markov chain, but interdependent. Although autocorrelation between samples cannot be eliminated perfectly, Hamiltonian Monte Carlo based subset simulation (HMC-SS) (Wang *et al.* 2019, Chen *et al.* 2022) is adopted to streamline the MCMC process in this chapter. The bias due to autocorrelation of samples and adaptive intermediate failure domains is asymptotically unbiased by more than 50 iterations (Au and Beck 2001).

4.3 Subset simulation for NRA

In NRA, connectivity is typically defined by a binary limit-state function as shown in Eq. (4.2). The property poses a major obstacle to combining subset simulation and network reliability analysis. The p_0 quantile of the samples is chosen to be either 0 or 1 in each intermediate domain due to the jump discontinuity of binary limit-state functions. Therefore, subset simulation cannot narrow down the failure domain and

consequently does not work at all.

4.3.1 Informative continuous network limit-state functions

4.3.1.1 Most reliable path-based function

For subset simulation, the existing binary network reliability function, $G_{\mathrm{OD}}^{\mathrm{Bi}}(\boldsymbol{z})$, is reformulate into a more physics-informed continuous function. More specifically, the continuous network reliability function, $G_{\mathrm{OD}}^{\mathrm{RP}}(\boldsymbol{z})$, is defined in terms of the vulnerability of the most reliable path between an OD pair as

$$G_{\mathrm{OD}}^{\mathrm{RP}}(\boldsymbol{z}) = \begin{cases} \dfrac{\min_{i \in \boldsymbol{RP}} z_i}{n_{\mathrm{RP}}}, & \text{if OD pair is connected in } \boldsymbol{z}, \\ 0, & \text{otherwise,} \end{cases} \tag{4.11}$$

where $\boldsymbol{RP}$ is a node set in the most reliable path between the OD pair consisting of the survival nodes in $\boldsymbol{z}$; and n_{RP} is the number of nodes on $\boldsymbol{RP}$. Eq (4.11) stems from the intuition that the detected $\boldsymbol{RP}$ is no longer available when any component fails (i.e., when any z_i for $i \in \boldsymbol{RP}$ becomes negative), and that the larger n_{RP}, the more likely components are to fail even for the same minimum z value. To expedite reliability-based pathfinding, all component failure events are assumed to be independent. Then, Dijkstra's algorithm (Ahuja *et al*. 1993; Cormen *et al*. 2009) is used to find the most reliable path $\boldsymbol{RP}$ between OD nodes that maximizes the product of the survival probabilities of nodes obtained from Eq (3.7), i.e., the sum of the log-scaled survival probabilities. Figures 4.2(a) and (b) show the proposed continuous network reliability functions for the two-component series and parallel systems, which are contrasted with the binary network reliability functions in Figures 4.1(a) and (b).

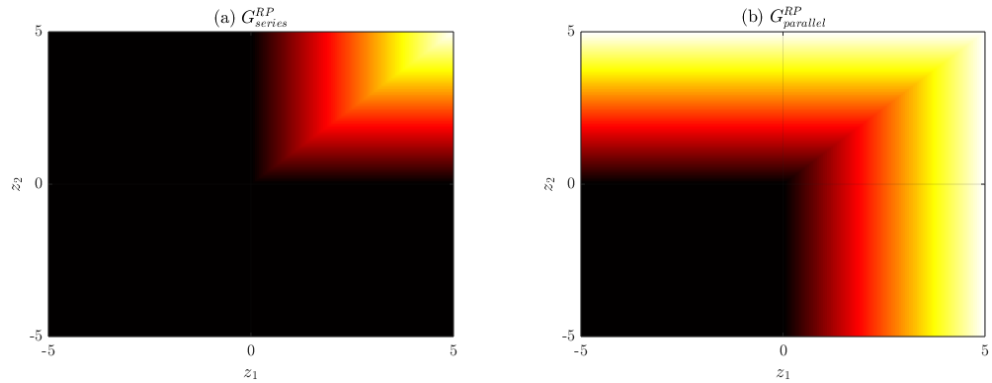

Figure 4.2. Proposed RP-based continuous network reliability function for (a) two-component series system, and (b) two-component parallel system

The proposed function decreases monotonically as it approaches the failure domain as shown in Figures 4.2, so that the current samples rarely bounce significantly from the previous ones. The intermediate domain gradually converges to the failure domain as the subset simulation progresses. Let the i^{th} intermediate failure domain $\mathcal{F}_i$ be $\{G^{\mathrm{RP}}_{\mathrm{OD}}(\boldsymbol{z}) \leq g_i\}$. Then, the failure probability P_f is expressed as a product of conditional probabilities as

$$\begin{aligned}\hat{P}_{f,SS} &= \prod_{i=1}^{M} P\left(G^{\mathrm{RP}}_{\mathrm{OD}}(\boldsymbol{z}) \leq g_i \middle| G^{\mathrm{RP}}_{\mathrm{OD}}(\boldsymbol{z}) \leq g_{i-1}\right) \\ &\cong \frac{p_0^{M-1}}{n} \sum_{j=1}^{n} \mathbb{I}\left(G^{\mathrm{RP}}_{\mathrm{OD}}\left(\boldsymbol{z}^{(j)}\right) \leq g_i \middle| G^{\mathrm{RP}}_{\mathrm{OD}}\left(\boldsymbol{z}^{(j)}\right) \leq g_{i-1}\right),\end{aligned} \tag{4.12}$$

where $g_1 > \cdots > g_M = 0$ denote intermediate thresholds; $g_0 = \infty$ denotes the initial failure threshold; and $\boldsymbol{z}^{(j)}$ is the state vector of the j^{th} network sample.

4.3.1.2 Shortest path-based function

However, the proposed function $G^{\mathrm{RP}}_{\mathrm{OD}}(\boldsymbol{z})$ has a critical flaw in terms of computation time for reliability analysis of large-scale networks; the time complexity of Dijkstra's

algorithm for the weighted graphs is given by $\mathcal{O}(|\boldsymbol{V}|^2)$ (Dijkstra 1959). This is quite time-consuming in comparison to breadth-first search (BFS) for the OD connectivity, i.e., $G_{\mathrm{OD}}^{\mathrm{Bi}}(\boldsymbol{z})$, which has a linear time $\mathcal{O}(|\boldsymbol{E}| + |\boldsymbol{V}|)$. Although subset simulation requires fewer simulations than the crude MCS, the computational cost of each simulation becomes significant on large-scale networks. To compensate for the weakness, another limit-state function using BFS is proposed, which replaces $\boldsymbol{RP}$ in Eq (4.11) with the node set in the shortest path, $\boldsymbol{SP}$, as

$$G_{\mathrm{OD}}^{\mathrm{SP}}(\boldsymbol{z}) = \begin{cases} \dfrac{\min_{i \in \boldsymbol{SP}} z_i}{n_{\mathrm{SP}}}, & \text{if OD pair is connected in } \boldsymbol{z}, \\ 0, & \text{otherwise,} \end{cases} \tag{4.13}$$

where n_{SP} is the number of nodes on $\boldsymbol{SP}$. Figures 4.3(a) and (b) show contour plots of the proposed SP-based network reliability function for the two-component series and parallel systems, $G_{\mathrm{series}}^{\mathrm{SP}}(\boldsymbol{z})$ and $G_{\mathrm{parallel}}^{\mathrm{SP}}(\boldsymbol{z})$. Since there is only a single path in a series system, i.e., $\boldsymbol{SP} \equiv \boldsymbol{RP}$, Figure 4.3(a) for $G_{\mathrm{series}}^{\mathrm{SP}}(\boldsymbol{z})$ is exactly the same as Figure 4.2(a) for $G_{\mathrm{series}}^{\mathrm{RP}}(\boldsymbol{z})$. On the other hand, there is an obvious difference between the two contour maps in the parallel system; while $G_{\mathrm{parallel}}^{\mathrm{RP}}(\boldsymbol{z})$ is a globally differentiable continuous function, $G_{\mathrm{parallel}}^{\mathrm{SP}}(\boldsymbol{z})$ has a jump discontinuity along the boundary between the first and second quadrants because $\boldsymbol{SP}$ based on BFS only considers component 1 if both survive (i.e., in the first quadrant in Figure 4.3(b)). Although this results in distinctively shaped intermediate failure domains during subset simulation, it allows for faster computation compared to $G_{\mathrm{parallel}}^{\mathrm{RP}}(\boldsymbol{z})$.

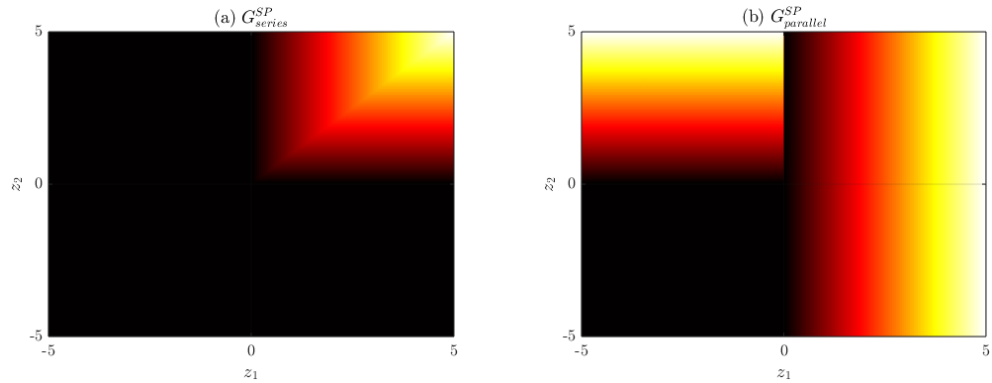

Figure 4.3. Proposed SP-based network reliability function for (a) two-component series system, and (b) two-component parallel system

4.3.2 Seismic reliability curve of network

Beyond the fragility curves of structures, this section proposes the concept of reliability curves of network connectivity and the way to compute them efficiently using the proposed variance-reduction sampling method.

4.3.2.1 Configuration of intermediate failure domains

The intermediate failure domains generated by HMC-SS are the spaces that should be traversed to reach the failure domain of interest, i.e., network failure domain. The analysis of network reliability curves using HMC-SS begins by extracting useful probabilities from these intermediate failure domains. If the target moment magnitude is set so that the failure probability is greater than p_0, the network reliability can be calculated without intermediate failure domains. This initial failure domain is used as an intermediate failure domain for lower moment magnitudes. It is noteworthy that only the mean of seismic demands changes with the moment magnitude, while the standard deviations of seismic demands, the distributions of

seismic capacities, and the correlation coefficients are independent of the moment magnitude as shown in Eqs. (3.7) and (3.9). As a result, the mean of the logarithmic safety margins, $E[z_i]$, depends on the magnitude of the earthquake, but the covariance matrix $\boldsymbol{R_{zz}} = \left[\rho_{z_i z_j}\right]_{i,j\in[1,m]}$ is independent of M_w. Figure 4.4 shows the failure domain of two-component parallel system and the contour map of $\boldsymbol{z}$ according to the magnitude.

Since $\boldsymbol{z}$ under each M_w shares the covariance matrix $\boldsymbol{R_{zz}} = \left[\rho_{z_i z_j}\right]_{i,j\in[1,m]}$, one can linearly transform the contour maps of $\boldsymbol{z}$ to overlap into one. A critical point is defined as the threshold point at which the network state changes, e.g., the origin in Figure 4.4. After the linear transformation, all the contour maps are completely overlapped, and only the failure domains or critical points under each M_w are distinguished from each other. Figure 4.5 shows the result of the linear transformation, where the failure domain under the larger M_w acts as an intermediate failure domain under the smaller M_w.

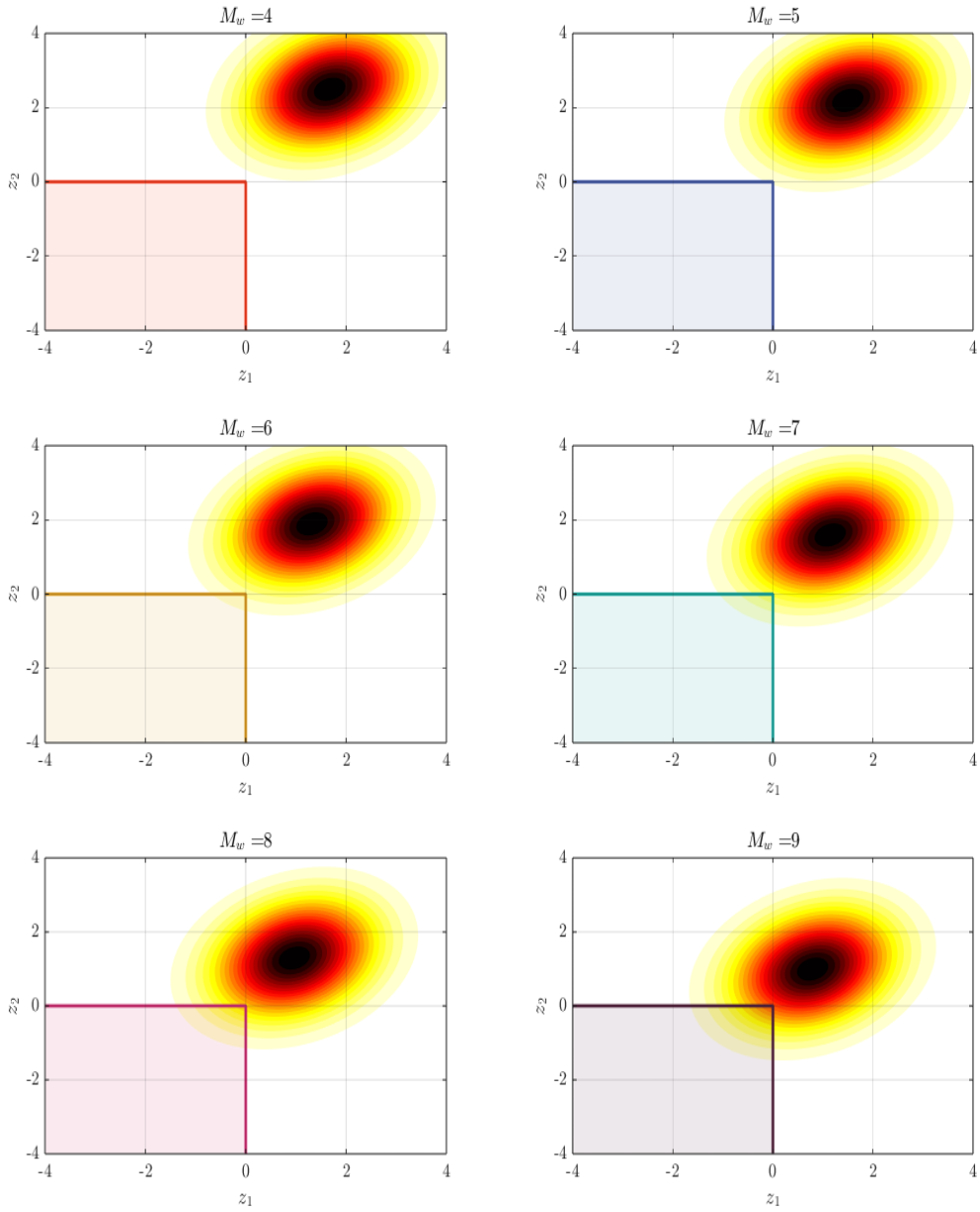

Figure 4.4. Failure domain of interest and contour map of logarithmic safety margins along magnitude changes

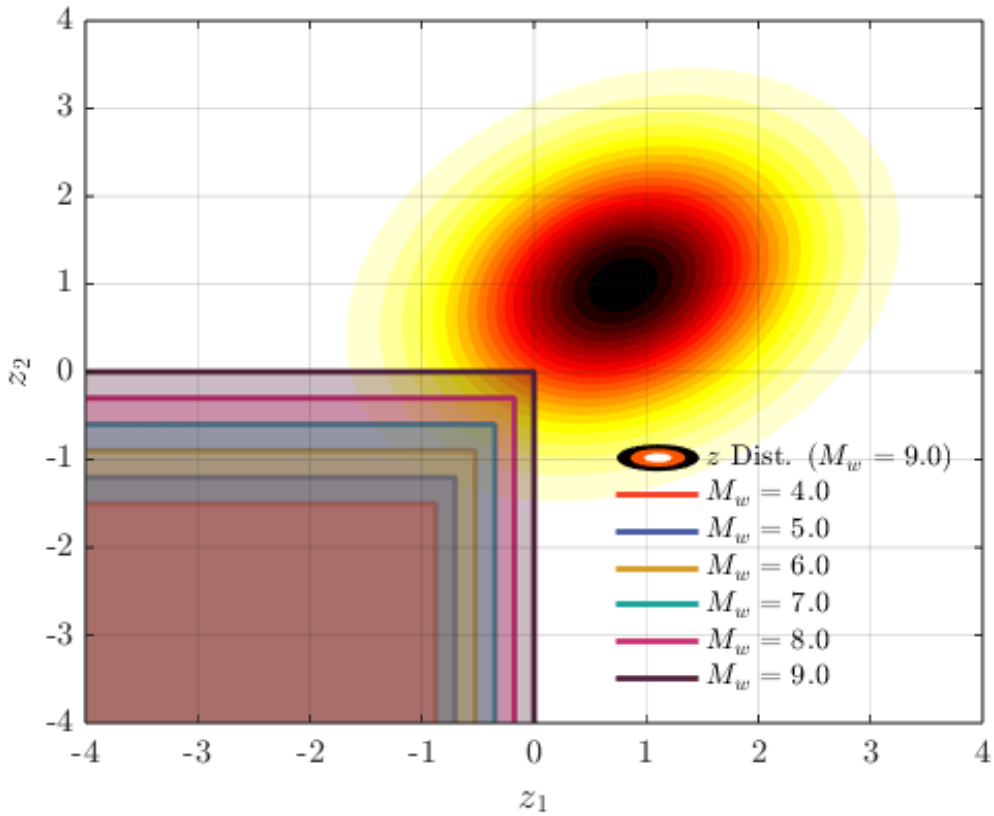

Figure 4.5. Overlapped failure domain of interest after linear transformation

4.3.2.2 Normalization of intermediate failure domains

There is one more hurdle to overcome to plot the network reliability curve by a single run of the subset simulation. Due to the different sensitivities of individual components for earthquake magnitude, the critical points are defined as vectors rather than scalars. By normalizing the sensitivity of each component to earthquake magnitude change, every critical point can be defined as a scalar as long as the earthquake magnitude change, ΔM_w is given as a constant. The normalization equation for $\boldsymbol{z}$ is given as follows:

$$\tilde{\boldsymbol{z}}(M_w) = \frac{\boldsymbol{z}(M_w)}{\Delta \boldsymbol{z}}, \tag{4.14}$$

where $\tilde{\boldsymbol{z}}(M_w)$ is the normalized logarithmic safety margin vector under M_w; and $\Delta \boldsymbol{z}$ denotes the difference in logarithmic safety margins for ΔM_w.

Figure 4.6 shows the normalized failure domains with the contour map of the joint probability distribution of $\tilde{\boldsymbol{z}}$. The critical point of the i^{th} normalized failure domain is given as $[1-i, 1-i, \ldots, 1-i]$, and the i^{th} objective function $G_i(\cdot)$ is given as

$$G_i(\tilde{\boldsymbol{z}}) = G(\tilde{\boldsymbol{z}}) - (i-1), \tag{4.15}$$

where $G(\cdot)$ is the proposed objective function in Eqs. (4.11) and (4.13).

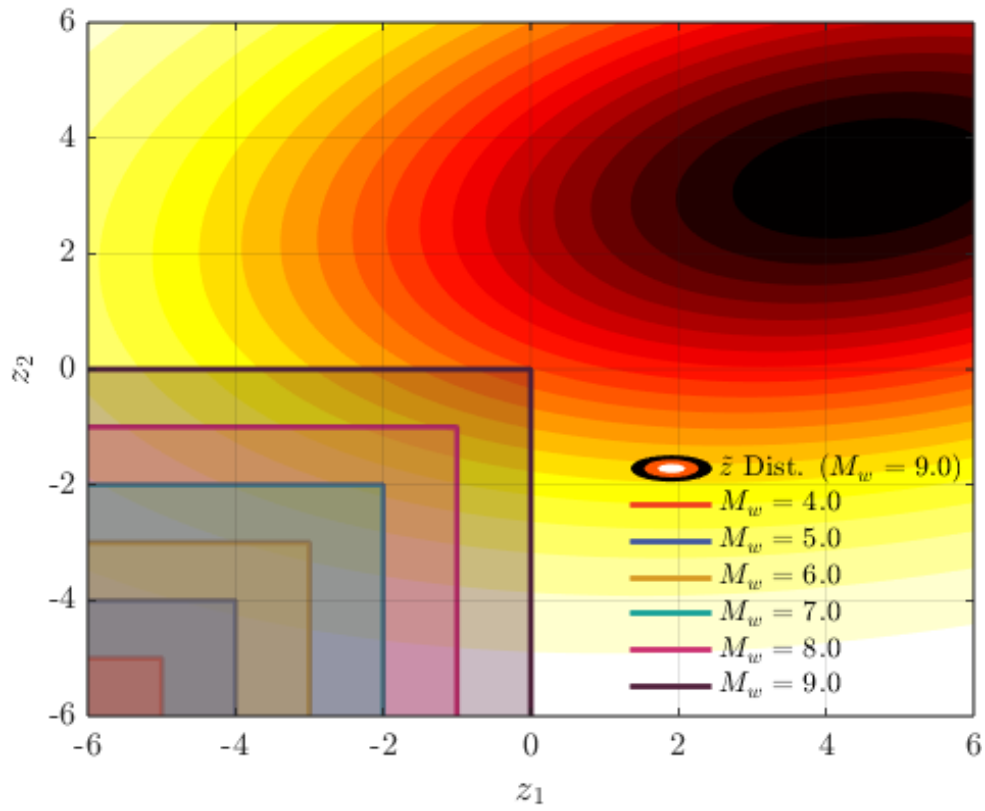

Figure 4.6. Normalized failure domains of interest and contour map

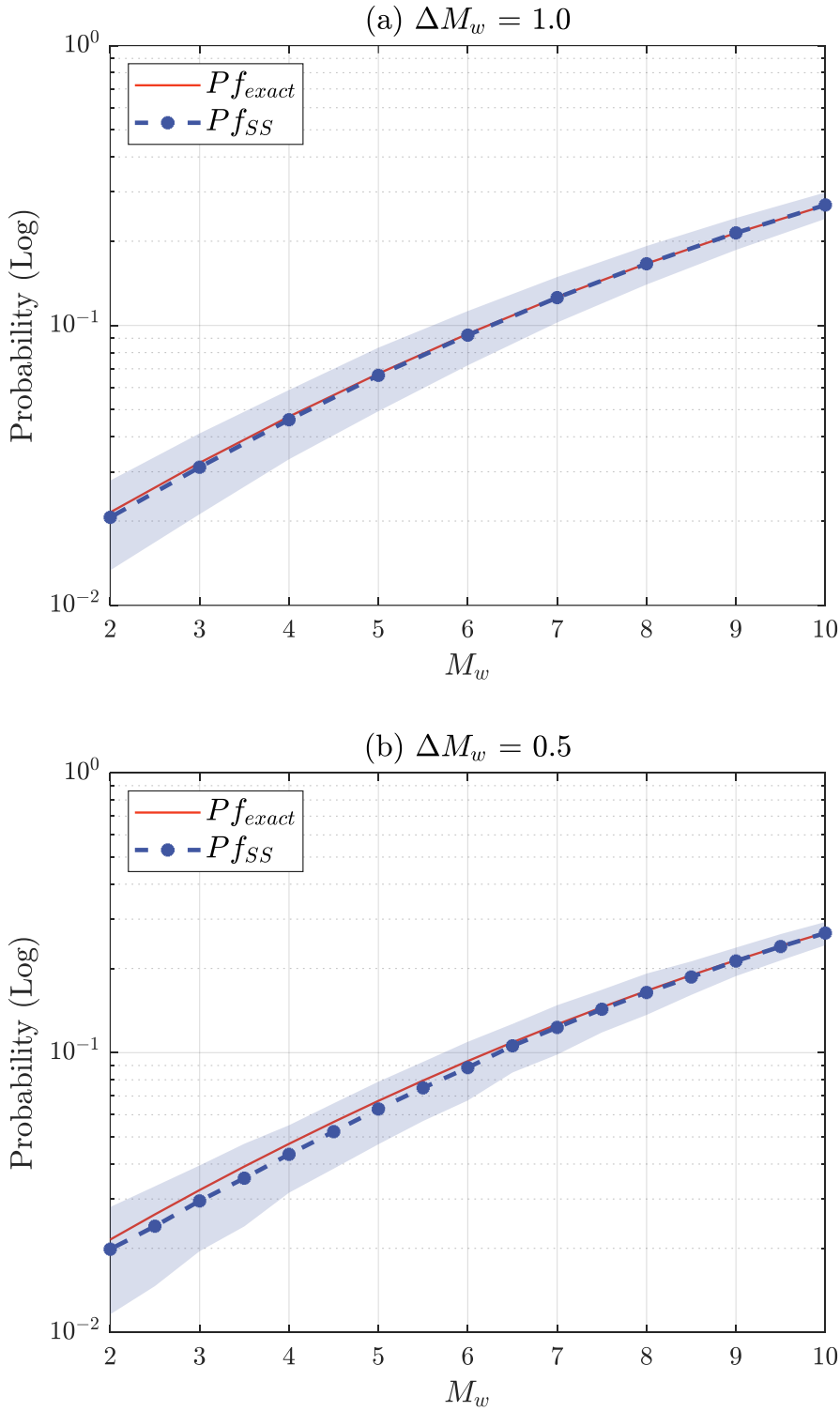

Figure 4.7. HMC-SS-based network reliability curve with different ΔM_w

4.3.2.3 Generation of network reliability curve

Using the proposed objective function in Eq. (4.14), the network reliability curve can be generated by a single implementation of HMC-SS. However, HMC-SS still provides biased estimates; the smaller ΔM_w, the more detailed the reliability curve, but the cumulative error increases as the number of subsets increases.

Figure 4.7 compares the reliability curve of a single component estimated by HMC-SS with the integral-based exact values, while varying the ΔM_w. The red solid line shows the exact solution, while the blue dashed line shows the HMC-SS-based estimates with blurred 95% confidence intervals. Both results are relatively similar to the exact solutions for $M_w \geq 7$, i.e., close to the initial failure domain, but the difference in accuracy becomes apparent for $M_w \leq 4$ due to the accumulated errors. When analyzing so many intermediate failure domains, increasing the number of seeds for HMC-SS may be a way to improve convergence.

4.4 Numerical examples

In general, *k*-terminal reliability analysis and *k*-out-of-*N* network reliability analysis, i.e., a part of capacity reliability analysis, are considered much more complex than two-terminal reliability analysis. They require different methods tailored to the characteristics of each reliability, e.g., BFS for connectivity, Ford-Fulkerson algorithm (Ford and Fulkerson 1956) for capacity reliability. In contrast, sampling-based analysis can be used for other reliability indices in essentially the same way as for two-terminal reliability, once their limit-state functions are well-defined. To this end, two-terminal reliability analyses are first performed for a two-component

parallel system and a hypothetical network (Lim *et al*. 2015) using two proposed network reliability functions, $G_{\mathrm{OD}}^{\mathrm{RP}}$ and $G_{\mathrm{OD}}^{\mathrm{SP}}$, in Section 4.1. Then, Section 4.2 discusses how to extend the two-terminal reliability analysis to *k*-terminal reliability and *k*-out-of-*N* network reliability. To test and demonstrate the accuracy and scalability of the proposed methods, they are applied to the highway bridge networks in San Jose (Guo *et al.* 2017; Nabian and Meidani 2018) and San Diego (Lee and Song 2021), respectively.

The seismic capacity parameters for two components in Example 1 and all the bridges in the highway networks in San Jose and San Diego are assumed to be 0.98 g for the median $\bar{C}_i$, and 0.69 for the logarithmic standard deviation ζ_i. For the components in the hypothetical network, the parameters are set to 0.85 g for $\bar{C}_i$, and 0.69 for ζ_i. In all the examples of Section 4, the parameters for the HMC-SS are set as $n = 1{,}000$, $p_0 = 0.1$, $t_f = \frac{\pi}{4}$, and $\alpha = 0$ (for the meaning of the last two parameters, refer to Wang *et al*. (2019)). All computations are implemented using MATLAB® on an 8-core MacBook Air (2022) with 8 GB of RAM.

4.4.1 Two-terminal reliability

4.4.1.1 Example I: Two-component parallel system

Consider the two-component parallel system with an earthquake scenario with a moment magnitude $M_w = 5.0$. The distance Δ_{12} between two components is set to 11.12 km, and the distances R_1 and R_2 of the two components from the epicenter are given as 3.46 km and 9.28 km, respectively. Figures 4.8 and 4.9 illustrate the 250 HMC samples and intermediate domains based on $G_{\mathrm{OD}}^{\mathrm{RP}}$ and $G_{\mathrm{OD}}^{\mathrm{SP}}$,

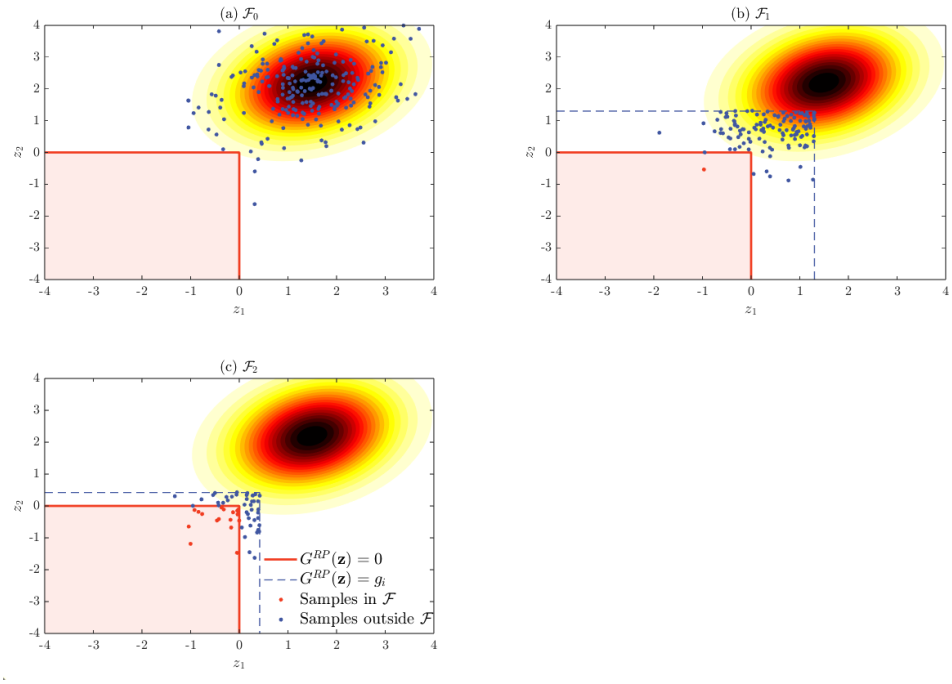

Figure 4.8. Samples from (a) entire domain, (b) first subset, and (c) second subset using $G_{\mathrm{OD}}^{\mathrm{RP}}$

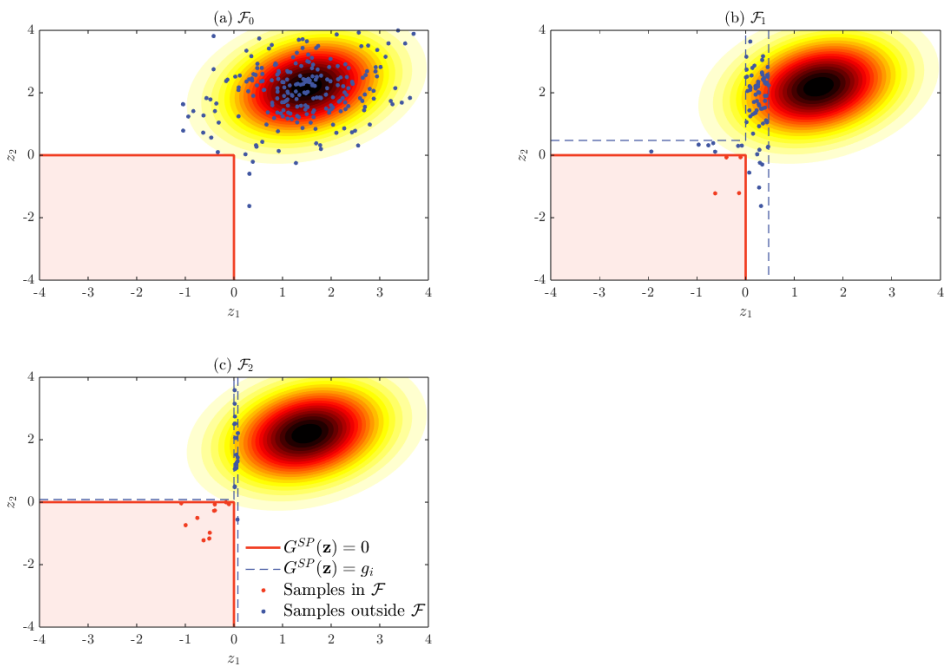

Figure 4.9. Samples from (a) entire domain, (b) first subset, and (c) second subset using $G_{\mathrm{OD}}^{\mathrm{SP}}$

respectively, with the system failure domain $\mathcal{F}$ and the contour plot of the joint PDF of the logarithmic safety margins, $f(\boldsymbol{z})$. Unlike the square intermediate domains of $G_{\mathrm{OD}}^{\mathrm{RP}}$, those of $G_{\mathrm{OD}}^{\mathrm{SP}}$ gradually converge to the failure domain in the form of the lowercase letter 'd', showing consistency with the contour plot in Figure 4.9(b). Although drawing identically distributed samples from the odd-shaped intermediate failure domains of $G_{\mathrm{OD}}^{\mathrm{SP}}$ is generally a major hurdle for subset simulation, the HMC-SS facilitates it with the high acceptance rate.

To evaluate $\hat{P}_{f,SS}$ and the coefficient of variation of $\hat{P}_{f,SS}$ (c.o.v.) for a sequence of moment magnitudes M_w ranging from 3.0 to 7.0, the HMC-SS with $G_{\mathrm{OD}}^{\mathrm{RP}}$ and $G_{\mathrm{OD}}^{\mathrm{SP}}$ are performed 500 times each. Table 4.1 shows the results of subset simulations with the exact P_f. Note that while the exact seismic failure probability of the two-component system can be evaluated via integration, it is usually infeasible for large-scale networks. Both estimated probabilities achieve quite high accuracy considering the exact solution, because estimates of subset simulation are asymptotically unbiased.

Table 4.1 also summarizes the computation time t_{ss} for a run of HMC-SS of each limit-state function. $eff = \mathrm{c.o.v.} \times \sqrt{NS}$ is introduced to measure the efficiency of variance-reduction sampling methods (Au and Beck 2001), where NS denotes the average number of network samples. A lower eff indicates higher sampling efficiency, i.e., lower c.o.v. with fewer samples. Figures 4.10(a) and (b) show the variation of eff and t_{ss} with M_w to compare the efficiency of the HMC-SS with $G_{\mathrm{OD}}^{\mathrm{RP}}$ and $G_{\mathrm{OD}}^{\mathrm{SP}}$ in terms of samples and time, respectively. One can clearly see the advantages of the two subset simulations; the former converges stably

owing to its low c.o.v., while the other requires only a quarter to a fifth of the t_{ss} of the $G_{\mathrm{OD}}^{\mathrm{RP}}$-based one. This speed-up comes from the BFS-based shortest path search, which is much faster than the Dijkstra algorithm mentioned in Section 4.3.1.2. Overall, regardless of the limit-state function, lower failure probabilities require more NS with longer t_{ss}, and eff increases monotonically with decreasing M_w.

On the other hand, there is a temporary inconsistency in t_{ss}, when $M_w = 6.0$. This is because the time to identify seismically damaged components in each network sample is proportional to M_w, even though NS is negatively correlated with M_w. Nevertheless, NS dominates the overall tendency because its variation is much larger than that of the component failure probabilities.

Figure 4.11 shows the network reliability curve generated by a single run of HMC-SS (blue dashed line) with the 95% confidence interval of the estimates (blue shaded area) and the exact values (red solid line). Table 4.2 compares the efficiency and accuracy of the NRA. The $G_{\mathrm{OD}}^{\mathrm{RP}}$-based HMC-SS is used for comparison in both cases, and n is set to 10,000 for more accurate reliability curves including other numerical examples. Although the single run has a little higher c.o.v., NS to complete the network reliability curve is only about one-third of that of the separate HMC-SS implementation. This efficiency is achieved by minimizing wasted samples or intermediate failure domains in the proposed method.

Table 4.1. Two-terminal reliability analysis results on two-component parallel system

M_w	$G_{\mathrm{OD}}^{\mathrm{RP}}$			$G_{\mathrm{OD}}^{\mathrm{SP}}$			Exact P_f
	$\hat{P}_{f,SS}$	c.o.v.	t_{ss}(s)	$\hat{P}_{f,SS}$	c.o.v.	t_{ss}(s)	
7.0	1.41×10^{-2}	0.149	0.447	1.41×10^{-2}	0.202	0.102	1.40×10^{-2}
6.0	6.34×10^{-3}	0.196	0.730	6.37×10^{-3}	0.265	0.169	6.31×10^{-3}
5.0	2.62×10^{-3}	0.196	0.635	2.63×10^{-3}	0.345	0.136	2.61×10^{-3}
4.0	1.00×10^{-3}	0.255	0.817	1.00×10^{-3}	0.478	0.176	0.98×10^{-3}
3.0	3.46×10^{-4}	0.286	0.837	3.50×10^{-4}	0.702	0.212	3.40×10^{-4}

Table 4.2. Efficiency and accuracy of single implementation of HMC-SS-based network reliability curve

M_w	Separate HMC-SS			Single implementation			Exact P_f
	$\hat{P}_{f,SS}$	c.o.v.	NS	$\hat{P}_{f,SS}$	c.o.v.	NS	
7.0	1.41×10^{-2}	0.047	19,270	1.41×10^{-2}	0.048	19,270	1.40×10^{-2}
6.5	9.50×10^{-3}	0.055	26,200	9.47×10^{-3}	0.068	9,000	9.49×10^{-3}
6.0	6.34×10^{-3}	0.062	27,910	6.29×10^{-3}	0.076	9,000	6.31×10^{-3}
5.5	4.15×10^{-3}	0.049	28,000	4.07×10^{-3}	0.090	9,000	4.10×10^{-3}
5.0	2.62×10^{-3}	0.062	28,000	2.59×10^{-3}	0.096	9,000	2.61×10^{-3}
4.5	1.62×10^{-3}	0.065	28,000	1.61×10^{-3}	0.102	9,000	1.62×10^{-3}
4.0	1.00×10^{-3}	0.081	32,896	0.99×10^{-3}	0.114	9,000	0.98×10^{-3}
3.5	5.82×10^{-4}	0.087	37,000	5.88×10^{-4}	0.127	9,000	5.85×10^{-4}
3.0	3.46×10^{-4}	0.090	37,000	3.41×10^{-4}	0.130	9,000	3.40×10^{-4}
Total NS			264,276			91,270	

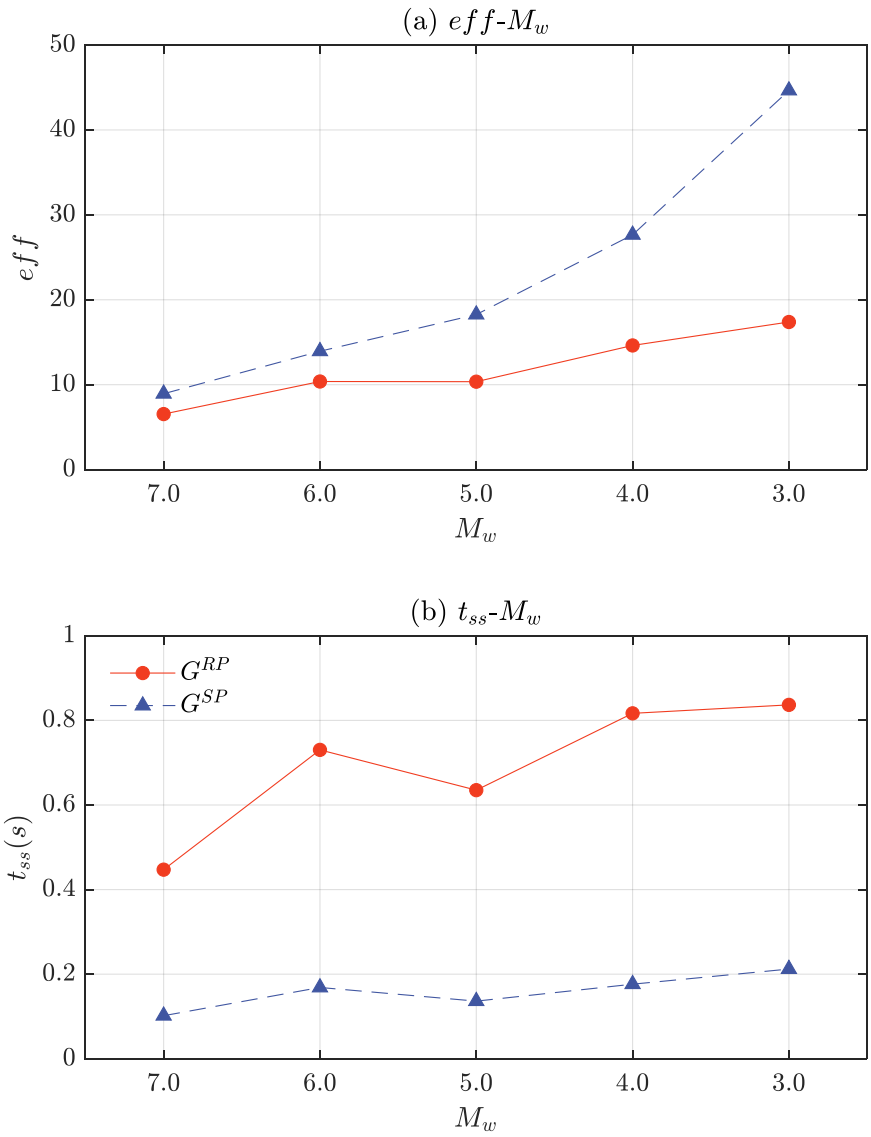

Figure 4.10. (a) eff-M_w, and (b) t_{ss}-M_w curves on two-component parallel system

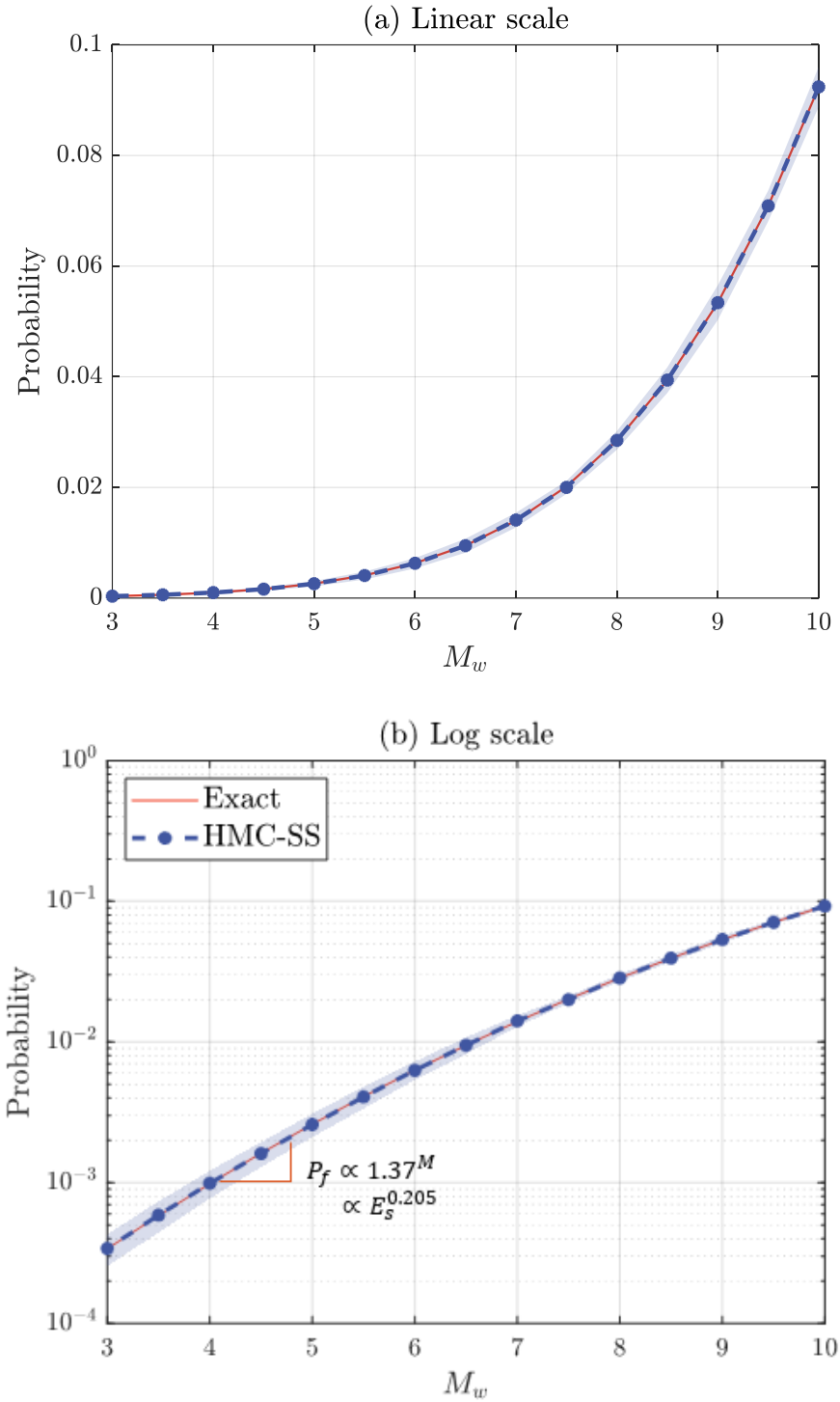

Figure 4.11. Seismic reliability curve of two-component parallel system at (a) linear-, and (b) log-scale

4.4.1.2 Example II: Hypothetical example

The hypothetical network introduced in Section 2.4.1 has 42 components, and the high-dimensional data makes it difficult to visualize samples as shown in Figures 4.8 and 4.9. Instead, Table 4.3 shows that HMC-SS using the two proposed network limit-state functions still performs well. For extremely small M_w, e.g., $M_w = 3.0$, the $G_{\mathrm{OD}}^{\mathrm{SP}}$-based HMC-SS is much closer to the MCS result than the $G_{\mathrm{OD}}^{\mathrm{RP}}$-based one despite much larger c.o.v. values. This is due to some overestimated outliers in the $G_{\mathrm{OD}}^{\mathrm{RP}}$-based method, which can be mitigated by increasing the number of samples.

Figure 4.12 shows the advantages of the two proposed continuous functions in terms of sampling efficiency and computation time, respectively, over all earthquake magnitudes. Meanwhile, the seismic reliability curve of the hypothetical network assessed by the single HMC-SS based on $G_{\mathrm{OD}}^{\mathrm{RP}}$ (yellow dots) is shown in Figure 4.13 with the results of direct MCS (red line) and the separate implemententation of HMC-SS (blue squares). Only the 95% confidence interval of the estimate from a single run of HMC-SS is shown in the yellow shaded area. The estimates by the single run are unbiased and have little difference from those of direct MCS or separate HMC-SS even at low M_w owing to the sufficiently large n.

Table 4.3. Two-terminal reliability analysis results on hypothetical network

M_w	$G_{\mathrm{OD}}^{\mathrm{RP}}$			$G_{\mathrm{OD}}^{\mathrm{SP}}$			MCS P_f
	$\hat{P}_{f,SS}$	c.o.v.	t_{ss}(s)	$\hat{P}_{f,SS}$	c.o.v.	t_{ss}(s)	
7.0	5.17×10^{-2}	0.111	0.819	5.14×10^{-2}	0.120	0.412	5.19×10^{-2}
6.0	1.37×10^{-2}	0.170	0.600	1.39×10^{-2}	0.194	0.220	1.37×10^{-2}
5.0	3.00×10^{-3}	0.233	0.772	3.05×10^{-3}	0.318	0.227	2.97×10^{-3}
4.0	5.46×10^{-4}	0.304	0.944	5.30×10^{-4}	0.566	0.247	5.28×10^{-4}
3.0	8.26×10^{-5}	0.363	1.067	7.88×10^{-5}	1.114	0.376	7.88×10^{-5}

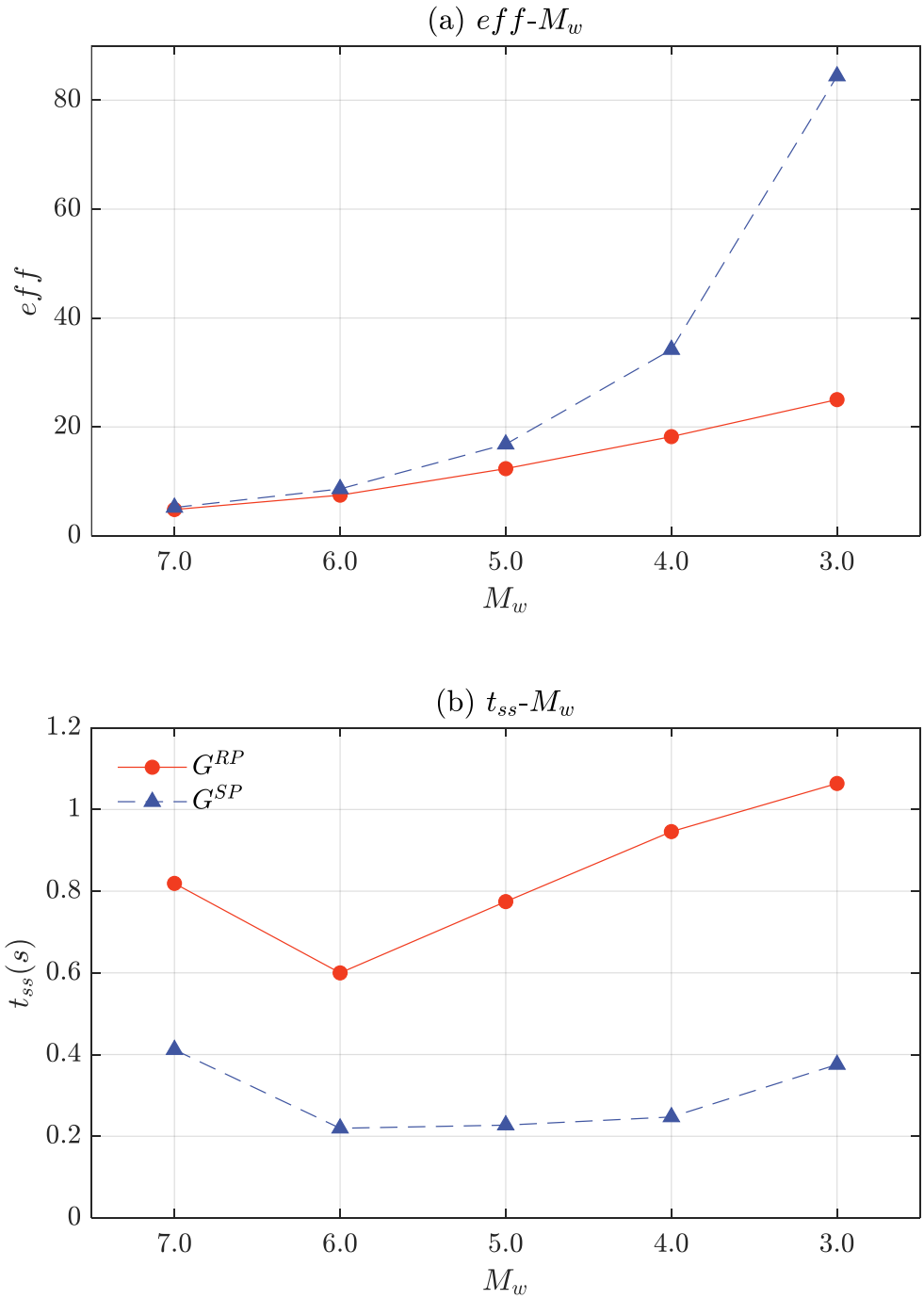

Figure 4.12. (a) eff-M_w, and (b) t_{ss}-M_w curves on hypothetical network

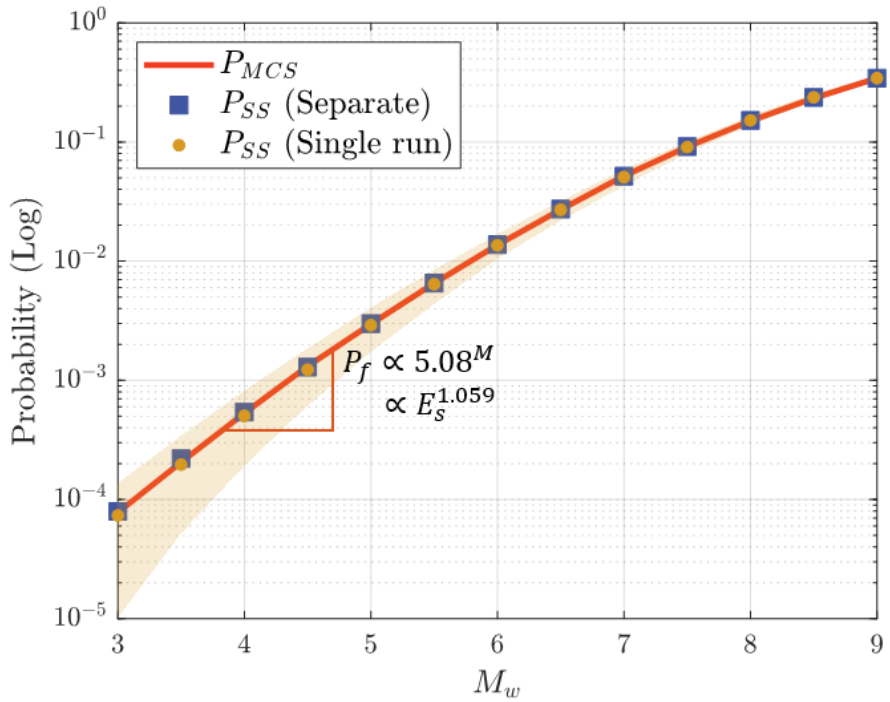

Figure 4.13. Seismic reliability curve of hypothetical network

4.4.2 *k*-terminal reliability & *k*-out-of-*N* network reliability

4.4.2.1 Example III: *k*-terminal reliability on San Jose highway network

Two-terminal reliability can be considered as a special case of *k*-terminal reliability with $k = 2$. In other words, the network reliability functions proposed in Eqs. (4.11) and (4.13) can be generalized to the limit-state function of *k*-terminal reliability, $G_{\boldsymbol{V}_k}(\boldsymbol{z})$, as

$$G_{\boldsymbol{V}_k}(\boldsymbol{z}) = \min_{o \in \boldsymbol{V}_O, d \in \boldsymbol{V}_D} G_{od}(\boldsymbol{z}), \tag{4.16}$$

where $\boldsymbol{V}_O$ and $\boldsymbol{V}_D$ denote the sets of origin and destination nodes, respectively; and $k = |\boldsymbol{V}_O| + |\boldsymbol{V}_D|$. The computational complexity for *k*-terminal reliability analysis grows linearly with the number of OD pairs, since the network connectivity is investigated by the number of OD pairs from each sample.

This *k*-terminal reliability analysis using subset simulation is applied to the San Jose highway network (Guo *et al.* 2017; Nabian and Meidani 2018) introduced in Section 2.4.2. Figure 4.14 shows the San Jose highway network with two origins and two destinations. Table 4.4 shows the results of the *k*-terminal reliability analysis using $G_{\mathrm{OD}}^{\mathrm{RP}}$ and $G_{\mathrm{OD}}^{\mathrm{SP}}$ according to Eq. (4.16), along with the direct MCS results. Moreover, Figure 4.15 shows eff and t_{ss} under each earthquake magnitude to compare the performance of each proposed function in terms of sampling efficiency and computational speed.

Figure 4.16 shows the seismic reliability curves of the San Jose highway network in terms of *k*-terminal reliability estimated by the direct MCS and the proposed method with and without physics-informed intermediate failure domains. As M_w decreases, the estimates by a single implementation of HMC-SS tend to be underestimated compared to the rest due to bias from accumulated errors. However, the single run outperforms separate runs in terms of computation time and samples required. The saved computational cost can be used for additional sampling to increase accuracy, depending on the user's needs.

Table 4.4. *k*-terminal reliability analysis results on San Jose highway network

M_w	$G_{\mathrm{OD}}^{\mathrm{RP}}$			$G_{\mathrm{OD}}^{\mathrm{SP}}$			MCS P_f
	$\hat{P}_{f,SS}$	c.o.v.	t_{ss}(s)	$\hat{P}_{f,SS}$	c.o.v.	t_{ss}(s)	
7.0	1.55×10^{-1}	0.076	0.796	1.54×10^{-1}	0.076	0.481	1.54×10^{-1}
6.0	7.30×10^{-2}	0.110	1.334	7.24×10^{-2}	0.107	0.741	7.22×10^{-2}
5.0	3.37×10^{-2}	0.124	0.943	3.31×10^{-2}	0.149	0.426	3.33×10^{-2}
4.0	1.59×10^{-2}	0.160	0.776	1.58×10^{-2}	0.185	0.281	1.61×10^{-2}
3.0	7.61×10^{-3}	0.189	1.081	7.58×10^{-3}	0.246	0.354	7.50×10^{-3}

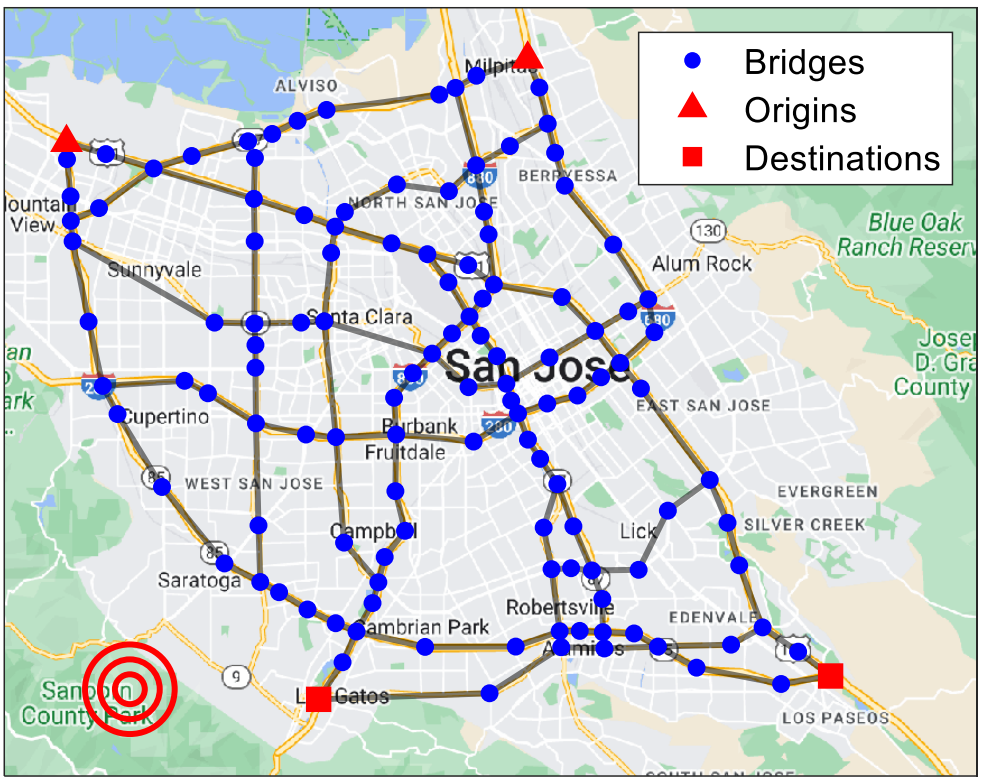

Figure 4.14. San Jose highway network with multiple OD nodes

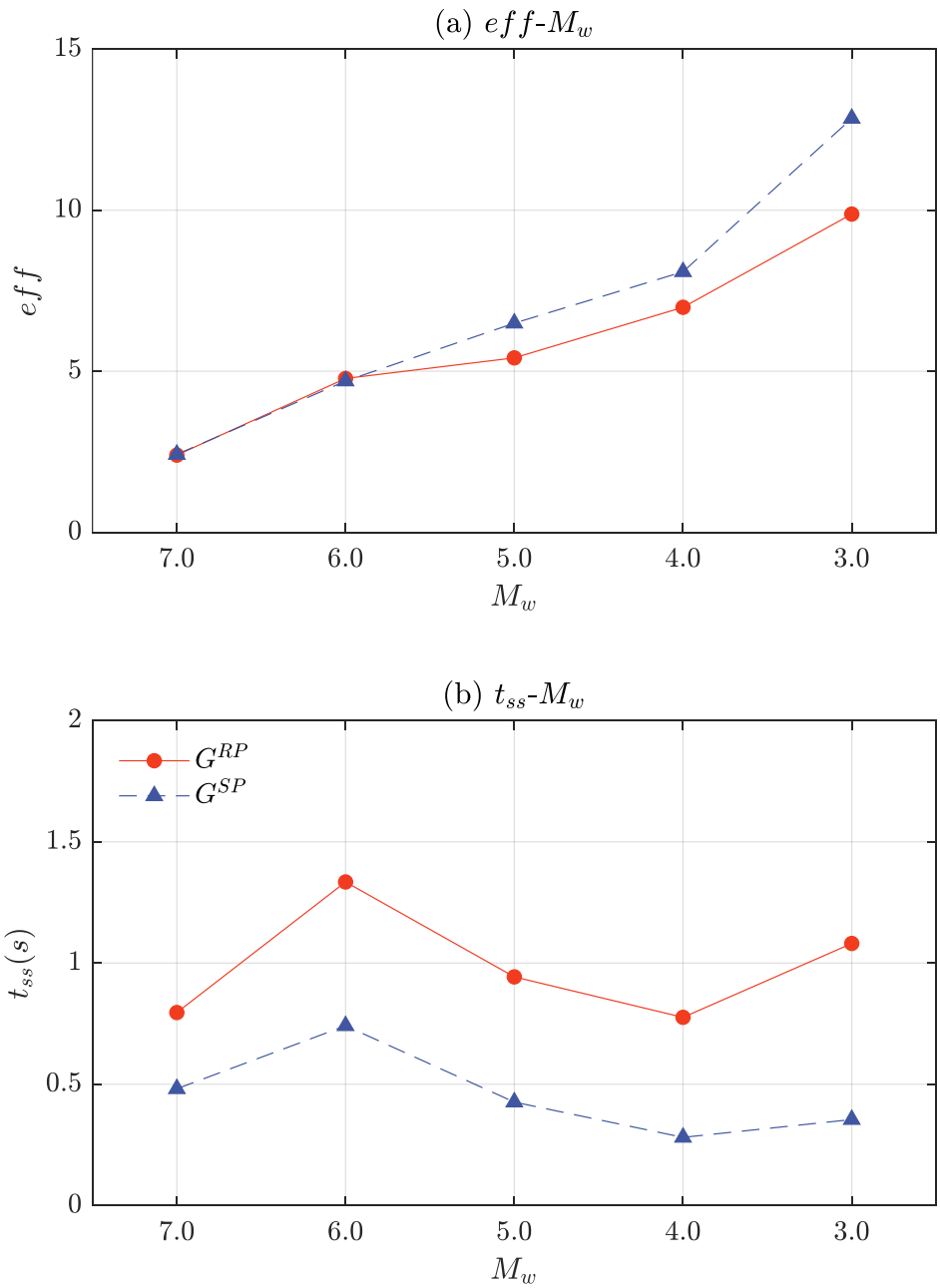

Figure 4.15. (a) eff-M_w, and (b) t_{ss}-M_w curves on San Jose highway network

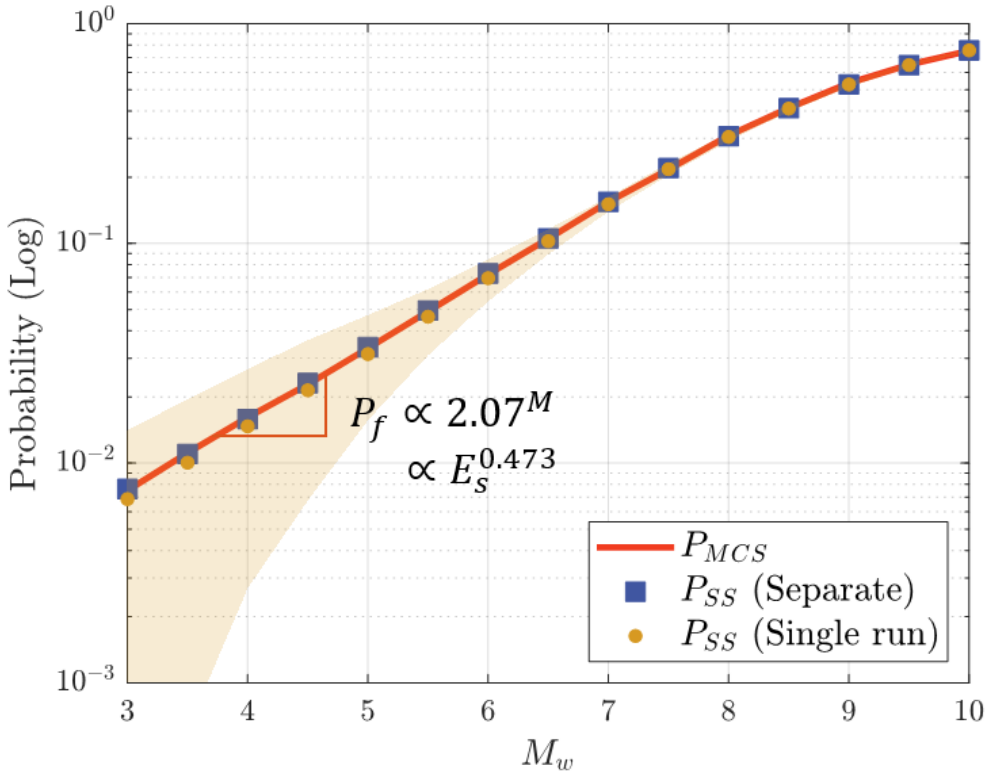

Figure 4.16. Seismic reliability curves of San Jose highway

4.4.2.2 Example IV: *k*-out-of-*N* reliability on San Diego highway network

Beyond the *k*-terminal reliability analysis, Eq. (4.16) can be extended to the limit-state function of the *k*-out-of-*N* network reliability for N OD pairs, $G_{k/N}$, as

$$G_{k/N}(\boldsymbol{z}) = \min_{i\in[1,N]}\!{}^{k}\ G_{OD_i}(\boldsymbol{z},k), \tag{4.17}$$

where $\min(\cdot,k)$ is defined as a function for an order statistic that returns the k^{th} smallest value.

Consider the *k*-out-of-*N* network reliability of the San Diego highway network in Section 2.4.3. More specifically, Southwest San Diego is set as the origin and five intercity highways connecting to neighboring cities are used as the destinations as shown in Figure 4.17. The target event is defined as an event that at least three destinations are accessible from the origin, i.e., $k = 3$ and $N = 5$.

Table 4.5. *k*-out-of-*N* reliability analysis results on San Diego highway network

M_w	$G_{\mathrm{OD}}^{\mathrm{RP}}$			$G_{\mathrm{OD}}^{\mathrm{SP}}$			MCS P_f
	$\hat{P}_{f,SS}$	c.o.v.	t_{ss}(s)	$\hat{P}_{f,SS}$	c.o.v.	t_{ss}(s)	
7.0	1.19×10^{-1}	0.089	1.766	1.18×10^{-1}	0.091	1.402	1.20×10^{-1}
6.0	3.43×10^{-2}	0.130	2.613	3.40×10^{-2}	0.135	1.978	3.46×10^{-2}
5.0	8.20×10^{-3}	0.202	2.891	7.95×10^{-3}	0.221	2.131	8.01×10^{-3}
4.0	1.75×10^{-3}	0.286	2.302	1.76×10^{-3}	0.350	1.470	1.72×10^{-3}
3.0	3.60×10^{-4}	0.357	2.694	3.55×10^{-4}	0.611	1.633	3.62×10^{-4}

Based on Eq. (4.17), the *k*-out-of-*N* network reliability can be easily evaluated by the proposed method, and Table 4.5 shows the results with two network limit-state functions at multiple M_w are very similar to those of the direct MCS. Meanwhile, Figure 4.18(a) shows the seismic reliability curves of the network assessed by the direct MCS, separate HMC-SS, and the single implementation of

HMC-SS with the 95% confidence intervals. In contrast, Figure 4.18(b) shows the results of HMC-SS split over two ranges, $3.0 \leq M_w \leq 6.0$ and $6.0 \leq M_w \leq 10.0$, compared to the single implementation. While the bias of the single run increases in the range of $M_w \leq 6.0$, the two split runs provide comparatively unbiased results. Ultimately, more finely partitioned implementations could provide the unbiased estimates, but the gain in terms of computational efficiency will be reduced compared to the independent separate executions.

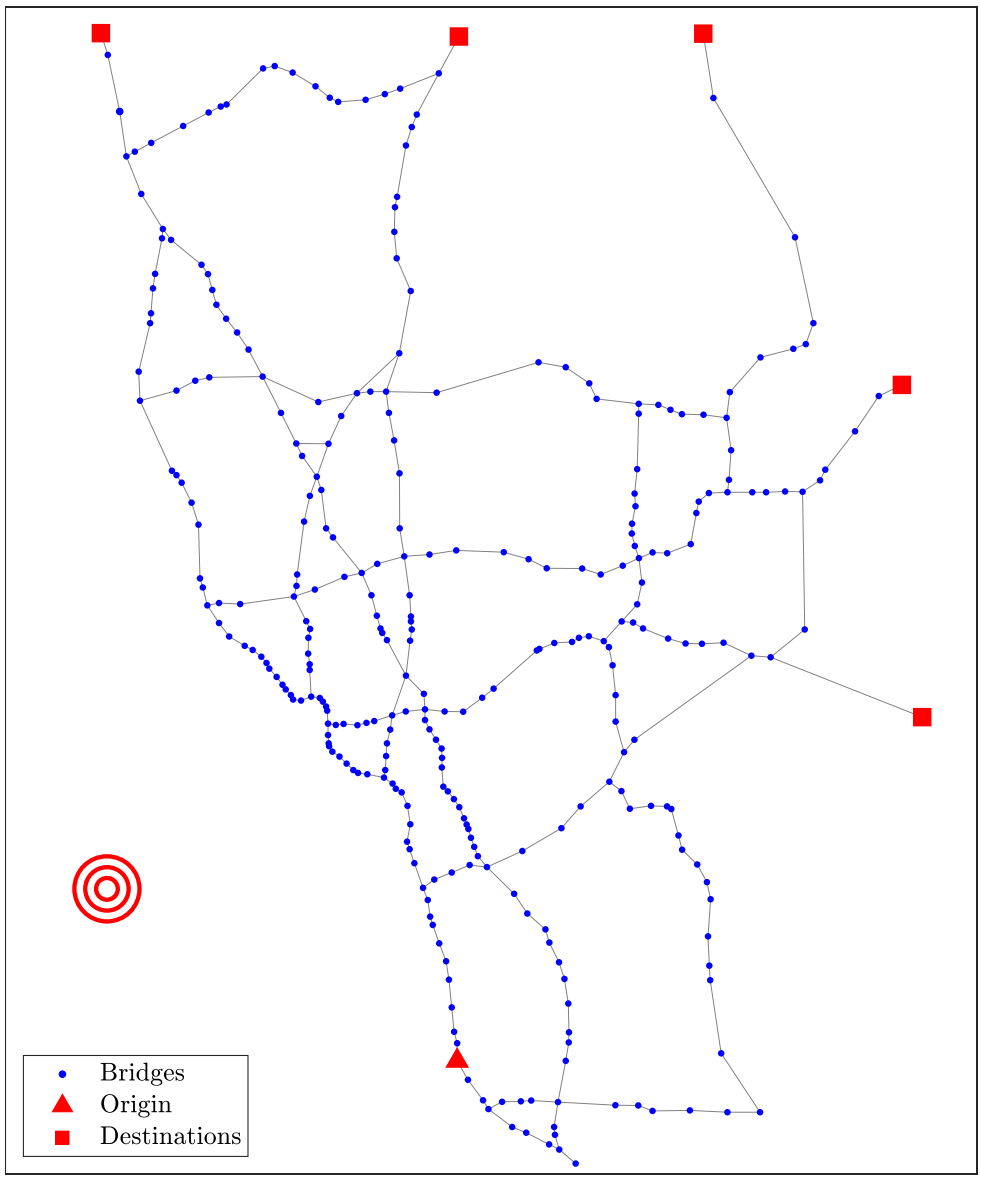

Figure 4.17. San Diego highway network with an origin and five destinations

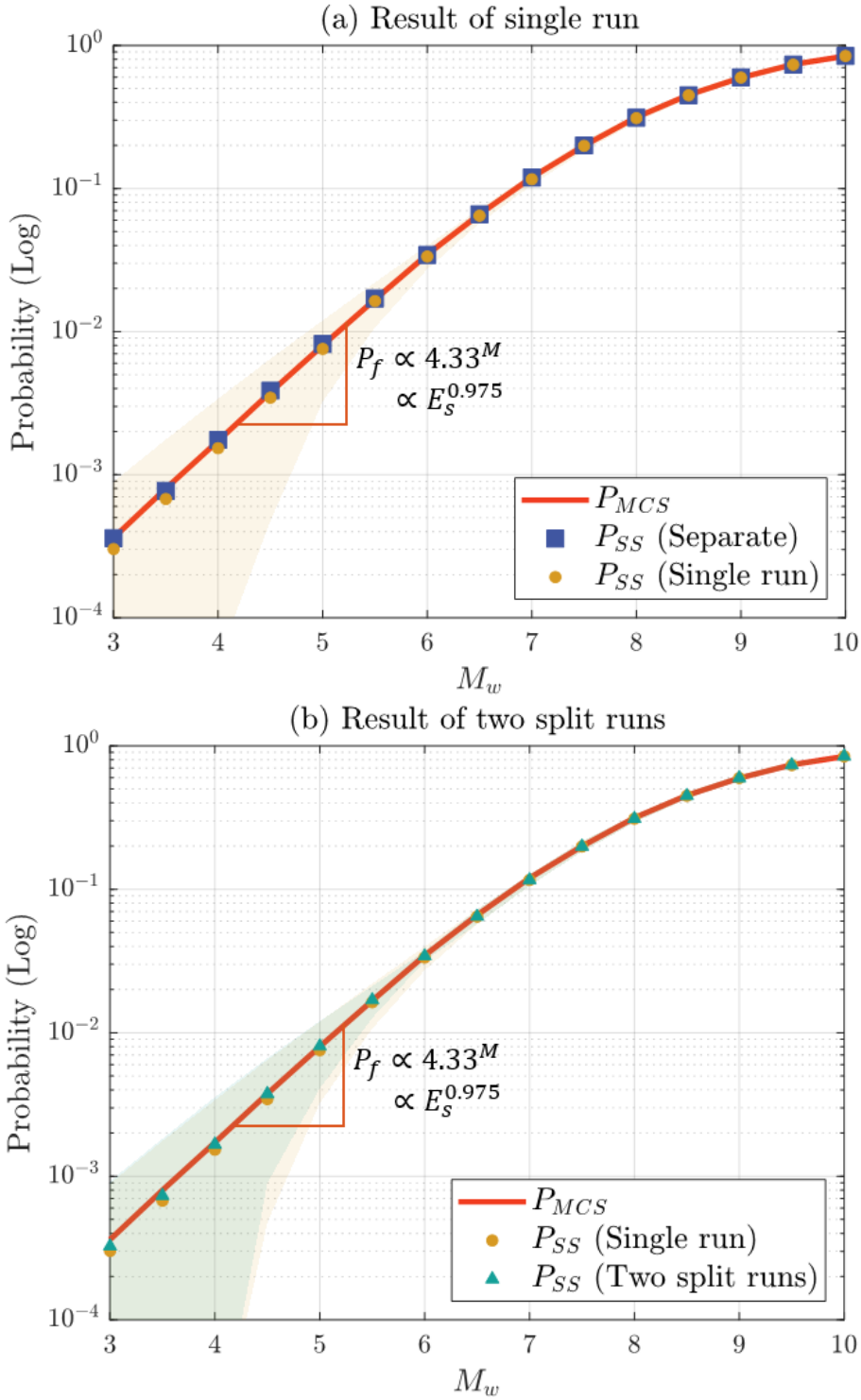

Figure 4.18. Seismic reliability curves of San Diego highway network under (a) single run, and (b) two split runs

Chapter 5. Conclusions

5.1 Introduction

This chapter summarizes the major developments and findings of this dissertation. Then, the current limitations and requirements that need further investigation are elaborated. The chapter is concluded by possible applications and recommendations for further research.

5.2 Summary and contributions of this dissertation

In order to perform seismic reliability analyses of large-scale networks with probabilistic inference and complexity quantification, this dissertation proposes and develops three kinds of NRA methods: (1) JT-based NRA and complexity quantification using BNs and dual representation of networks; (2) multi-scale NRA approach using CS-RDA; and (3) variance-reduction sampling method for reliability curves of networks based on subset simulations. The major findings and contributions of this dissertation are graphically presented in Figures 5.1 and 5.2 and summarized as follows:

- Exact seismic reliability of complex directional networks other than serial or parallel systems can be obtained in near real-time by the proposed JT-based NRA method. The generation of JT for the method is automated with a BN that is identical to the dual representation of the network. Furthermore, the method

can deal with networks with multi-state components.

- The required memory is governed by the maximum clique size of JT, thereby quantifying the complexity of the NRA. It allows users to determine whether the NRA is feasible or not on a given resource.
- JT-based NRA method has inherent limitations in dealing with cyclic networks due to the nature of BNs utilizing DAGs. However, the proposed preprocessing decomposes the cyclic network into multiple DAGs, thereby making the method applicable. Besides, the preprocessing of the network simplification shortens the computation time by removing components irrelevant to the OD pair.
- Numerical examples show that the JT-based NRA method can be effectively applied to various types of network, including cyclic networks or realistic large-scale networks. Moreover, probabilistic inference is successfully performed, taking advantage of the near real-time NRA.
- CS-RDA is a non-simulation-based NRA method using a decomposition approach. The main objective of CS-RDA is achieved by reducing the number of network decompositions, i.e., subnetworks, required to narrow down the upper and lower bounds of seismic network reliability. To this end, the method uses BC to integrates the non-simulation-based NRA method and the hierarchical clustering method. In addition, analytically derived correlation coefficients assess interdependencies between component failures accurately and quickly.
- CS-RDA effectively captures the critical components expected to be included in the minimum cut-set. Numerical examples were investigated to test and demonstrate the efficiency and accuracy of CS-RDA with multi-scale

approaches. In each example, the proposed method outperforms the existing RDAs, as well as MCS without compromising accuracy.

- Variance–reduction sampling using two proposed continuous network limit-state functions allows efficient evaluation of sparse failure probabilities of large-scale networks. The formulated continuous limit-state functions implicitly provide information about the location of the failure domain. HMC-SS is adopted for stable and efficient convergence of estimates.
- Numerical examples show that the proposed HMC-SS-based NRA can efficiently evaluate the seismic failure probability of large-scale networks that are infeasible with traditional sampling-based methods. In addition, the proposed NRA method can be easily extended to analyze other network reliability indices, including *k*-terminal reliability and *k*-out-of-*N* reliability.
- The most prominent application of the proposed method is the evaluation of reliability curves of network reliability. In general, intermediate failure domains have no special meaning in subset simulation. In contrast, the proposed framework discusses the configuration of each intermediate failure domain as a network failure event under a given earthquake intensity, and the generation of network reliability curves using the intermediate failure probabilities.

5.3 Limitations and recommendations for future investigation

To advance the frontiers of theories and applications relevant to the proposed methods, the followings are identified as further research topics:

- The proposed JT-based NRA can manage cyclic networks through cycle decomposition, but the number of required subnetworks grows exponentially with the number of cycles. As a result, it is infeasible to apply the JT-based NRA to the reliability analysis of undirected networks. To compensate for this, combinations of the JT-based NRA with sampling techniques may be considered.
- Dependent component events result in the generation of a giant single clique in the JT, consequently making the computation infeasible. As mentioned in Section 2, conditioning can be a solution to reflect the correlation coefficients.
- Because CS-RDA uses Boolean simplification to decompose a network event into combinations of binary structure events, it cannot handle multi-state components. Therefore, unlike other proposed methods, CS-RDA is limited in its extension to max-flow analysis. However, by considering the different damage states of structures, CS-RDA can perform a discretized multi-state network analysis.
- While the failure probabilities and the correlations between the individual components can be evaluated using closed-form equations, these equations are not valid for those of super-components in CS-RDA. Although MCS is used to assess the seismic risk of super-components, it may be limited in terms of scalability. Therefore, an efficient seismic risk assessment framework for super-components is required to apply CS-RDA to large-scale networks.
- For probabilistic inference, such as CPIM, the network-level outputs should be analyzed as a function of input values. In sampling-based approaches, however, probabilistic inference requires many evaluations of the NRA. To this end, one

can employ the sampling-based sensitivity analysis methods that have recently been developed for the NRA (Wang and Jia 2020).

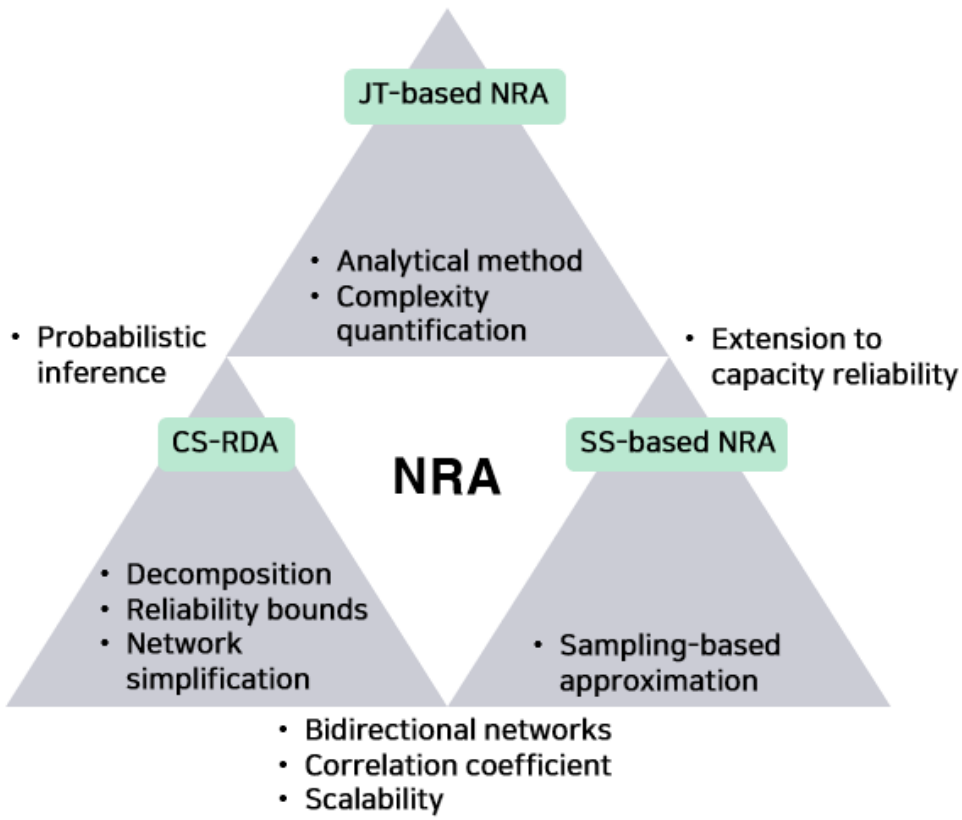

Figure 5.1. Diagram of main contribution and findings of the dissertation

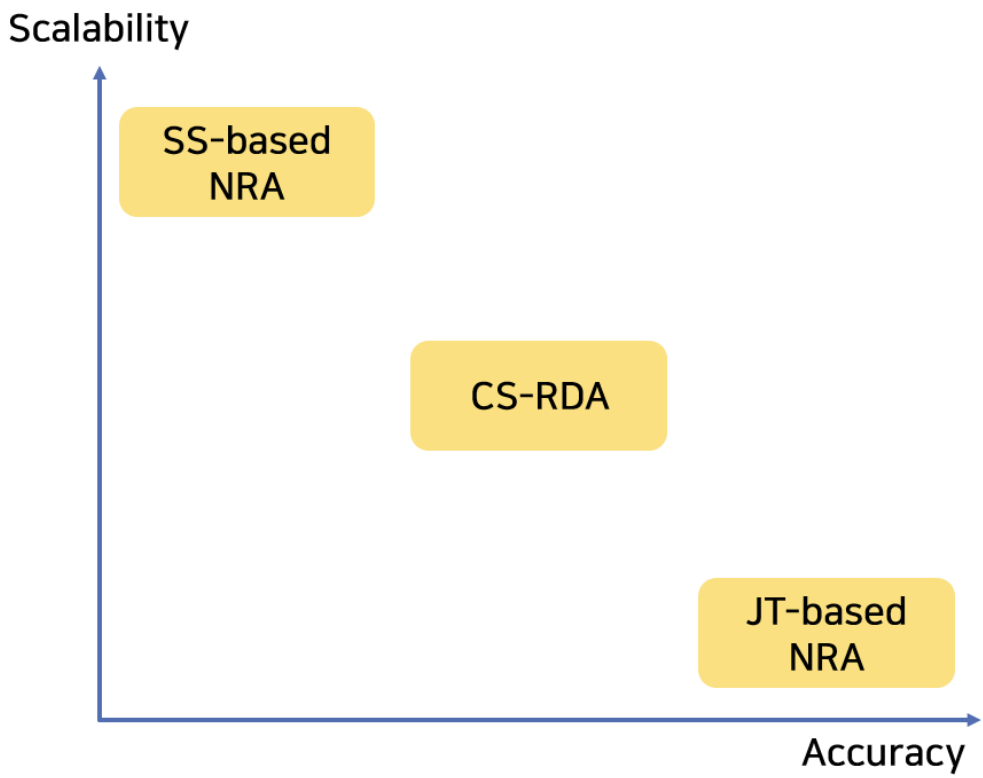

Figure 5.2. Trade-off between accuracy and scalability in proposed methods

References

Abraham, J. A. (1979). An improved algorithm for network reliability. *IEEE Transactions on Reliability*, *28*(1), 58-61.

Abrahamson, N. A., and Youngs, R. R. (1992). A stable algorithm for regression analyses using the random effects model. *Bulletin of the Seismological Society of America*, *82*(1), 505-510.

Ahuja, R. K., Magnanti, T. L., and Orlin, J. B. (1993). *Network flows: theory, algorithms and applications.* Prentice Hall.

Au, S. K., and Beck, J. L. (2001). Estimation of small failure probabilities in high dimensions by subset simulation. *Probabilistic Engineering Mechanics*, *16*(4), 263-277.

Aziz, M. A., Sobhan, M. A., and Samad, M. A. (1993). Enumeration of pathsets of reliability graphs by repeated indexing. *Microelectronics Reliability*, *33*(4), 481-487.

Ball, M. O. (1986). Computational complexity of network reliability analysis: An overview. *IEEE Transactions on Reliability*, *35*(3), 230-239.

Ball, M. O., Colbourn, C. J., and Provan, J. S. (1995). Network reliability. *Handbooks in operations research and management science*, 7, 673-762.

Barber, D. (2012). *Bayesian reasoning and machine learning*. Cambridge University Press.

Beauchamp, M. A. (1965). An improved index of centrality. *Behavioral Science*, *10*(2), 161-163.

Bensi, M., Der Kiureghian, A., and Straub, D. (2011). Bayesian network modeling of correlated random variables drawn from a Gaussian random field. *Structural Safety*, 33(6), 317-332.

Boore, D. M., and Atkinson, G. M. (2008). Ground-motion prediction equations for the average horizontal component of PGA, PGV, and 5%-damped PSA at spectral periods between 0.01 s and 10.0 s. *Earthquake Spectra*, *24*(1), 99-138.

Brandes, U., Delling, D., Gaertler, M., Gorke, R., Hoefer, M., Nikoloski, Z., and Wagner, D. (2007). On modularity clustering. *IEEE Transactions on Knowledge and Data Engineering*, *20*(2), 172-188.

Brown, D. B. (1971). A computerized algorithm for determining the reliability of redundant configurations. *IEEE Transactions on Reliability*, *20*(3), 121-124.

Byun, J. E. and Song, J. (2021a). Generalized matrix-based Bayesian network for multi-state systems. *Reliability Engineering and System Safety*, *211*, 107468.

Byun, J. E. and Song, J. (2021b). A general framework of Bayesian network for system reliability analysis using junction tree. *Reliability Engineering and System Safety*, *216*, 107952.

Cetinay, H., Devriendt, K., and Van Mieghem, P. (2018). Nodal vulnerability to targeted attacks in power grids. *Applied Network Science*, *3*(1), 1-19.

Chen, W., Wang, Z., Broccardo, M., and Song, J. (2022). Riemannian Manifold Hamiltonian Monte Carlo based subset simulation for reliability analysis in non-Gaussian space. *Structural Safety*, *94*, 102134.

Colbourn, C. J. (1987). Network resilience. *SIAM Journal on Algebraic Discrete Methods*, *8*(3), 404-409.

Cormen, T. H., Leiserson, C. E., Rivest, R. L., and Stein, C. (2009). *Introduction to algorithms*. MIT press.

Der Kiureghian, A., Ditlevsen, O. D., and Song, J. (2007). Availability, reliability and downtime of systems with repairable components. *Reliability Engineering and System Safety*, *92*(2), 231-242.

Dijkstra, E. W. (1959). A note on two problems in connexion with graphs. *Numerische Mathematik*, *1*, 269-271.

Federal Emergency Management Agency (FEMA). *Hazus-MH 2.1: Technical Manual*. Washington, DC, USA.

Ford, L. R., and Fulkerson, D. R. (1956). Maximal flow through a network. *Canadian Journal of Mathematics*, *8*, 399-404.

Freeman, L. C. (1977). A set of measures of centrality based on betweenness. *Sociometry*, 35-41.

Genz, A. (1992). Numerical computation of multivariate normal probabilities. *Journal of computational and graphical statistics*, *1*(2), 141-149.

Goda, K., and Hong, H. P. (2008). Spatial correlation of peak ground motions and response spectra. *Bulletin of the Seismological Society of America*, *98*(1), 354-365.

Gomez, C., Sanchez-Silva, M., Dueñas-Osorio, L., and Rosowsky, D. (2013). Hierarchical infrastructure network representation methods for risk-based decision-making. *Structure and Infrastructure Engineering*, *9*(3), 260-274.

Guo, A., Liu, Z., Li, S., and Li, H. (2017). Seismic performance assessment of highway bridge networks considering post-disaster traffic demand of a transportation system in emergency conditions. *Structure and Infrastructure Engineering*, *13*(12), 1523-1537.

Hastings, W. K. (1970). Monte Carlo sampling methods using Markov chains and their applications.

Henley, E. J., and Kumamoto, H. (1981). *Reliability engineering and risk assessment*. Prentice Hall, NJ.

Hohenbichler, M., and Rackwitz, R. (1982). First-order concepts in system reliability. *Structural Safety*, *1*(3), 177-188.

Joyner, W. B., and Boore, D. M. (1993). Methods for regression analysis of strong-motion data. *Bulletin of the Seismological Society of America*, *83*(2), 469-487.

Kang, W. H., and Song, J. (2010). Evaluation of multivariate normal integrals for general systems by sequential compounding. *Structural Safety*, *32*(1), 35-41.

Koller, D., and Friedman, N. (2009). *Probabilistic graphical models: principles and techniques*. MIT press.

Lee, D., and Song, J. (2021). Multi-scale seismic reliability assessment of networks by centrality-based selective recursive decomposition algorithm. *Earthquake Engineering and Structural Dynamics*, *50*(8), 2174-2194.

Li, J., and He, J. (2002). A recursive decomposition algorithm for network seismic reliability evaluation. *Earthquake Engineering and Structural Dynamics*, *31*(8), 1525-1539.

Lim, H. W., and Song, J. (2012). Efficient risk assessment of lifeline networks under spatially correlated ground motions using selective recursive decomposition algorithm. *Earthquake Engineering and Structural Dynamics*, *41*(13), 1861-1882.

Lim, H. W., Song, J., and Kurtz, N. (2015). Seismic reliability assessment of lifeline networks using clustering-based multi-scale approach. *Earthquake Engineering and Structural Dynamics*, *44*(3), 355-369.

Metropolis, N., Rosenbluth, A. W., Rosenbluth, M. N., Teller, A. H., and Teller, E. (1953). Equation of state calculations by fast computing machines. *The Journal of Chemical Physics*, *21*(6), 1087-1092.

Nabian, M. A., and Meidani, H. (2018). Deep learning for accelerated seismic reliability analysis of transportation networks. *Computer-Aided Civil and Infrastructure Engineering*, *33*(6), 443-458.

Newman, M. E., and Girvan, M. (2004). Finding and evaluating community structure in networks. *Physical Review E*, *69*(2), 026113.

Nieminen, J. (1974). On the centrality in a graph. *Scandinavian Journal of Psychology*, *15*(1), 332-336.

Özgür, A., Vu, T., Erkan, G., and Radev, D. R. (2008). Identifying gene-disease associations using centrality on a literature mined gene-interaction network. *Bioinformatics*, *24*(13), i277-i285.

Petreska, I., Tomovski, I., Gutierrez, E., Kocarev, L., Bono, F., and Poljansek, K. (2010). Application of modal analysis in assessing attack vulnerability of complex networks. *Communications in Nonlinear Science and Numerical Simulation*, *15*(4), 1008-1018.

Porta, S., Crucitti, P., and Latora, V. (2006). The network analysis of urban streets: A dual approach. *Physica A: Statistical Mechanics and its Applications*, 369(2), 853-866.

Rosenthal, A. (1977). Computing the reliability of complex networks. *SIAM Journal on Applied Mathematics*, *32*(2), 384-393.

Rosenthal, A. (1979). Approaches to comparing cut-set enumeration algorithms. *IEEE Transactions on Reliability*, *28*(1), 62-65.

Song, J., and Der Kiureghian, A. (2003). Bounds on system reliability by linear programming. *Journal of Engineering Mechanics*, *129*(6), 627-636.

Song, J. and Kang, W. H. (2009). System reliability and sensitivity under statistical dependence by matrix-based system reliability method. *Structural Safety*, 31(2), 148-156.

Valiant, L. G. (1979). The complexity of enumeration and reliability problems. *SIAM Journal on Computing*, 8(3), 410-421.

Wang, Z., Broccardo, M., and Song, J. (2019). Hamiltonian Monte Carlo methods for subset simulation in reliability analysis. *Structural Safety*, *76*, 51-67.

Wang, Z., and Jia, G. (2020). Augmented sample-based approach for efficient evaluation of risk sensitivity with respect to epistemic uncertainty in distribution parameters. *Reliability Engineering and System Safety*, *197*, 106783.

Zhang, J., Pourazarm, S., Cassandras, C. G., and Paschalidis, I. C. (2018). The price of anarchy in transportation networks: Data-driven evaluation and reduction strategies. *Proceedings of the IEEE*, 106(4), 538-553.

Zuev, K. M., Beck, J. L., Au, S. K., and Katafygiotis, L. S. (2012). Bayesian post-processor and other enhancements of Subset Simulation for estimating failure probabilities in high dimensions. *Computers and Structures*, *92*, 283-296.

초 록

이동규

건설환경공학부

서울대학교 대학원

현대 사회에서 기술이 발전하고 도시가 고밀화됨에 따라 사회기반시설물이 상호간에 긴밀하게 연결되어 하나의 거대한 사회기반시설 네트워크(infrastructure network)를 형성하고 있으며, 지진에 의한 개별 구조물의 손상은 라이프라인 네트워크 전반에 막대한 피해를 초래할 수 있다. 네트워크의 위험성을 정량화하고 효율적인 유지보수가 이루어질 수 있도록, 네트워크 차원의 내진 신뢰성 분석의 필요성이 대두된다. 이를 위해서는 다수의 구조물의 지진에 의한 손상 및 파괴 확률과 더불어, 구조물의 상태 조합에 따른 네트워크의 연결성 및 흐름 용량이 평가되어야 한다. 이러한 네트워크의 내진 신뢰성 분석은 지진이 네트워크 전반에 공통적으로 미치는 불확실성(common source effect)과 상호 의존적인 구조물의 상태 변화, 구조물의 개수에 기하급수적으로 비례하여 증가하는 연산 복잡도 등으로 인해 대규모 네트워크에 확대 적용하는 데에 어려움을 겪어왔다. 이를 극복하기 위해 몬테카를로 시뮬레이션(Monte Carlo Simulation, MCS)이 사용되나, 확률이 희박한 사건에 대한 시뮬레이션의 비효율성과 확률적 추론의 어려움 등 여러 한계를 지닌다.

본 논문에서는 이러한 종전의 한계를 극복하기 위해, 세 가지의 네트워크 내진 신뢰성 분석 방법론을 제안한다. 먼저, 베이지안 네트워크(Bayesian network, BN)와 정션 트리(junction tree, JT)에 기반한 네트워크 신뢰성 평가 및 복잡도 정량화 방법론이 제안된다. 네트워크 쌍대 표현(dual representation)을 이용하여 구축된 BN과 그에 기반하여 형성된 JT에서는 단방향 메시지 전달만으로 사이클이 없는 방향성 네트워크 신뢰성의 정해를 평가할 수 있다. 네트워크가 사이클을 갖는 경우에도,

사이클을 순차적으로 분해하여 제거함으로써 신뢰성을 정확히 평가할 수 있다. 한편, 네트워크 신뢰성의 복잡도는 구성요소의 개수로 평가하는 것이 일반적이나, 실제로는 네트워크 위상 또한 연산 복잡도에 영향을 미친다. 수치 예제를 통해 제안된 방법이 정확한 네트워크 신뢰성과 구성요소의 중요도 지표를 단시간 내에 평가할 뿐만 아니라, 다양한 위상의 네트워크 신뢰성 복잡도를 JT의 최대 클리크(clique)의 크기를 통해 정량화할 수 있음을 보였다.

또한, 중심성 기반 선택적 재귀 분해 알고리듬(Centrality-based selective recursive decomposition algorithm, CS-RDA)은 네트워크의 중심성을 기반으로 연결성에 핵심적인 영향을 미친다고 판단되는 구성요소를 파악함으로써, (1) 다중 스케일 접근법을 위해 네트워크 간소화를 수행하고, (2) 재귀 분해 알고리듬(Recursive decomposition algorithm, RDA)의 수렴성을 크게 증가시킨다. CS-RDA에서는 이를 통해 RDA에 비해 훨씬 적은 하위그래프 개수만으로, 동일한 수준의 네트워크 신뢰도 범위를 달성할 수 있다. 실제 대규모 교량 네트워크를 이용한 수치 예제를 통해, 향상된 CS-RDA의 효율성 및 정확성을 증명하고, 네트워크 간소화 정도에 따른 효율성과 정확성의 변화를 분석하였다.

마지막으로, 종전에 사용되던 MCS의 확장성과 효율성을 향상시키기 위한 분산 감소 시뮬레이션 기법이 제안된다. 기존 연결성 측면의 이진 한계상태 함수는 네트워크 실패 도메인까지의 거리를 정량화하는 연속 함수로 재정의되며, 이는 하위집합 시뮬레이션 기반의 네트워크 신뢰성 해석을 가능하게 한다. 더 나아가, 하위집합 시뮬레이션의 각 중간 실패 도메인이 특정 지진 강도에서의 네트워크 파괴 이벤트에 대응하도록 구성함으로써, 단일 하위집합 시뮬레이션으로 네트워크 취약도 곡선을 생성할 수 있다. 수치 예제를 통하여 제안된 방법론이 2단자 신뢰성(two-terminal reliability) 분석은 물론, k단자 신뢰성(k-terminal reliability), 네트워크 흐름 용량 분석에 손쉽게 확장되어 높은 효율성과 정확성을 가짐을 보였다.

주요어: 네트워크 신뢰성 분석; 내진 신뢰성; 사회기반시설 네트워크;

대규모 네트워크; 그래프 이론; 베이지안 네트워크; 정션 트리 알고리듬; 복잡도 정량화; 확률적 추론; 다중 스케일 접근법; 클러스터링; 재귀적 분해 알고리듬; 하위집합 시뮬레이션; 해밀토니안 몬테카를로; 네트워크 신뢰도 곡선.

학번: 2017-27849